2022

User-Friendly, Low-Cost, Microfluidic Devices With Capillary Circuits For Multiplexed, Isothermal, Point-Of-Care, Nucleic Acid Amplification Tests

Huiwen Bai
University of Pennsylvania

User-Friendly, Low-Cost, Microfluidic Devices With Capillary Circuits For Multiplexed, Isothermal, Point-Of-Care, Nucleic Acid Amplification Tests

Abstract

Rapid, sensitive, and specific detection of causative pathogens is key to personalized medicine and the prompt implementation of appropriate mitigation measures to reduce disease transmission, mortality, morbidity, and cost. Conventional molecular detection methods require trained personnel, sophisticated equipment, and specialized laboratories, which limits their use to centralized laboratories. To enable molecular diagnostics at the point of need and in resource-poor settings, inexpensive, simple devices that combine multiple unit operations and are capable of co-detecting endemic pathogens are needed.

In this work, I have developed microfluidic devices with capillary circuits to automate liquid distribution, eliminating the need for expensive equipment, sophisticated laboratory facilities, and skilled personnel to enable molecular diagnostics at the point of need. Capillary valves with different sizes were developed and implemented to aliquot samples and reagents to multiple reaction chambers and to enable draining liquids from supply lines without affecting liquids in the various reaction chambers, enabling bubble-free operation. The sealing of my microfluidic devices to prevent evaporation during incubation is facilitated with phase-change materials and capillary-induced motion. When my microfluidic chip is heated to its incubation temperature, the phase-change material melts and flows to seal ports of entry and air vent. Numerical simulations were carried out to assess the viability of on-chip, in-house developed, two-stage isothermal nucleic acid amplification in the presence of diffusion and advection. An Android-based smartphone application was developed to automate real-time signal monitoring, time series image analysis, and diagnostic result interpretation. Three 3D-printed, portable, microfluidic devices with capillary circuits were designed, fabricated, and tested for single-stage and two-stage, isothermal nucleic acid amplification with either liquid reagents or pre-stored dry reagents that do not require a cold chain. All devices have proved successful for rapid, sensitive, and specific multiplexed detections of human and animal pathogens.

Degree Type

Dissertation

Degree Name

Doctor of Philosophy (PhD)

Graduate Group

Mechanical Engineering & Applied Mechanics

First Advisor

Haim H. Bau

Subject Categories

Mechanical Engineering

USER-FRIENDLY, LOW-COST, MICROFLUIDIC DEVICES WITH CAPILLARY CIRCUITS FOR MULTIPLEXED, ISOTHERMAL, POINT-OF-CARE, NUCLEIC ACID AMPLIFICATION TESTS

Huiwen Bai

A DISSERTATION

in

Mechanical Engineering and Applied Mechanics

Presented to the Faculties of the University of Pennsylvania

in

Partial Fulfillment of the Requirements for the

Degree of Doctor of Philosophy

2022

Supervisor of Dissertation

_____

Haim H. Bau

Richard H. & S. L. Gabel Professor, Mechanical Engineering and Applied Mechanics

Graduate Group Chairperson

_____

Jennifer R. Lukes

Professor, Mechanical Engineering and Applied Mechanics

Dissertation Committee

Howard H. Hu Professor, Mechanical Engineering and Applied Mechanics

Mark G. Allen Alfred Fitler Moore Professor, Electrical and Systems Engineering & Mechanical Engineering and Applied Mechanics

USER-FRIENDLY, LOW-COST, MICROFLUIDIC DEVICES WITH CAPILLARY CIRCUITS FOR MULTIPLEXED, ISOTHERMAL, POINT-OF-CARE, NUCLEIC ACID AMPLIFICATION TESTS

ACKNOWLEDGEMENT

I would like to express my heartful gratitude to my advisor, Dr. Haim H. Bau, for his guidance, support, and supervision throughout my Ph.D. study at Penn. It is my great pleasure to come to Penn and work with him. I would also like to thank my thesis committee members, Dr. Howard H. Hu and Dr. Mark G. Allen, for their valuable time and constructive insights.

I am thankful to my lab mates, the members and alumni from Dr. Haim Bau's and Dr. Changchun Liu's Group: Dr. Mohamed El-Tholoth, Dr. Youngung Seok, Dr. Karteek Kadimisetty, Dr. Ruijie Li, Qingtian Yin, Dr. Changchun Liu, Dr. Kun Yin, Dr. Junman Chen, Dr. Chen Zhao, Dr. Cheng Qian, Dr. Michael G. Mauk, Dr. Mazhar Sher, Joshua Clark, and Marziyeh Hajialyani. We had a great time and joyful collaborations. In particular, I would like to say special thanks to Dr. Mohamed El-Tholoth and Dr. Youngung Seok. Dr. Mohamed El-Tholoth was a visiting professor in our group and the assay designer of the multiplexed detection of the pig viruses discussed in Chapter 2 and the chicken virus discussed in Chapter 4. Dr. Youngung Seok is a postdoctoral fellow in our group and the assay designer of the multiplexed detection of the human bloodborne viruses discussed in Chapter 3.

Lastly but most importantly, I would like to thank my wife, Dongyang Wei, our parents, Xiujun Bai, Xianyun Hou, Yi Wei, and Lixia Zhou, for their encouragement, endless love, unconditional support, and companionship.

ABSTRACT

USER-FRIENDLY, LOW-COST, MICROFLUIDIC DEVICES WITH CAPILLARY CIRCUITS FOR MULTIPLEXED, ISOTHERMAL, POINT-OF-CARE, NUCLEIC ACID AMPLIFICATION TESTS

Huiwen Bai

Haim H. Bau

Rapid, sensitive, and specific detection of causative pathogens is key to personalized medicine and the prompt implementation of appropriate mitigation measures to reduce disease transmission, mortality, morbidity, and cost. Conventional molecular detection methods require trained personnel, sophisticated equipment, and specialized laboratories, which limits their use to centralized laboratories. To enable molecular diagnostics at the point of need and in resource-poor settings, inexpensive, simple devices that combine multiple unit operations and are capable of co-detecting endemic pathogens are needed.

In this work, I have developed microfluidic devices with capillary circuits to automate liquid distribution, eliminating the need for expensive equipment, sophisticated laboratory facilities, and skilled personnel to enable molecular diagnostics at the point of need. Capillary valves with different sizes were developed and implemented to aliquot samples and reagents to multiple reaction chambers and to enable draining liquids from supply lines without affecting liquids in the various reaction chambers, enabling bubble-free operation. The sealing of my microfluidic devices to prevent evaporation during incubation is facilitated with phase-change materials and capillary-induced motion. When my microfluidic chip is heated to its incubation temperature, the phase-change material melts and flows to seal ports of entry and air vent. Numerical simulations were carried out to assess the viability of on-chip, in-house developed, two-stage isothermal nucleic acid amplification in the presence of diffusion and advection. An Android-based smartphone application was developed to automate real-time signal monitoring, time series image analysis, and diagnostic result interpretation. Three 3D-printed, portable, microfluidic devices with capillary circuits were designed, fabricated, and tested for single-stage and two-stage, isothermal nucleic acid amplification with either liquid reagents or pre-stored dry

reagents that do not require a cold chain. All devices have proved successful for rapid, sensitive, and specific multiplexed detections of human and animal pathogens.

TABLE OF CONTENTS

LIST OF TABLES

LIST OF ILLUSTRATIONS

Chapter 1 Introduction

1.1 Microfluidics in Point-of-care (POC) Nucleic-acid Amplification Tests (NAATs)

Rapid, sensitive, and specific detection of biomarkers associated with diseases is key to the prompt implementation of therapeutics and mitigation measures to reduce disease transmission, thereby reducing morbidity, mortality, and cost. For example, the COVID-19 outbreak has introduced significant challenges to global health and dramatically changed the lives of everyone. This outbreak has claimed millions of lives worldwide and caused substantial economic losses. As new variants continue to emerge, the negative impacts brought by this pandemic have not yet come to an end. The availability of sensitive and rapid tests for SARS-Cov-2 is an essential tool in the effort to minimize the spread of this disease.

Nucleic-acid amplification tests (NAATs) and antigen tests are two types of commonly used diagnostic tests. Compared to antigen tests, NAATs offer higher sensitivity and specificity and an earlier detection window prior to seroconversion. Standard NAATs require trained personnel and specialized equipment that are only available within centralized laboratories, prolonging the time from sample collection to results. In resource-limited settings, and especially in less-developed countries, few centralized laboratories are available, and the turnaround times for NAATs may take up to a few days. Point-of-care testing (POCT) refers to the diagnostic tests performed near the patient outside of centralized laboratories, which eliminates the need for sending samples to the lab and therefore reduces turnaround times.

Microfluidics is the technology of fluid manipulation at the microscale and has been proved effective for POCT, including molecular detection [1-9]. Microfluidics has a number of advantages for POCT such as (1) small reagent volumes, reducing reagent costs, (2) small sample volumes, (3) miniaturization that makes it possible to integrate multiple unit operations onto a single chip, improving portability, (4) amenability for multiplexing that allows performing multiple diagnostic tests for different targets in parallel, and (5) comparable sensitivity and specificity to laboratory-based tests. Overall, currently used microfluidic devices offer relatively low-cost and portable

solutions to POC NAATs but still require trained personnel and some laboratory equipment such as syringe pumps and pipettes for reliable fluid control.

My Ph.D. research focuses on reducing diagnostic cost and operational complexity by developing microfluidic devices for rapid POC NAATs that are affordable and user-friendly for resource-poor settings while maintaining the same level of sensitivity and specificity as laboratory-based tests.

1.2 Isothermal Nucleic-acid Amplification Tests (NAATs)

Isothermal NAATs have many distinct advantages for POCT over the laboratory-based PCR that requires thermal cycling. Most importantly, isothermal reaction simplifies the design complexity and reduces the cost of heating/incubation systems. Incubation can even be carried out electricity-free with chemical heating regulated by phase-change materials (PCMs) [5, 10]. Our group has developed a two-stage isothermal nucleic acid amplification assay dubbed Penn RAMP that combines two isothermal amplification processes - recombinase polymerase amplification (RPA) and loop-mediated isothermal amplification (LAMP) [11, 12] to enable extensive multiplexing and higher sensitivity than can be obtained with a single-stage process. Isothermal NAATs were adopted in all the devices discussed in this thesis.

1.3 Capillary Circuits

A typical microfluidic setup for isothermal NAATs consists of a microfluidic chip with miniaturized unit operations, syringe pumps and pipettes to provide precise fluid control, a microscope to monitor the amplification process, and a heating system for incubation. An inexpensive homemade heating system meets the requirement of isothermal NAATs, and a smartphone can be used to replace microscopes to monitor amplification. A simple method of flow control is still needed to replace syringe pumps.

Capillary circuits are the combination of capillary “pumps” and valves that regulate fluid flow on chip with capillary forces. Different from mechanical pumps and valves powered by external driving forces, capillary pumps and valves rely on surface tension, materials’ wettability,

and microchannels' geometry. By judicious selection of materials with desired wettability and by properly designing microchannels' geometries, a capillary circuit can be formed to achieve spontaneous, complex liquid distribution on chip. Compared to mechanical pumps and valves that require movable components such as flexible membranes, capillary pumps and valves offer simpler design and lower manufacturing complexity.

To understand the working principle of capillary circuits, the concepts of contact angle, surface tension, and capillary pressure need to be discussed. The contact angle is the equilibrium angle formed between the liquid-vapor interface and the solid surface (on the liquid's side) at the contact line. The relationship is quantitatively described by the Young equation

$$\gamma_{lv}\cos\theta + \gamma_{ls} = \gamma_{sv}, \tag{1.1}$$

where θ is the static contact angle measured between the tangent line of the liquid-vapor interface and the solid substrate. γ_{lv}, γ_{ls} and γ_{sv} are, respectively, the surface energies of the liquid-vapor, liquid-solid, and solid-vapor interfaces. Since γ_{lv}, γ_{ls} and γ_{sv} are material properties, the static contact angle is constant for a given set of materials at a given temperature and pressure. Across the curved liquid-vapor interface, there is a capillary pressure jump Δp_c that can be described by the Young-Laplace equation

$$\Delta p_c = -\gamma\left(\frac{1}{R_1} + \frac{1}{R_2}\right), \tag{1.2}$$

where R_1 and R_2 are the principal radii of the liquid-vapor interface's curvature. The capillary pressure for a microfluidic channel with a rectangular cross-section can be approximated with the following equation [13]

$$p_c = \gamma\left(\frac{\cos\theta_u + \cos\theta_b}{H} + \frac{\cos\theta_l + \cos\theta_r}{W}\right), \tag{1.3}$$

where H is the height and W is the width of the microchannel's cross-section, and $\theta_u, \theta_b, \theta_l, \theta_r$ are the contact angles formed with the upper, bottom, left, and right channel walls, respectively. For a microchannel with a circular cross-section, the capillary pressure is described with the following equation

$$p_c = \frac{2\gamma\cos\theta}{r}, \tag{1.4}$$

where r is the radius of the microchannel and θ is the contact angle. Equations 1.3 and 1.4 show that the magnitude of capillary pressure is inversely proportional to the characteristic dimension of the microchannel, which makes it more favorable for the microfluidic format.

A substrate with a static water contact angle smaller than 90° is considered hydrophilic, while materials with static water contact angles larger than 90° are hydrophobic. When a hydrophilic glass capillary tube is placed vertically into a water reservoir, a concave meniscus will be formed and the hydraulic pressure near the liquid-vapor interface will be smaller than the atmospheric pressure. Since the hydraulic pressure at the tube's bottom is equal to or greater than the atmospheric pressure, water will imbibe into the glass capillary until the capillary force is balanced by the weight of the liquid column inside the glass capillary. This phenomenon is called capillary suction and explains the working principle of capillary pumps.

To better understand the theories for capillary valves, it is essential to discuss contact line motion and contact angle hysteresis. The contact line is the intersection line of liquid-vapor, liquid-solid, and solid-vapor interfaces. Consider a case that water is slowly added into a water droplet that sits on a smooth substrate. Initially, the contact line stays still, and the contact angle increases until a critical value is reached. Then, the contact line advances. This critical contact angle θ_A is called the advancing contact angle. Similarly, when water is slowly removed from a stationary water drop, which can be done with either evaporation or aspirating liquids with a pipette, the contact line remains static until the receding contact angle θ_R is formed, at which time the contact angle recedes. Transforming the contact angle from the equilibrium contact angle to either the advancing or receding contact angle requires energy. The contact angle hysteresis - the difference between the advancing and receding contact angles - describes the need for activation energy to trigger the contact line motion [14].

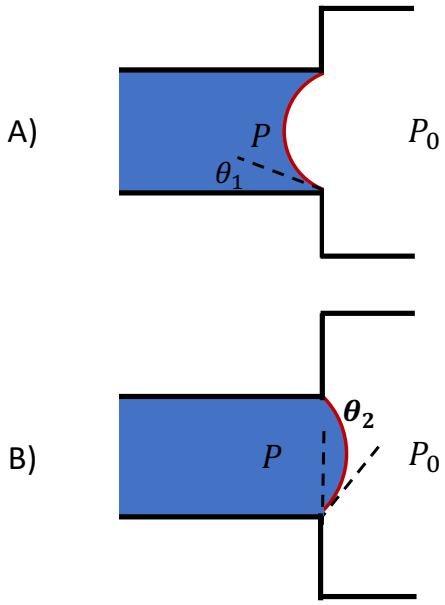

Fig. 1.1: Working principle of a capillary valve: The capillary valve is defined as the abrupt dimension enlargement in a microchannel. A) The critical state of the meniscus when the advancing contact line is halted by the capillary valve. B) The critical state of the meniscus when the liquid is about to bridge the capillary valve. θ_1 and θ_2 are critical advancing contact angles with respect to the horizontal and vertical wall, respectively.

Based on the notions of contact line motion and contact angle hysteresis, the advancing angle is required for a liquid to propagate along a microchannel. A capillary valve is formed in the presence of an abrupt enlargement of the conduit's cross-section. Consider a hydrophilic microchannel with the shape illustrated in Fig. 1.1 with a water inlet on the left. Water will flow into the channel spontaneously driven by the negative Laplace pressure beneath the concave liquid-air interface until the meniscus reaches the location of the abrupt change in the cross-section dimensions (capillary valve, Fig. 1.1A), at which point the contact line is pinned. To move beyond the enlargement in the cross-section, the meniscus must assume a convex shape with a positive Laplace pressure (Fig. 1.1B). The pressure needed to reverse the meniscus from concave to

convex in a capillary with radius r, when the entire structure is made of the same material, can be expressed as

$$\Delta p = \frac{2\gamma}{r}(\cos\theta_1 + \sin\theta_2), \tag{1.5}$$

θ_1 and θ_2 are critical advancing contact angles with respect to the horizontal and vertical wall, respectively. Equation 1.5 illustrates that the maximum pressure a capillary valve can sustain is inversely proportional to the channel's radius r.

1.4 3D-printed Microfluidics

Over the past two decades, the fabrication method of microfluidics has been dominated by soft lithography, micromachining, and injection molding, which are now challenged by rapidly developing 3D printing technologies [15, 16]. 3D printing refers to various additive-based, rapid prototyping techniques. Stereolithography (SLA) is the most widely used 3D printing technique to manufacture microfluidic chips with enclosed channels [17] and was adopted to fabricate all the devices discussed in this thesis.

Compared to conventional manufacturing methods, the 3D printing technique has the following advantages. First, 3D printers are inexpensive and highly automated. There are many inexpensive resin 3D printers (Phrozen Sonic Mini, Phrozen Technology, Taiwan, China; Anycubic Photon Mono X, Anycubic Photon, Shenzhen, China; Formlabs Form 3, Formlabs, Somerville, MA) commercially available that provide fair enough printing resolutions (e.g., Formlabs Form 3 offers 25-micron resolution in both the XY plane and the Z direction) to fabricate microfluidic chips. The printers accept files in standardized formats and provide a one-button start. Second, 3D printing manufactures complex 3D structures with short turnaround times. Depending on the dimension of a microfluidic chip, a typical turnaround time for 3D printing is usually hours while it may take up to days for soft lithography and milling and weeks for injection modeling [18]. Third, the biocompatibility of 3D printed devices is well established and is comparable to benchtop equipment [6].

1.5 Microfluidics Chips for Molecular Detection

Over the past two decades, the development of microfluidic devices has proved successful for molecular detection. The previously reported microfluidic devices can be categorized, based on their approaches to fluid manipulation, into conventional microfluidics [5, 6, 11, 19-25], paper-based microfluidics [26-28], Lab-on-a-disc (LoD) microfluidics [29-31], and droplet-based microfluidics [32, 33]. The Lab-on-a-disc (centrifugal) microfluidic system requires a rotational system that controls the liquid flow with centrifugal, Euler, and Coriolis forces combined with on-chip valving techniques [29]. The droplet-based microfluidics needs flow-focusing geometry and fluid velocity control to produce uniform droplets [34]. Different from the two above-mentioned types that require velocity control, the control requirement of the conventional microfluidic is on the volume level, which is easier to be achieved. A conventional microfluidic device usually requires a fixed volume of reagents to be loaded into the corresponding chamber on chip, which can be satisfied with pipetting [11, 21]. Different from the other types of devices that usually require pumping systems, the paper-based microfluidic devices are pump-free, reducing the complexity of the systems' design and operation [35]. The operational complexity and device cost have an order of paper-based < conventional < Lab-on-a-disk and droplet-based [35], while the complexity of fluid flow that can be achieved has a reversed order. Considering the complexity of fluid distribution required by implementing Penn RAMP in a microfluidic format, our group focuses on developing conventional microfluidic devices to pursue cost-effectiveness and user-friendliness. In this section, we review three representative works in the field of interest and explain how our studies further improve the robustness, cost-effectiveness, and usability of conventional microfluidic devices for molecular detection.

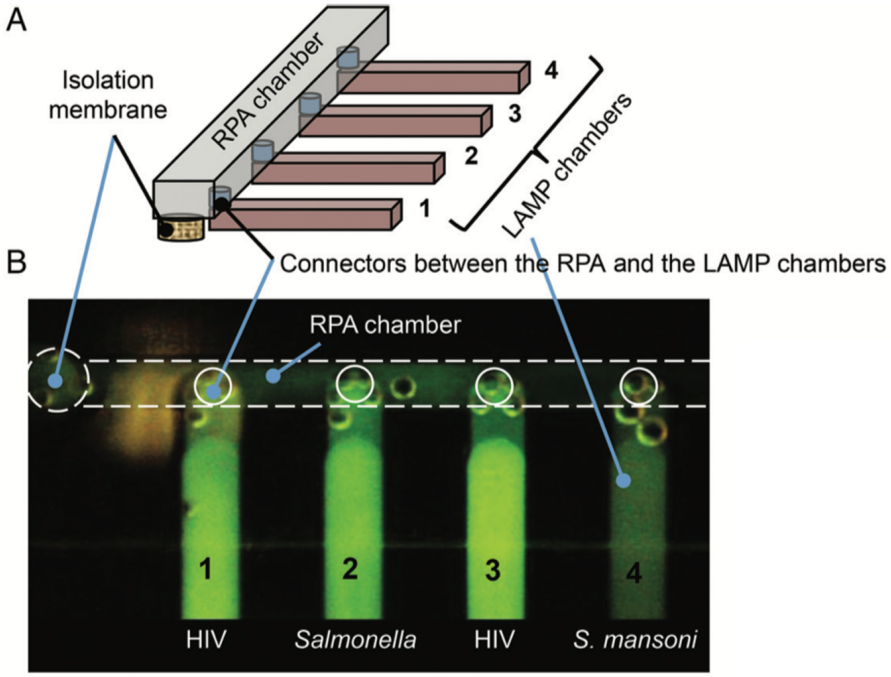

Fig. 1.2: Illustration of the chip design and fluorescence image during NA amplification [11].

Song [11] developed a microfluidic chip for Penn RAMP. The chip comprises one RPA and four LAMP chambers for multiplexed detection. The four identical LAMP chambers connect to the RPA chamber on one end and to four independent inlets on the other end. The chip is made of three CNC machined polymethyl methacrylate (PMMA) layers and assembled with acetonitrile bonding. Prior to the two-stage amplification, LAMP solutions are first pipetted into each LAMP chamber one by one. Next, the surfaces around the four LAMP inlets are thoroughly dried. The LAMP inlets are then sealed with a PCR tape to prevent the solution from leaving LAMP reactors when filling the RPA chamber. Last, the same loading, drying, and sealing operations are repeated for the common RPA chamber. Overall, this chip (Fig. 1.2) successfully demonstrates Penn-RAMP in a microfluidic format. However, this chip lacks the internal control of fluid flow, and the chip operation requires multiple manual operations, risking severe consequences due to potential operational errors. For example, when the LAMP solution is accidentally overloaded, the excess LAMP solution will immediately flow into the RPA chamber and eventually penetrate into other LAMP reactors. Since the LAMP solution in each LAMP

chamber contains a unique primer set corresponding to a specific target, the overload can introduce cross-contamination of primers and eventually present false positives. In another case when LAMP solutions are accidentally removed when drying the surface around the LAMP inlets, the recession of LAMP solutions will introduce air bubbles between RPA and LAMP chambers and cut off the connection between RPA and LAMP chambers. Besides the risks of malfunction, there is also an opportunity to simplify the chip operation where the same LAMP loading is repeated four times via four separate inlets.

Kadimisetty [6] reported a fully 3D-printed microfluidic chip with four independent reactors that can perform multiple LAMP amplifications in parallel. The chip is fabricated with an inexpensive 3D printer (Formlab Form 2, Formlabs, Somerville, MA) in two parts (Fig. 1.3), enabling the insertion of nucleic acid isolation membranes (Qiagen Silica) into the chip. The inner surface of the chip is treated with PEG for improved biocompatibility. The chip can perform both NA isolation and amplification. During NA isolation, sample solutions and washing buffers are sequentially pipetted into the chip through the inlets, pass through the nucleic acid isolation membrane, and leave the chip via the outlets. The same sequence of operations is repeated for each LAMP reactor. For NA amplification, LAMP solutions are pipetted into the chip, and all ports (inlets and outlets) are then dried and sealed with a PCR tape [6]. Overall, Kadimisetty's work is a successful demonstration of 3D-printed microfluidics for a single-stage isothermal NAAT and has proved the biocompatibility of the 3D printed material. However, similar to Song's work [11], the chip operation of Kadimisetty's design lacks built-in controls, requiring manual operations to provide fluid control, and the whole operation procedure needs to be repeated for each reactor to achieve multiplexing.

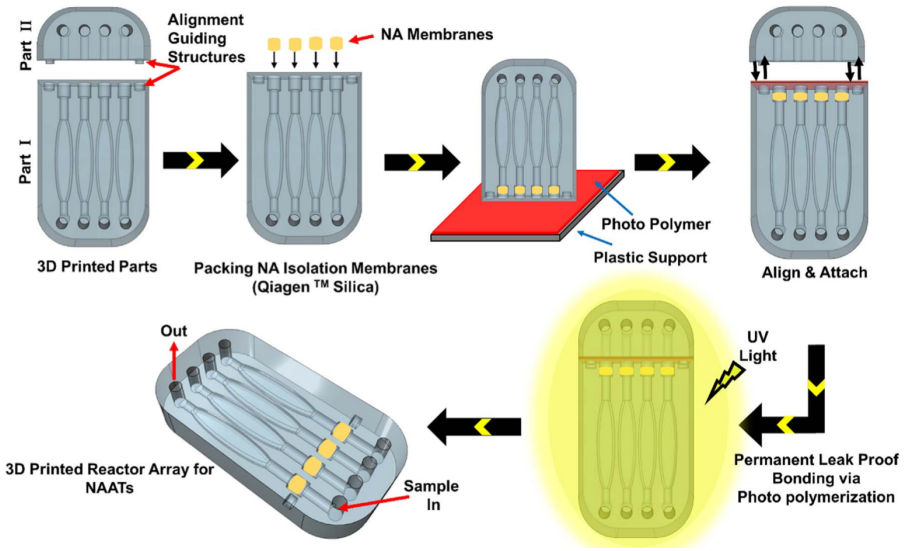

Fig. 1.3: Assembly of the chip with 3D printing [6].

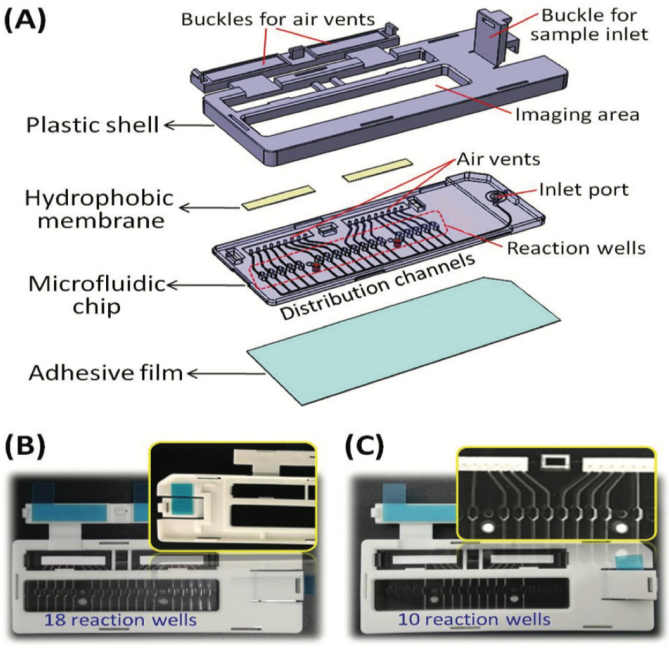

Fig. 1.4: Detailed chip design. (A) Exploded view. (B) Pressure sealing component. (C) Multiplexed reactors [9].

In a recently published paper, Zhong [9] developed a microfluidic system with up to eighteen LAMP reactors for single-stage NAATs. The chip is manufactured with polycarbonate

(PC) substrate by injection molding. Hydrophobic membranes combined with pipetting are used to provide on-chip fluid control. After loading the chip with a pipette, buckles are pushed down to provide sealing (Fig. 1.4). The key innovation of Zhong's work is to simplify operational complexity, allowing the filling of multiple reaction chambers with a single loading step and developing a user-friendly sealing method. However, to achieve one-stage loading, all reactors are connected to the inlet and therefore are interconnected with each other. The cross-communication among reactors is unavoidable but can be delayed by increasing the distances between adjacent reactors. Additionally, like the devices discussed above [6, 11], pipettes are still needed to load the sample.

We developed user-friendly, low-cost microfluidic devices with capillary circuits for multiplexed NAATs. First, the fluid flow on chip is spontaneously driven by capillary forces and regulated by capillary valves, eliminating the need for external instruments such as syringe pumps. This both automates the liquid distribution on chip, enabling untrained personnel to perform POC NAATs, and reduces the device's cost, making it affordable for eventual home use. Second, we developed means to pre-dry primers in individual reaction chambers during chip manufacturing, enabling us to fill the chip with a universal reaction mix and avoiding the need to fill individual reaction chambers separately. Third, we developed a method to drain the common distribution channel, eliminating the risk of cross-contamination. Fourth, we automated the sealing step with the use of phase-change materials (PCMs) that melt when the chip temperature is increased to its incubation value, cover the inlet and exit ports to provide evaporation barriers during incubation, and solidify after the conclusion of amplification to tomb the reaction products, preventing them from contaminating the workspace. Fifth, we developed an Android-based smartphone application for real-time signal monitoring and image analysis. Sixth, our devices are fully 3D-printed can be easily reproduced with an inexpensive 3D printer that is commonly available.

1.6 Organization of the Dissertation

Chapter two describes a 3D-printed microfluidic device with capillary circuits for multiplexed reverse-transcription loop-mediated isothermal amplification (RT-LAMP). The chip comprises four LAMP reactors, each with a unique primer set for a specific target. The liquid distribution on chip is controlled by capillary forces without reliance on external instruments. An innovative draining process is used to remove excess liquids in connecting channels while LAMP reaction mixes in the various reactors remain intact. The draining process isolates individual LAMP reactors and prevents cross-contamination. Additionally, we adopted a thermally actuated sealing with phase-change materials (PCMs). The chip has proved successful for multiplexed detection of pig viruses [36].

Chapter three adapts the design of the chip described in chapter two to accommodate the storage of in-situ dried reagents and colorimetric detection. Pre-storage of dried LAMP reagents on chip allows room temperature storage, while a standard liquid form of LAMP mix requires storage at -20 °C. The colorimetric detection method enables reading diagnostic results by the naked eye, which further reduces cost by eliminating the need for a fluorescence camera. An Android-based smartphone application was developed for real-time signal monitoring and automated image analysis. These are important steps toward a fully instrument-free multiplexed LAMP in a microfluidic format for untrained personnel. The chip has proved successful for multiplexed detection of human immunodeficiency virus and human hepatitis viruses.

Chapter four discusses a microfluidic device with more complicated capillary circuits for the two-stage isothermal NAAT Penn RAMP that combines RPA and LAMP to achieve a higher level of multiplexing and sensitivity. The chip consists of one RPA chamber connected with four LAMP reactors. The biggest challenge we faced was distributing first-stage amplicons into multiple second-stage reactors evenly. A numerical simulation of Penn RAMP was developed to guide chip design, estimating the efficiency of first-stage amplicon distribution and potential cross-contamination. The chip has proved successful in implementing Penn RAMP on chip, and the on-chip Penn RAMP has proved more sensitive for the detection of chicken infectious laryngotracheitis virus compared to the standalone LAMP assay.

Chapter five concludes the thesis.

References

[1] J. Kim, D. Byun, M. G. Mauk, and H. H. Bau, "A disposable, self-contained PCR chip," *Lab Chip,* vol. 9, no. 4, pp. 606-612, 2009, doi: 10.1039/b807915c.

[2] D. Chen *et al.*, "An integrated, self-contained microfluidic cassette for isolation, amplification, and detection of nucleic acids," *Biomedical Microdevices,* vol. 12, no. 4, pp. 705-719, 2010/08/01 2010, doi: 10.1007/s10544-010-9423-4.

[3] M. Keller, J. Naue, R. Zengerle, F. von Stetten, and U. Schmidt, "Automated Forensic Animal Family Identification by Nested PCR and Melt Curve Analysis on an Off-the-Shelf Thermocycler Augmented with a Centrifugal Microfluidic Disk Segment," *PLoS One,* vol. 10, no. 7, p. e0131845, 2015, doi: 10.1371/journal.pone.0131845.

[4] M. G. Mauk, C. Liu, M. Sadik, and H. H. Bau, "Microfluidic Devices for Nucleic Acid (NA) Isolation, Isothermal NA Amplification, and Real-Time Detection," in *Mobile Health Technologies: Methods and Protocols*, A. Rasooly and K. E. Herold Eds. New York, NY: Springer New York, 2015, pp. 15-40.

[5] S. C. Liao *et al.*, "Smart cup: A minimally-instrumented, smartphone-based point-of-care molecular diagnostic device," *Sensor Actuat B-Chem,* vol. 229, pp. 232-238, Jun 28 2016, doi: 10.1016/j.snb.2016.01.073.

[6] K. Kadimisetty *et al.*, "Fully 3D printed integrated reactor array for point-of-care molecular diagnostics," *Biosensors and Bioelectronics,* vol. 109, pp. 156-163, 2018/06/30/ 2018, doi: https://doi.org/10.1016/j.bios.2018.03.009.

[7] J. Song, C. Liu, M. G. Mauk, J. Peng, T. Schoenfeld, and H. H. Bau, "A Multifunctional Reactor with Dry-Stored Reagents for Enzymatic Amplification of Nucleic Acids," *Analytical Chemistry,* vol. 90, no. 2, pp. 1209-1216, 2018/01/16 2018, doi: 10.1021/acs.analchem.7b03834.

[8] A. Ganguli *et al.*, "Rapid isothermal amplification and portable detection system for SARS-CoV-2," *Proceedings of the National Academy of Sciences,* vol. 117, no. 37, pp. 22727-22735, 2020, doi: 10.1073/pnas.2014739117.

[9] R. Zhong, S. Liu, G. Zhang, M. Wang, and Y. Sun, "iso-μmGene: an isothermal amplification-based portable microfluidic system for simple, reliable and flexibly multiplexed genetic identification and quantification," *Analyst,* 10.1039/D0AN00560F vol. 145, no. 13, pp. 4627-4636, 2020, doi: 10.1039/D0AN00560F.

[10] R. J. Li, M. G. Mauk, Y. Seok, and H. H. Bau, "Electricity-free chemical heater for isothermal nucleic acid amplification with applications in COVID-19 home testing," *Analyst,* 10.1039/D1AN00309G vol. 146, no. 13, pp. 4212-4218, 2021, doi: 10.1039/D1AN00309G.

[11] J. Song *et al.*, "Two-Stage Isothermal Enzymatic Amplification for Concurrent Multiplex Molecular Detection," *Clinical Chemistry,* Article vol. 63, p. 714, 2017.

[12] M. El-Tholoth, E. Anis, and H. H. Bau, "Two stage, nested isothermal amplification in a single tube," *The Analyst,* vol. 146, no. 4, pp. 1311-1319, 2021, doi: 10.1039/d0an01835j.

[13] E. Delamarche, A. Bernard, H. Schmid, A. Bietsch, B. Michel, and H. Biebuyck, "Microfluidic networks for chemical patterning of substrates: design and application to bioassays," *Journal of the American Chemical Society,* vol. 120, no. 3, pp. 500-508, 1998.

[14] L. Gao and T. J. McCarthy, "Contact angle hysteresis explained," *Langmuir,* vol. 22, no. 14, pp. 6234-6237, 2006.

[15] H. Becker and C. Gärtner, "Polymer microfabrication methods for microfluidic analytical applications," *ELECTROPHORESIS: An International Journal,* vol. 21, no. 1, pp. 12-26, 2000.

[16] A. Waldbaur, H. Rapp, K. Länge, and B. E. Rapp, "Let there be chip—towards rapid prototyping of microfluidic devices: one-step manufacturing processes," *Analytical Methods,* 10.1039/C1AY05253E vol. 3, no. 12, pp. 2681-2716, 2011, doi: 10.1039/C1AY05253E.

[17] A. K. Au, W. Huynh, L. F. Horowitz, and A. Folch, "3D-printed microfluidics," *Angewandte Chemie International Edition,* vol. 55, no. 12, pp. 3862-3881, 2016.

[18] N. Bhattacharjee, A. Urrios, S. Kang, and A. Folch, "The upcoming 3D-printing revolution in microfluidics," *Lab Chip,* vol. 16, no. 10, pp. 1720-1742, 2016.

[19] J. Song *et al.*, "Smartphone-Based Mobile Detection Platform for Molecular Diagnostics and Spatiotemporal Disease Mapping," (in eng), *Anal Chem,* vol. 90, no. 7, pp. 4823-4831, Apr 3 2018, doi: 10.1021/acs.analchem.8b00283.

[20] A. G. Boyle *et al.*, "Detection of Streptococcus equi subsp. equi in guttural pouch lavage samples using a loop-mediated isothermal nucleic acid amplification microfluidic device," *Journal of Veterinary Internal Medicine,* vol. 35, no. 3, pp. 1597-1603, 2021, doi: 10.1111/jvim.16105.

[21] J. Kim *et al.*, "A PCR reactor with an integrated alumina membrane for nucleic acid isolation," *Analyst,* vol. 135, no. 9, pp. 2408-2414, 2010.

[22] M. Dou, D. C. Dominguez, X. Li, J. Sanchez, and G. Scott, "A Versatile PDMS/Paper Hybrid Microfluidic Platform for Sensitive Infectious Disease Diagnosis," *Analytical Chemistry,* vol. 86, no. 15, pp. 7978-7986, 2014, doi: 10.1021/ac5021694.

[23] X. Fang, H. Chen, S. Yu, X. Jiang, and J. Kong, "Predicting Viruses Accurately by a Multiplex Microfluidic Loop-Mediated Isothermal Amplification Chip," *Analytical Chemistry,* vol. 83, no. 3, pp. 690-695, 2011, doi: 10.1021/ac102858j.

[24] X. Jiang *et al.*, "High-Throughput Microfluidic Device for LAMP Analysis of Airborne Bacteria," *ACS Sensors,* vol. 1, no. 7, pp. 958-962, 2016, doi: 10.1021/acssensors.6b00282.

[25] Y. Liu, Y. Zhao, Y. Qin, X. Du, Q. Wang, and J. Lyu, "A novel microfluidic device that integrates nucleic acid extraction, amplification, and detection to identify an EGFR mutation in lung cancer tissues," *RSC Advances,* vol. 6, no. 16, pp. 13399-13406, 2016, doi: 10.1039/c5ra26225a.

[26] K. Kaarj, P. Akarapipad, and J.-Y. Yoon, "Simpler, Faster, and Sensitive Zika Virus Assay Using Smartphone Detection of Loop-mediated Isothermal Amplification on Paper Microfluidic Chips," *Scientific Reports,* vol. 8, no. 1, 2018, doi: 10.1038/s41598-018-30797-9.

[27] Y. Seok *et al.*, "A Paper-Based Device for Performing Loop-Mediated Isothermal Amplification with Real-Time Simultaneous Detection of Multiple DNA Targets," (in eng), *Theranostics,* vol. 7, no. 8, pp. 2220-2230, 2017, doi: 10.7150/thno.18675.

[28] Y. Seok, B. S. Batule, and M.-G. Kim, "Lab-on-paper for all-in-one molecular diagnostics (LAMDA) of zika, dengue, and chikungunya virus from human serum," *Biosensors and Bioelectronics,* vol. 165, p. 112400, 2020.

[29] L. X. Kong, A. Perebikovsky, J. Moebius, L. Kulinsky, and M. Madou, "Lab-on-a-CD," *Journal of Laboratory Automation,* vol. 21, no. 3, pp. 323-355, 2016, doi: 10.1177/2211068215588456.

[30] A. A. Sayad *et al.*, "A microfluidic lab-on-a-disc integrated loop mediated isothermal amplification for foodborne pathogen detection," *Sensors and Actuators B: Chemical,* vol. 227, pp. 600-609, 2016, doi: 10.1016/j.snb.2015.10.116.

[31] L. Zhou *et al.*, "Microfluidic-RT-LAMP chip for the point-of-care detection of emerging and re-emerging enteric coronaviruses in swine," *Analytica Chimica Acta,* vol. 1125, pp. 57-65, 2020, doi: 10.1016/j.aca.2020.05.034.

[32] T. D. Rane, L. Chen, H. C. Zec, and T.-H. Wang, "Microfluidic continuous flow digital loop-mediated isothermal amplification (LAMP)," *Lab Chip,* vol. 15, no. 3, pp. 776-782, 2015, doi: 10.1039/c4lc01158a.

[33] F. Schuler *et al.*, "Digital droplet LAMP as a microfluidic app on standard laboratory devices," *Analytical Methods,* vol. 8, no. 13, pp. 2750-2755, 2016, doi: 10.1039/c6ay00600k.

[34] R. Seemann, M. Brinkmann, T. Pfohl, and S. Herminghaus, "Droplet based microfluidics," *Reports on Progress in Physics,* vol. 75, no. 1, p. 016601, 2011/12/22 2011, doi: 10.1088/0034-4885/75/1/016601.

[35] H. Zhang, Y. Xu, Z. Fohlerova, H. Chang, C. Iliescu, and P. Neuzil, "LAMP-on-a-chip: Revising microfluidic platforms for loop-mediated DNA amplification," *TrAC Trends in Analytical Chemistry,* vol. 113, pp. 44-53, 2019/04/01/ 2019, doi: https://doi.org/10.1016/j.trac.2019.01.015.

[36] M. El-Tholoth, H. Bai, M. G. Mauk, L. J. Saif, and H. H. Bau, "A Portable, 3-D Printed, Microfluidic Device for Multiplexed, Real Time, Molecular Detection of Porcine Epidemic Diarrhea Virus, Transmissible Gastroenteritis Virus, and Porcine Deltacoronavirus at the Point of Need," *Lab Chip,* 10.1039/D0LC01229G 2021, doi: 10.1039/D0LC01229G.

Chapter 2 Auto-distribution and Auto-sealing based on Capillary Circuits for Single-stage NAATs

2.1 Introduction

In this chapter, we introduce a low-cost, rapid, semi-quantitative, field-deployable, 3D-printed microfluidic device for auto-distribution of samples and self-sealing for real-time reverse transcription-loop-mediated isothermal amplification (RT-LAMP), enabling the co-detection of the porcine epidemic diarrhea virus (PEDV), transmissible gastroenteritis virus (TGEV), and porcine deltacoronavirus (PDCoV) at the point of need within 30 minutes.

The Coronaviridae family of the Nidovirales order comprises four genera: Alphacoronavirus, Betacoronavirus, Gammacoronavirus, and Deltacoronavirus. The porcine epidemic diarrhea virus (PEDV) and transmissible gastroenteritis virus (TGEV) are members of the Alphacoronavirus genus, while the porcine deltacoronavirus (PDCoV) is a Deltacoronavirus [1]. Coronaviruses are positive-sense, single-stranded, enveloped RNA viruses and have an RNA genome of 25-30 kb (kilobases), the largest ever reported. The virion RNA contains 5' and 3' untranslated regions (UTRs), capped at the 5' end and polyadenylated at the 3' end. The 5'-terminal two-thirds of the genome contain open reading frames (ORFs) 1a and 1ab that encode two replicase polyproteins (pp1a and pp1ab). The 3'-terminal one-third of the genome encodes structural proteins, including spike (S), envelope (E), membrane (M), and nucleocapsid (N) proteins [2, 3].

PEDV, TGEV, and PDCoV are emerging/reemerging coronaviruses (CoVs) of neonatal pigs and cause great economic losses to the pig industry [4]. All three viruses affect the animals' enteric system, are antigenically distinct, lack cross-immunity protection, and cause acute gastroenteritis in neonatal piglets with similar clinical manifestations. Infected intestinal epithelial cells necrosis causes atrophy of the intestinal villi, diarrhea, growth retardation, dehydration, and death of piglets [1, 5]. Currently, among these three viral infections, the PEDV infection is the most significant and consequential in the USA. This is likely because PEDV has been only recently introduced to the USA, and pigs in the USA lack immunity against it [4].

Effective prevention and control of these diseases can be achieved by stringent biosecurity measures, disease containment within and among farms, and vaccination. Vaccines are available against TGEV and PEDV [1, 2, 6]. Rapid co-detection of these viruses would be followed by rapid initiation of appropriate control measures, reducing the expected economic losses.

Currently, confirmative diagnosis of these diseases is performed in centralized laboratories by the enzyme-linked immunosorbent assay (ELISA), virus isolation, virus neutralization (VN) and immunofluorescence techniques, quantitative real-time-reverse transcription-PCR (qRT-PCR), and conventional RT-PCR. However, all the above-mentioned detection methods challenge implementing specific, rapid, and simple diagnoses in laboratories with insufficient resources. These challenges stem from excessive labor and time in testing, lack of skilled personnel, adequate specificity and sensitivity, and costly equipment requirements [7-16].

Recently, RT-loop-mediated isothermal amplification (RT-LAMP) has been demonstrated to have sensitivity equal to RT-PCR for the detection of swine enteric coronaviruses [17-20]. LAMP utilizes four to six primers and strand-displacing DNA polymerase. LAMP is carried out at a constant temperature, without a need for temperature cycling [21]. Furthermore, LAMP is compatible with multiple amplicon detection methods, including visual inspection with the naked eye based on color changes or increased turbidity, gel electrophoresis, fluorescence, and bioluminescence detection [22-26], and lateral flow strip immunochromatography, detecting labeled amplicons using conjugated primer sets. Fluorescence and bioluminescence-based detection methods enable real-time amplicon monitoring and quasi-quantification [27].

To implement diagnostic assays at the point of need, it is desirable to minimize manual operations. This is best accomplished with microfluidic technology that enables the integration of various unit operations. Here, we describe a 3D printed microfluidic device for real-time reverse-transcription-LAMP that enables rapid, on-site molecular multiplexed detection and quasi-quantification of PEDV, TGEV, and PDCoV (Fig. 2.1).

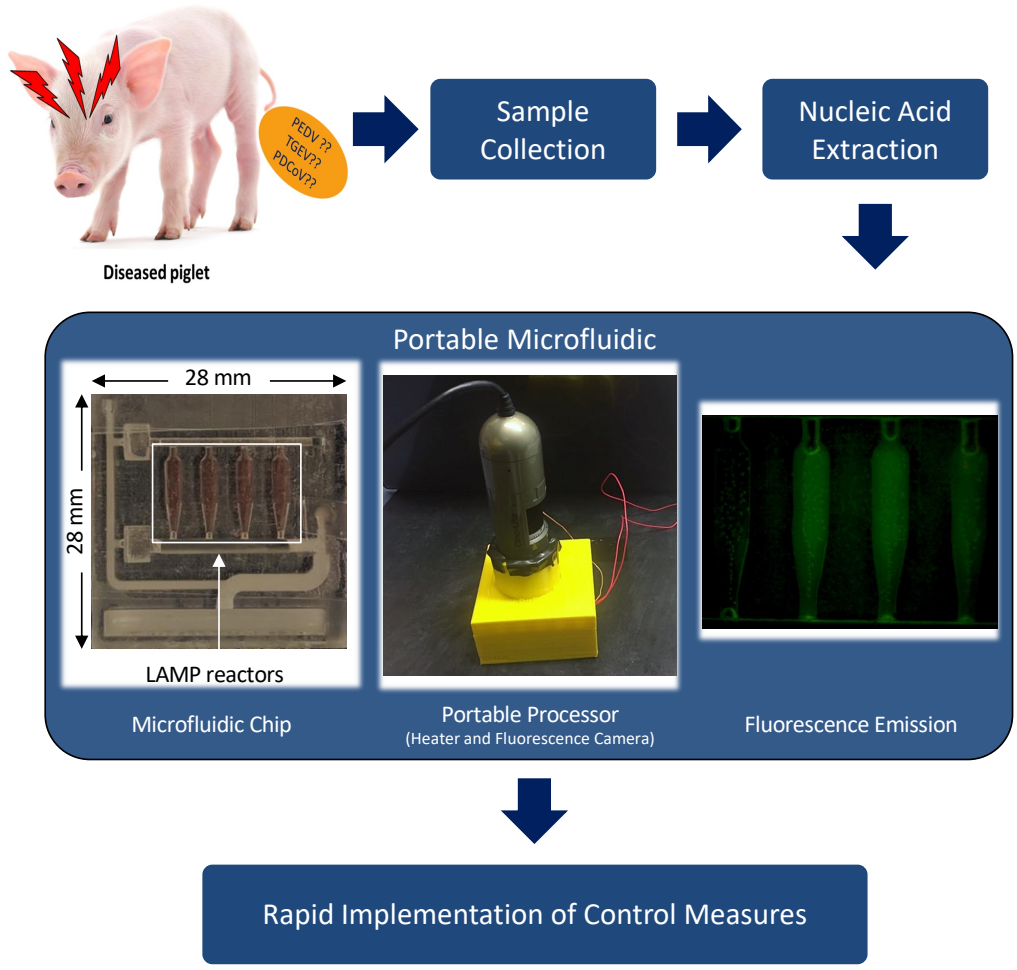

Fig. 2.1: Workflow for the molecular diagnosis of PEDV, TGEV, and PDCoV in pigs. A sample is collected with a rectal swab from a piglet and lysed to release and solubilize pathogenic viral nucleic acids. The extracted nucleic acids are enzymatically amplified with RT-LAMP using the microfluidic chip. The chip is incubated with a portable processor at a constant temperature. The amplification products are monitored in real-time with an intercalating fluorescent dye and a low-cost CCD camera. Alternatively, end-point detection of amplicons using colorimetric dyes is also feasible.

2.2 Materials and Methods

2.2.1 3D-printed chip design and fabrication

Our 28 mm (*L*) x 28 mm (*W*) x 4 mm (*H*) microfluidic cartridge 'chip' (Fig. 2.2) features four reaction chambers of 20 ± 1 µL volume each, connecting conduits, and passive capillary valves to assist in flow control and sample distribution among the reaction chambers. The chip was designed with SolidWorks 2018 software (DS SolidWorks™) that produces CAD files in STL format compatible with most 3D printers. The chip was then fabricated with a Low Force Stereolithography (LFS) resin-based 3D printer (Formlabs™, Form 3). The chip material is a clear photopolymer resin (Formlabs™, FLGPCL04) with a specific mass of 1.1 g cm^{-3} and thermal conductivity of 0.110 W m^{-1} K^{-1}. Portions of the 3D-printed chip are left uncapped to enable the introduction of reagents. After printing, printing supports were removed, and the chips were thoroughly washed with Form Wash (Formlabs™) for 15 min, followed by a 15 min post-cure at 60 °C with Form Cure (Formlabs™). To reduce the absorption of the enzymes and sample to the reaction chambers' surfaces that would adversely affect the efficiency of nucleic acid amplification, we coated reactors' inner surfaces with a 2% aqueous solution of Polyethylene glycol (PEG) 3350 [28].

Next, primers specific to individual targets were dried in three of the (test) reaction chambers, one primer set in each chamber. The fourth chamber was left primer-free to serve as a negative (non-primer) control. To this end, we pipetted an aqueous solution of the designated primer set specific to each target through the uncapped common conduit into each test reactor (Fig. 2.3) and then dried the chip at room temperature for 2 h. Next, we placed the chip on a cooled plate for molten PEG 930 loading. PEG 930 has a melting temperature of 36 ± 1 °C and solidified in the PEG chamber (opening II, Fig. 2.2 and Fig. 2.3) soon after filling. Finally, the chip was capped with a PCR tape (Bio-Rad™, MSB1001), leaving only two open ports, one for sample introduction and the other to allow air to escape during sample loading (Fig. 2.3). All the operations described above are to be carried out during the chip manufacturing process.

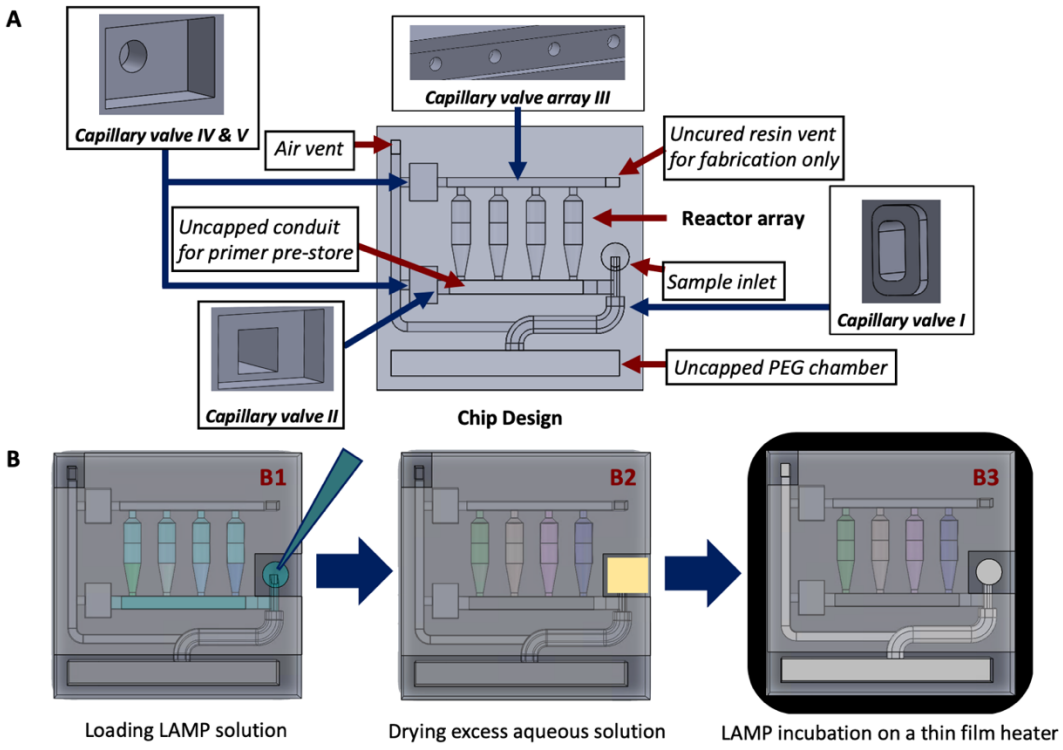

Fig. 2.2: A schematic depiction of the design principles and fluid control with capillary circuits and passive capillary valves. (A) 3D printed chip design. (B1) Driven by capillary force, the LAMP solution (including templates) flows into reactors automatically. In the future, the LAMP mix will be pre-stored in the reaction chambers in dry form, and only the sample will be introduced into the chip. (B2) By placing an absorption pad at the sample inlet, capillary force helps dry any excess aqueous solution in the common conduit and therefore cut off the connections between different reactors. (B3) The chip is then paired with the processor and heated to its operating temperature (63 °C). During the heating process, PEG 930 (with a melting temperature of around 37 °C) melts and flows into the common conduits driven by capillary force to seal the chip.

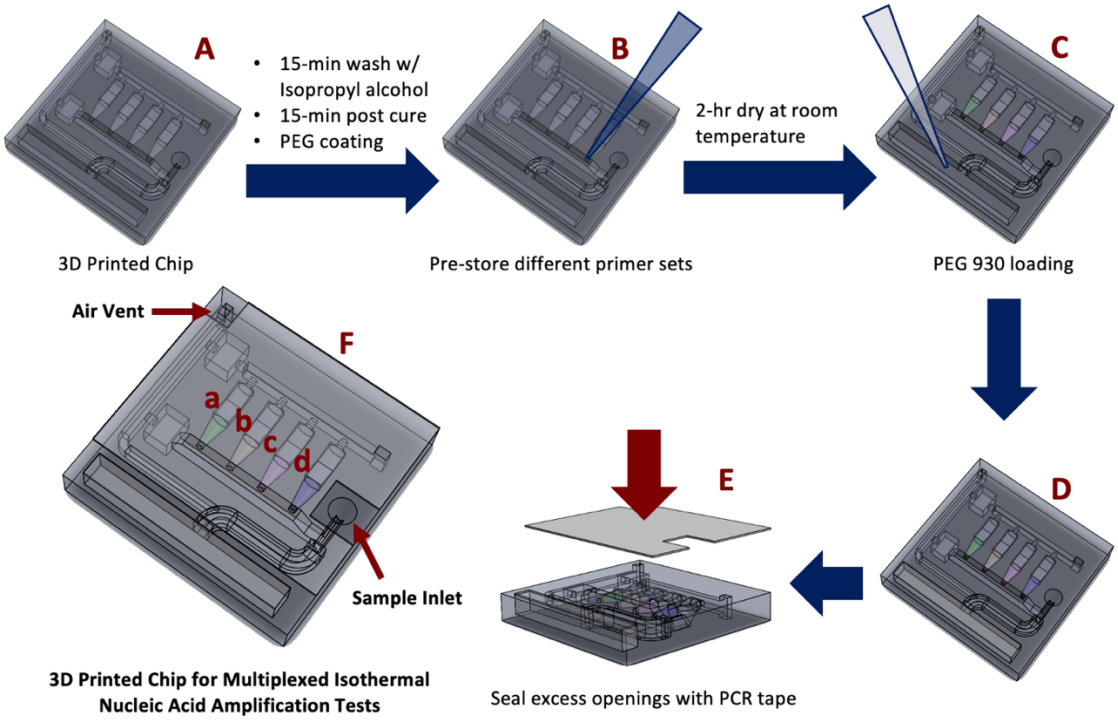

Fig. 2.3: Chip preparation: (A) after 3D printing, the chip is washed, post-cured, and coated with PEG 3350. (B) Aqueous solutions of primer sets for PEDV, TGEV, and PDCoV are, respectively, pipetted into chambers a, b, and c. Chamber d is left primer-free. (C) The melt of PEG 930 is inserted into the PEG chamber and (D) allowed to solidify. (E) The chip is capped with a PCR tape to seal the open conduits, leaving only the sample inlet, the air vent, and the PEG chambers open. (F) The chip is then ready for sample introduction and LAMP incubation.

2.2.2 Auto-distribution and self-sealing

The microfluidic chip houses capillary circuits, passive capillary valves, and phase-change materials to control the flow in the chip, thereby minimizing the need for actuators and manual operations. Since the 3D-printed resin is hydrophilic with a static water contact angle of 47 degrees (Formlabs™ Inc.), any abrupt enlargement in a conduit's cross-section provides a passive capillary valve that pins a liquid column's advancing meniscus [29] and halts the flow. Our microfluidic chip has four different capillary valves of various dimensions that require different pressures to bridge, enabling us to achieve our desired flow control objectives.

Our sample solution includes the LAMP reaction mix and targets (RNA extracted from the samples) but not primers. In the future, the LAMP reaction mix will be dry-stored in the reaction chambers, and the sample solution will include only the extracted nucleic acids in a hydration buffer. The sample is introduced at the sample inlet port (Fig. 2.2A). The liquid is driven into the chip by capillary forces. As the sample imbibes into the chip, it fills the common conduit and the LAMP reaction chambers and is halted with capillary valves I, II, and III (Fig. 2.2A). Then, the inlet port is brought into contact with an absorption pad that drains liquid only from the common conduit (Fig. 2.2B). Among the capillary valves, valve III has the smallest hydrodynamic diameter of 0.8 mm and therefore the greatest pinning force, followed by valve II with an intermediate hydrodynamic diameter of 1.5 mm (smallest pinning force), and valve I with a hydrodynamic diameter of 1.3 mm. Therefore, during the draining process, valve III pins the menisci and retains the LAMP reaction chambers filled with the sample while the liquid is removed from the connecting conduit to prevent crosstalk during incubation and cleared from the vicinity of the inlet port to facilitate subsequent sealing with PEG. The chip is now ready for incubation.

Next, we place the chip on the heater in our custom-made processor and heat it to the LAMP incubation temperature of ~63 °C. The PEG melts at 36 ± 1 °C and flows by capillary force, effectively isolating the LAMP reaction chambers from the ambient to minimize evaporation during incubation. When the chip is cooled back to room temperature after incubation, the PEG solidifies, sealing the LAMP chambers and preventing the release of amplicons to the ambient air.

2.2.3 Viruses, clinical samples, and LAMP primer design

PEDV (PC22A strain) propagated in Vero cells [9], TGEV (virulent Miller-M6 strain) propagated in ST cells, and PDCoV strain OH-FD22 propagated in LLC-PK cells [11] were provided by the Department of Veterinary Preventive Medicine, The Ohio State University, Wooster, OH, United States, through a Material Transfer Agreement. RNA was extracted with an AM1836 5X MagMax 96 viral extraction kit (Life Technologies Corp.), following the manufacturer's instructions.

The number of copies of genomic RNAs of PEDV, TGEV, and PDCoV were quantified [30] and diluted to 10^5 genomic copies per µL of each virus.

Eleven rectal swabs were collected from piglets that previously tested positive for PEDV, TGEV, or PDCoV with the gold standard virus-specific RT-PCR assays [7, 11, 12], and one negative control rectal swab was collected from a non-infected gnotobiotic pig at Ohio State University. Sample collection from pigs and extracted nucleic acid transportation were carried out in compliance with the ethical guidelines of both Ohio State University and the University of Pennsylvania, USA.

2.2.4 LAMP primer design

Sequences of various PEDV, TGEV, and PDCoV strain complete genomes were obtained from the GeneBank and aligned to determine the conserved sequences with MEGA X software (http://www.megasoftware.net/). A 277-nt sequence and 233-nt sequence in PEDV and PDCoV nucleocapsid gene, respectively**,** and a 258-nt sequence in the ORF1ab gene of TGEV were targeted as templates due to their homology among the analyzed strains and their divergence from sequences of other organisms. LAMP primers (Fig. 2.4, Fig. 2.5, and Fig. 2.6) were designed using the PrimerExplorer software (V5, Eiken Chemical Co. Ltd.). The designed primers were checked for cross-hybridization with sequences of other viruses in the NCBI database BLAST (http://www.ncbi.nlm.nih.gov) that infect the digestive tract of pigs, including swine acute diarrhea syndrome-coronavirus (SADS-CoV), porcine respiratory coronavirus (PRCV), porcine hemagglutinating encephalomyelitis virus (PHEV), porcine calicivirus, porcine parvovirus, and porcine rotaviruses. There was no cross-reaction with any of these viruses. The LAMP primers were synthesized (IDT Company, Coralville, IA), provided lyophilized, then suspended in nuclease-free water (Invitrogen, Carlsbad, CA, USA) to a concentration of 100 μM.

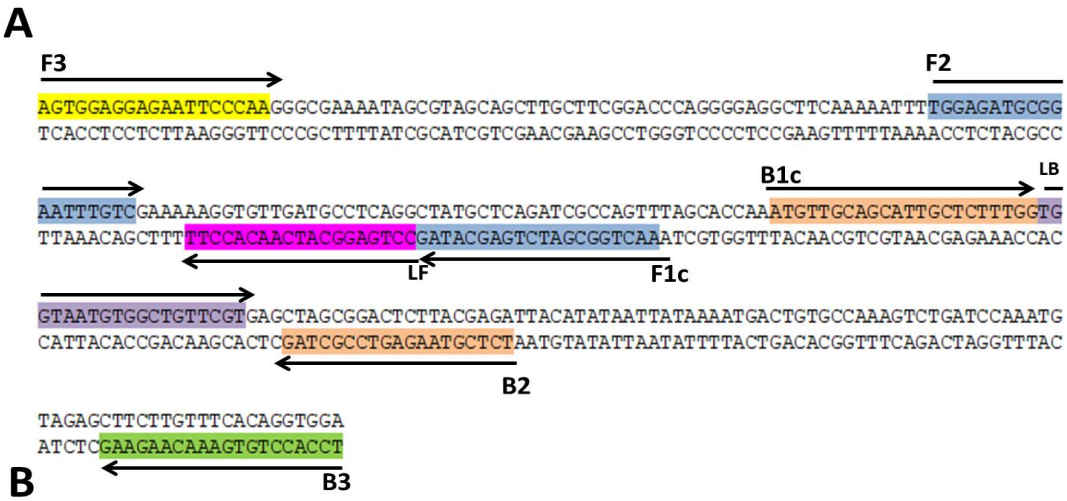

Target Gene	Primer Name	Primers sequences(5' to 3')	Concentration (µM)
Nucleocapsid protein coding gene of PEDV	F3	AGTGGAGGAGAATTCCCAA	0.2
	B3	TCCACCTGTGAAACAAGAAG	0.2
	FIP (F1c +F2)	AACTGGCGATCTGAGCATAGCTGGAGATGCGGAATTTGTC	1.6
	BIP (B1c +B2)	ATGTTGCAGCATTGCTCTTTGGTCTCGTAAGAGTCCGCTAG	1.6
	Loop F	CCTGAGGCATCAACACCTT	0.8
	Loop B	TGGTAATGTGGCTGTTCGY	0.8

Y: C/T

Fig. 2.4: Template regions and sequences of the LAMP primers for PEDV: (A) PEDV amplicon gene sequence with the six primer locations: B3, F3, FIP, BIP, LF, and LB; arrows indicate the direction of extension. (B) Sequences of the primers for the PEDV LAMP reaction.

A

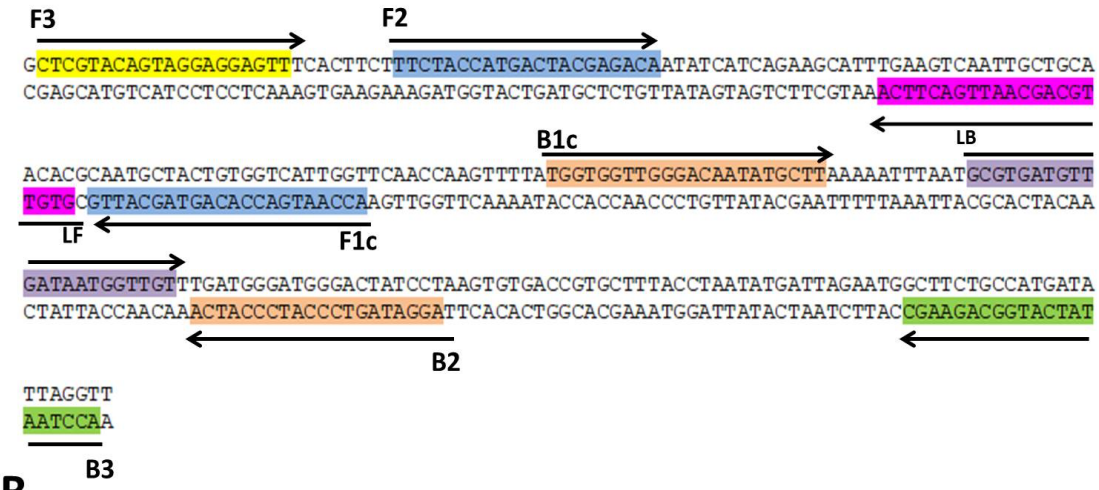

B

Target Gene	Primer Name	Primers sequences(5' to 3')	Concentration (μM)
Polymerase (Pol) protein gene of TGEV	F3	CTCGTACAGTAGGAGGAGTT	0.2
	B3	ACCTAATATCATGGCAGAAGC	0.2
	FIP (F1c +F2)	ACCAATGACCACAGTAGCATTGTTCTACCATGACTACGAGACA	1.6
	BIP (B1c +B2)	TGGTGGTTGGGACAATATGCTTGGATAGTCCCATCCCATCA	1.6
	Loop F	GTGTTGCAGCAATTGACTTCA	0.8
	Loop B	GCGTGATGTTGATAATGGTTGT	0.8

Fig. 2.5: Target regions and sequences of the LAMP primers for TGEV: (A) TGEV polymerase gene sequence with the six primer locations: B3, F3, FIP, BIP, LF, and LB; arrows indicate the direction of extension. (B) Sequences of the primers for the TGEV LAMP reaction.

A

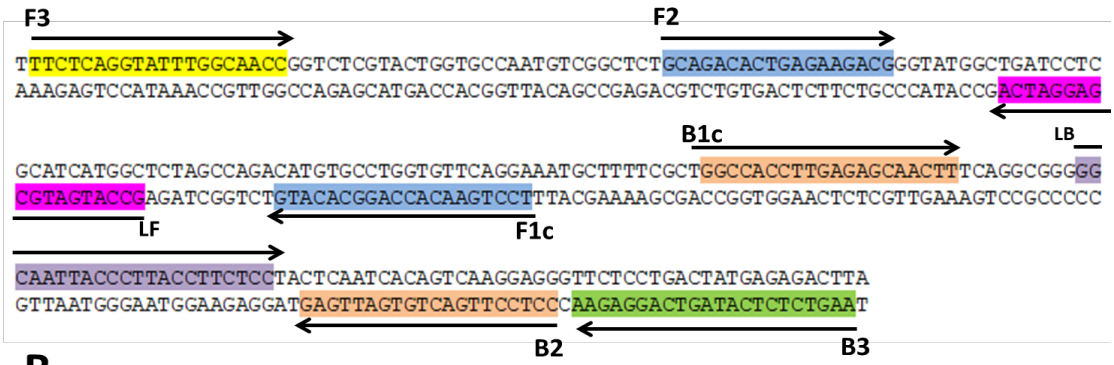

B

Target Gene	Primer Name	Primers sequences(5' to 3')	Concentration (μM)
Nucleocapsid protein coding gene of PDCoV	F3	TTCTCAGGTATTTGGCAACC	0.2
	B3	AAGTCTCTCATAGTCAGGAGAA	0.2
	FIP (F1c +F2)	TCCTGAACACCAGGCACATGGCAGACACTGAGAAGACG	1.6
	BIP (B1c +B2)	GGCCACCTTGAGAGCAACTTCCTCCTTGACTGTGATTGAG	1.6
	Loop F	GCCATGATGCGAGGATCA	0.8
	Loop B	GGCAATTACCCTTACCTTCTCY	0.8

Y: C/T

Fig. 2.6: Target regions and sequences of the LAMP primers for PDCoV: (A) PDCoV nucleoprotein gene sequence with the six primer locations: B3, F3, FIP, BIP, LF, and LB; arrows indicate the direction of extension. (B) Sequences of the primers for the PDCoV LAMP reaction.

2.2.5 Benchtop RT-LAMP reaction conditions

The RT-LAMP reaction mix with a volume of 10 μL contained F3 and B3 primers (0.2 μM of each), LoopF and LoopB primers (0.8 μM of each), FIP and BIP primers (1.6 μM of each), 6 μL of Isothermal MasterMix (ISO-001, OptiGene, USA), 0.4 μL of 1 × EvaGreen® dye (Biotium Inc., Hayward, CA, USA), 0.2 μL of AMV reverse transcriptase (200 U μL^{-1}) (Promega Corp., Madison, WI, USA), and 1 μL of the extracted RNA template, and nuclease-free water was added to bring the total volume to 10 μL. Fluorescence emission of DNA amplicons was monitored with the 7500 Fast Real-Time PCR system (Applied Biosystems, Carlsbad, CA, USA) at 65 °C for 30 minutes, then analysis of the melting curve from 50 °C to 95 °C with 1.0 °C increment per second was performed. Positive and negative controls were included in each run. Positive controls were

PEDV (PC22A strain), TGEV (virulent Miller-M6 strain), and PDCoV (OH-FD22 strain), while non-template rectal swabs from non-infected gnotobiotic pigs were used as negative controls.

2.2.6 Benchtop qRT-PCR reaction conditions

Each RT-PCR reaction volume comprised SsoFast EvaGreen® Supermix (Bio-Rad, USA) (5 µL), primers F3 and B3 (10 µM), 0.2 µL of AMV reverse transcriptase (200 U μL^{-1}), 1 µL of viral RNA, and nuclease-free water to a 10 µL final volume. The cycling conditions were as follows: incubation at 50 °C for 30 min (for reverse transcription), followed by incubation at 95 °C for 10 min (melting), and then 45 cycles at 95 °C for 10 s and at 60 °C for 30 s, followed by the analysis of the melting curve in the temperature range from 50 °C to 95 °C with 1.0 °C increment per second. Monitoring of fluorescence emission was carried out using the 7500 Fast Real-Time PCR system (Applied Biosystems, Carlsbad, CA, USA). Positive and negative controls were involved in each run.

2.2.7 On-chip detection and data analysis

During the test, the LAMP master mix is loaded into the 3D-printed microfluidic chip (Fig. 2.2) via the inlet port, and each LAMP reactor is filled with 20 ± 1 µL of the master mix, which includes 12 µL of Isothermal MasterMix (ISO-001, OptiGene, USA), 0.8 µL 1 × EvaGreen® dye, and 0.8 µL AMV reverse transcriptase (200 U μL^{-1}), along with 1.4 µL RNA template of one of these viruses and nuclease-free water to 20 µL.

The chip was then incubated in an inexpensive, homemade, portable heating system. Our heating system is controlled with a Raspberry Pi (Raspberry Pi Foundation®, Pi 4 Model B) and equipped with a polyimide Thermofoil™ heater (Minco®, HK6911) and a Type-K thermocouple (Omega®, TT-K30-SLE). The microcontroller Raspberry Pi, the thin-film heater, and the thermocouple are used to create a closed-loop proportional-integral-derivative (PID) control system. During incubation, the chip is first heated up to 45 °C for 6 min to ensure auto-

sealing prior to the LAMP amplification. Then, the heater's temperature is increased to and maintained at 65 °C for 30 minutes to incubate the LAMP reaction.

A portable USB fluorescence microscope (Dino-Lite®, AM4115T-GFBW) emitted ultraviolet light to excite the EvaGreen® dye incorporated in the amplified DNA and to read the real-time fluorescence emission (Fig. 2.1). The fluorescence microscope has seven built-in blue LEDs (light-emitting diodes) for fluorescence excitation and a 510 nm emission filter suitable for observing the EvaGreen® dye intercalated in the amplified DNA. The microscope is mounted on top of the heating system to monitor all LAMP reactors simultaneously (Fig. 2.1).

Images of the chip during incubation were captured with the fluorescence microscope once every minute. Regions selected by the user were analyzed with MATLAB (MathWorks™, R2019a). The camera records red, green, and blue (RGB) intensity values for each pixel. DinoCapture™ 2.0 software (AnMo Electronics Corp., Taiwan) bundled with the portable fluorescence microscope then extracts the G (green) value from the RGB matrix of each pixel and calculates the average G value among all pixels included in the region of interest. The average G values of each LAMP reactor represent the relative fluorescence intensities. The averaged and normalized G values are plotted as functions of time. The threshold time is defined as the time that it takes the G value to reach half its peak intensity.

2.2.8 Limit of detection (LOD)

To determine the smallest number of copies of the PEDV, TGEV, and PDCoV genomes that could be detected with our microfluidic device, benchtop real-time RT-LAMP, and qRT-PCR assays, we prepared serial dilutions of the three virus RNAs suspended in nuclease-free water.

2.2.9 Clinical performance

We extracted nucleic acids from the eleven samples of diseased piglets and one negative control rectal swab from a non-infected gnotobiotic pig. These samples were previously tested for PEDV, TGEV, and PDCoV with RT-PCR assays [7, 11, 12]. Among the tested samples, five samples showed positive results for PEDV, three tested positive for TGEV, and three were PDCoV-

positive. The negative control sample was negative for all three viruses. We retested all the samples concurrently with our microfluidic RT-LAMP, benchtop RT-LAMP, and benchtop qRT-PCR. Negative and positive controls were included in all these tests. Furthermore, we carried out with our microfluidic device co-detection of samples containing nucleic acids from two different viral species (e.g., PEDV + TGEV, PEDV + PDCoV, and TGEV + PDCoV) and all three virus species (PEDV + TGEV + PDCoV).

2.3 Results

2.3.1 Analytical performance of benchtop RT-LAMP and RT-PCR

Fig. 2.7 (RT-LAMP) and Fig. 2.8 (RT-PCR) depict, respectively, the fluorescence emission intensities (arbitrary units) as functions of time and number of cycles for different target concentrations of gRNAs of PEDV, TGEV, and PDCoV and the signals' threshold times/cycles as functions of each target concentration. The threshold time Tt is defined as the time until the amplification curve achieves half its saturation value. The RT-LAMP and RT-PCR threshold times are nearly linear functions of the log of the target concentration. RT-LAMP and RT-PCR have similar limits of detection. The lowest detectable concentration (limit of detection) is 10 genome copies per reaction for PEDV and PDCoV and 10^2 for TGEV. Analysis of the melting curve revealed a single peak for both RT-LAMP and RT-PCR products (Fig. 2.9), revealing the absence of non-specific products such as primer dimers. Negative controls and non-template controls did not show any signal of positive amplification.

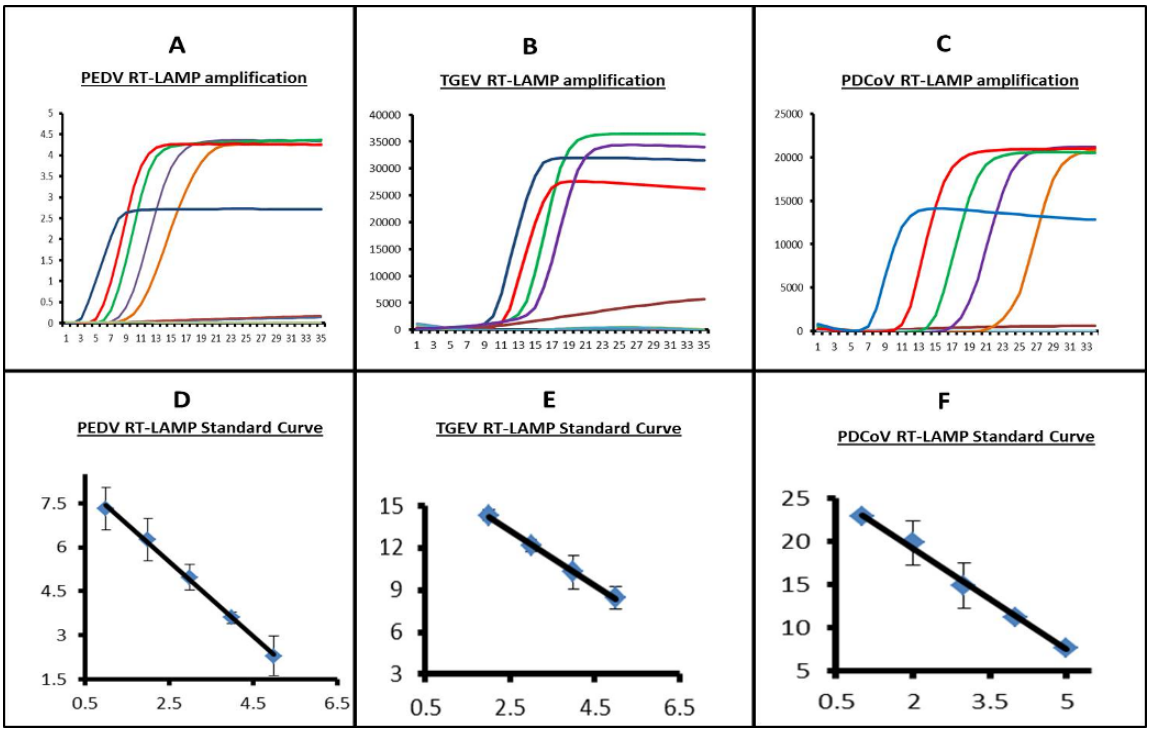

Fig. 2.7: Benchtop real-time LAMP results with template concentration ranging from 0 to 10^5 copies per reaction. RT-LAMP amplification curves: (A) PEDV, (B) TGEV, and(C) PDCoV. Standard curves with threshold times: (D) PEDV, (E) TGEV, and (F) PDCoV.

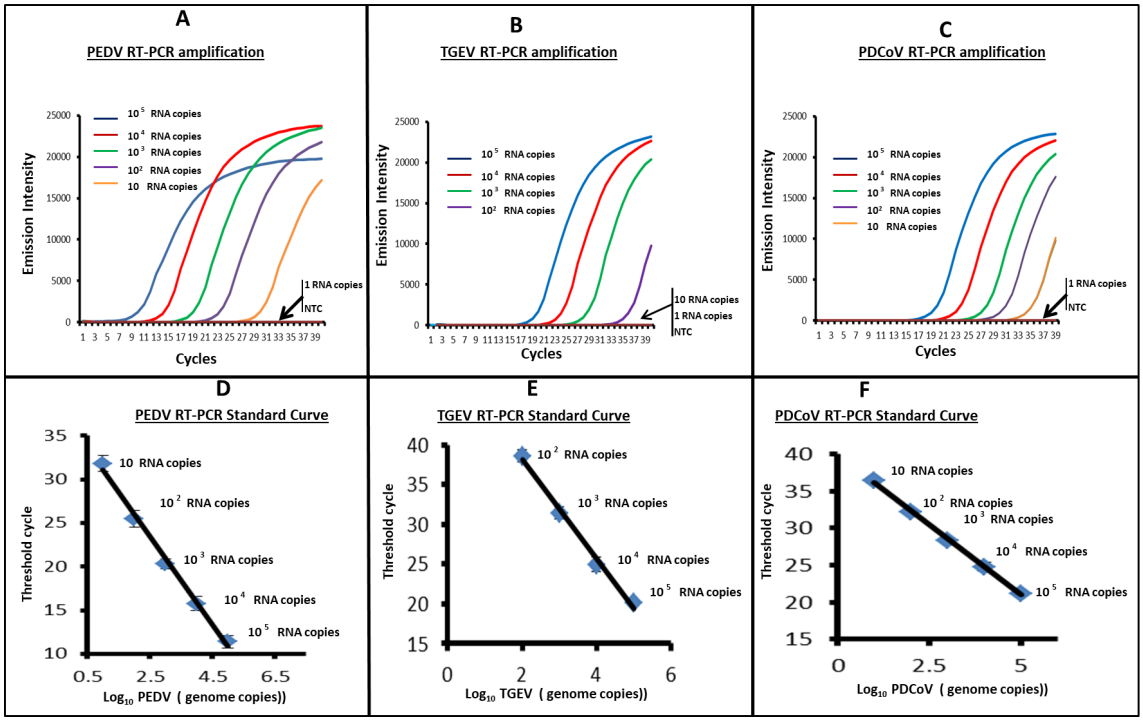

Fig. 2.8: Real-time PCR amplification curves of PEDV (A), TGEV (B) and PDCoV (C). The number of templates ranged from 0 to 10^5 genomic copies per reaction. The threshold times (minutes) are depicted as functions of PEDV (D), TGEV (E), and PDCoV (F) concentration (genome copies per reaction). N = 3.

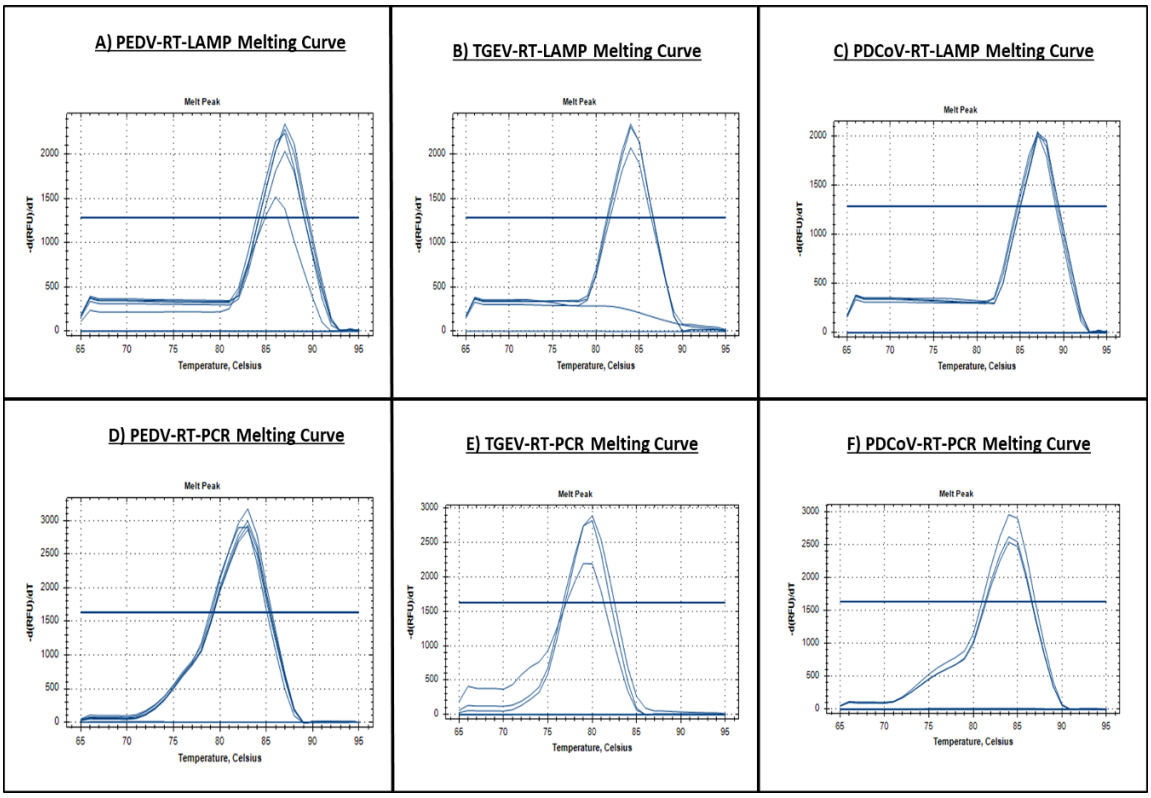

Fig. 2.9: Melting curve analysis of both RT-LAMP and RT-PCR products reveals a single peak.

2.3.2. Microfluidic chip analytical performances

Our microfluidic chip (Fig. 2.2) comprises four independent isothermal amplification reactors, each with a dry-stored primer set specific to a designated target. The identity of the amplicon is determined by the reaction chamber's location. All four reactors are within the camera's field of view, enabling us to concurrently monitor the fluorescence emission from all the LAMP reactors in real time during LAMP incubation. When only one of the targets is present in the sample, the corresponding LAMP reactor lights up, while the other reactors and the non-primer control (NPC) remain dark (Fig. 2.10A - 2.10C). The analytical performance of the chip was evaluated in the template concentration range from 0 to 10^2 genome copies per reaction and showed similar results to the benchtop assays.

One of the advantages of our chip is its ability to concurrently test for the presence of multiple targets in a sample, thus indicating comorbidities. To demonstrate this feature, we

contrived samples spiked with one, two, and all three different viruses. In the presence of comorbidities, either two test reactors or all three test reactors light up (Fig. 2.10D - 2.10G). Our assay co-detected successfully PEDV + TGEV, PEDV + PDCoV, TGEV + PDCoV, and (PEDV + TGEV + PDCoV).

A1

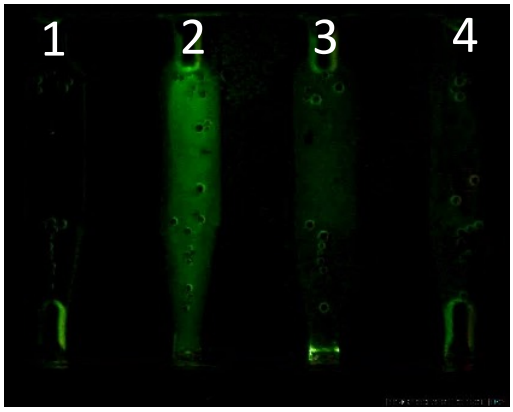

A2

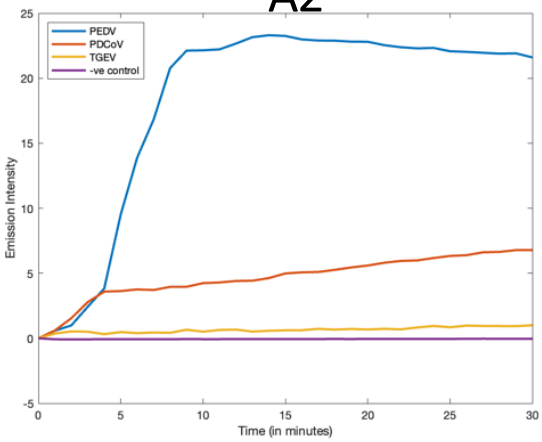

B1

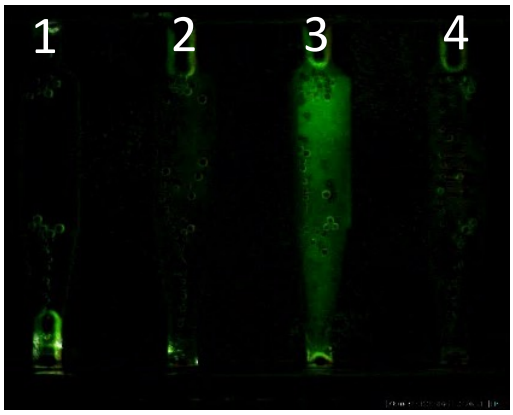

B2

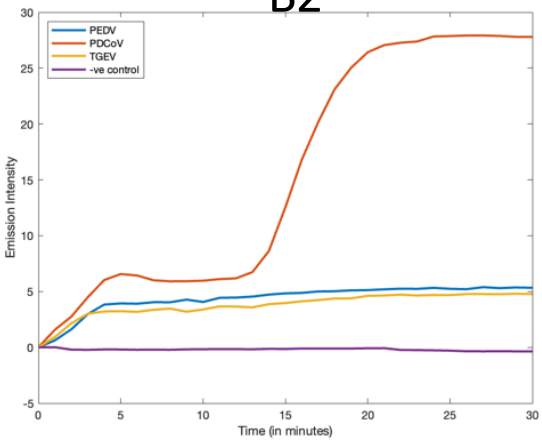

C1

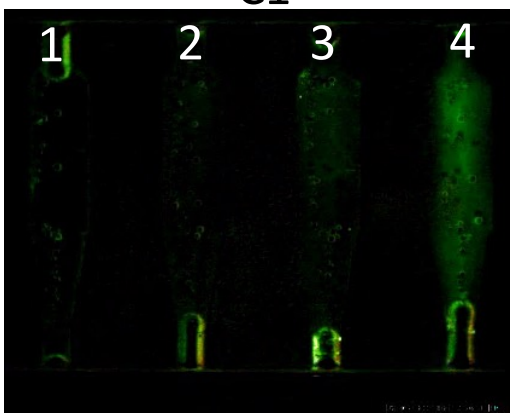

C2

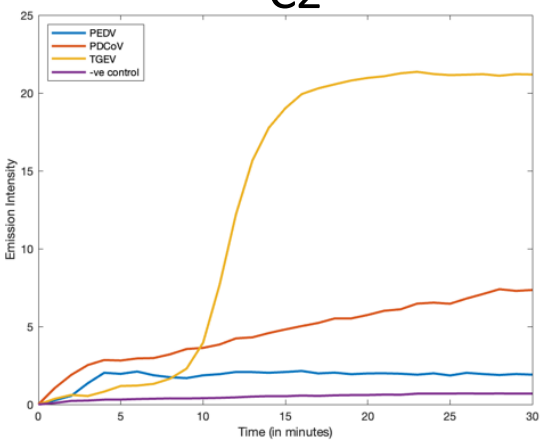

D1

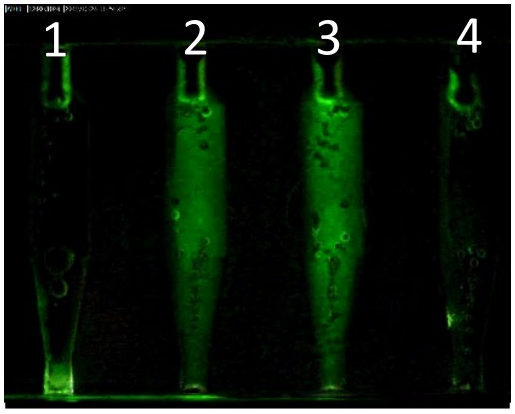

D2

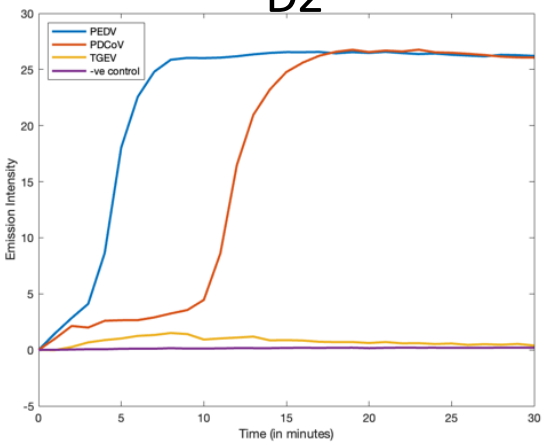

E1

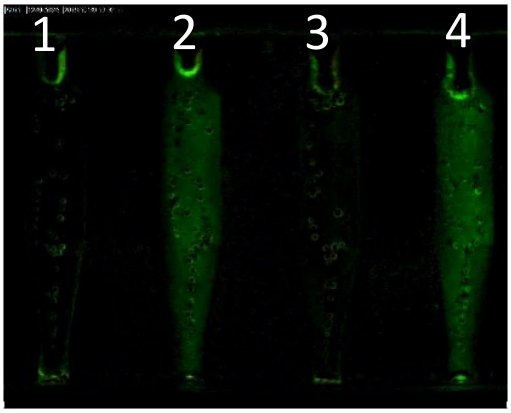

E2

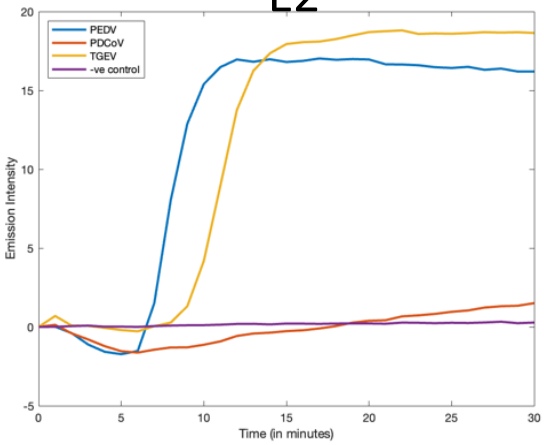

F1

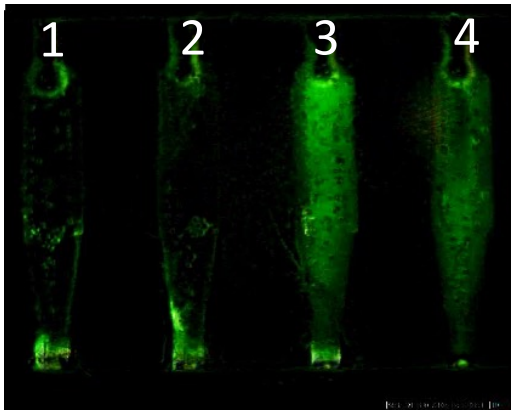

F2

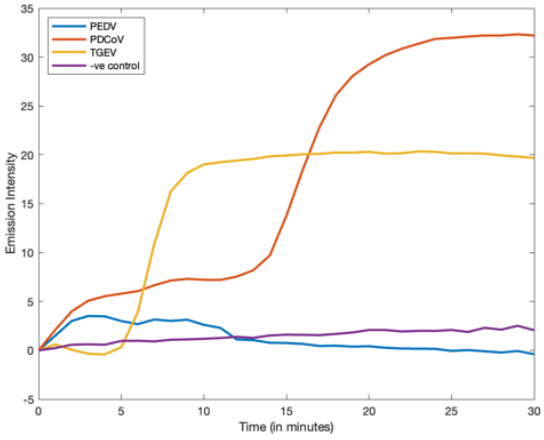

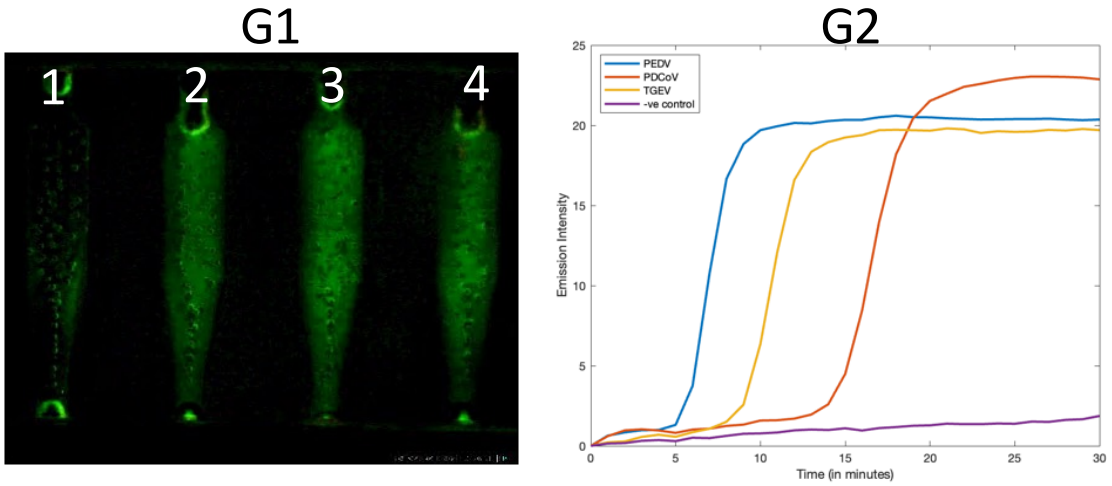

Fig. 2.10: Images of fluorescence emission at the end of the amplification process and reaction chambers' average fluorescence intensities as functions of time. Samples contain (A) PEDV only – chamber no. 2, (B) PDCoV only – chamber 3, (C) TGEV only – chamber 4, (D) PEDV and PDCoV – chambers 2 and 3, (E) PEDV and TGEV - chambers 2 and 4, (F) PDCoV and TGEV - chambers 3 and 4, and (G) PEDV, PDCoV, and TGEV - chambers 2, 3, and 4.

Four parallel LAMP reactors enable our chip to perform multiplexed RT-LAMP to detect all three targets concurrently with a non-primer control. To demonstrate this, we prepared mixed samples with all combinations of PEDV, TGEV, and PDCoV for multiplexed test on chip. Our assay managed to co-detect all combinations of the three viruses (Fig. 2.10 and Fig. 2.11).

2.3.3 Performance of the benchtop assays with clinical samples

The eleven samples from diseased piglets were tested for PEDV, TGEV, and PDCoV with our benchtop RT-LAMP assays, our chips running RT-LAMP assays, and qRT-PCR (Fig. 2.11 and Table 2.1). Based on earlier qPCR, five samples were positive for PEDV, three were positive for TGEV, three were positive for PDCoV, and one was negative for all these pathogens. All the samples were retested with qRT-PCR in our lab in proximity to our RT-LAMP tests. All benchtop RT-LAMP and chip-based RT-LAMP assays had 100% selectivity and 100% sensitivity compared

to our qRT-PCR and with the data provided by the laboratory from which the clinical samples originated.

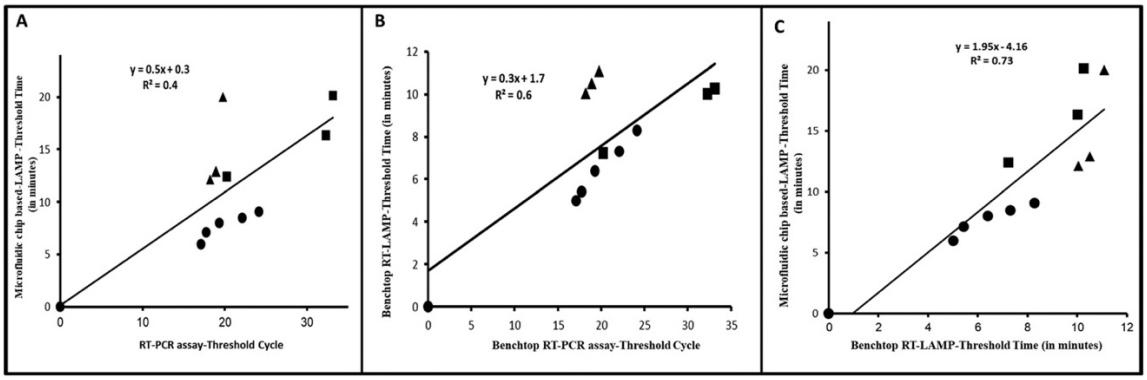

Fig. 2.11: Testing of the clinical samples from diseased piglets with the microfluidic-based LAMP, benchtop RT-LAMP, and benchtop RT-PCR assays. (A) Microfluidic-based LAMP threshold time as a function of qRT-PCR threshold cycle. (B) Benchtop RT-LAMP threshold time as a function of benchtop qRT-PCR threshold time. (C) Chip RT-LAMP threshold time as a function of benchtop RT-LAMP threshold time (● for PEDV samples; ■ for TGEV samples; ▲ for PDCoV).

Table 2.1: Threshold LAMP times (min) and threshold RT-PCR cycles of our microfluidic and benchtop tests of our clinical samples.

Sample #	Our RT-PCR	Our benchtop RT-LAMP	Our chip-based RT-LAMP
PEDV 1	22.1	7.3	8.5
PEDV 2	19.3	6.4	8.0
PEDV 3	17.8	5.4	7.1
PEDV 4	17.1	5.0	6.0
PEDV 5	24.1	8.3	9.1
TGEV 1	33.1	10.3	20.1
TGEV 2	20.2	7.2	12.4
TGEV3	32.3	10.0	16.4
PDCoV 1	18.2	10.1	12.1
PDCoV 2	18.9	10.5	12.9
PDCoV3	19.8	11.1	20.0
Control	0.0	0.0	0.0

The benchtop RT-LAMP and the microfluidic RT-LAMP threshold times were shorter than the qRT-PCR and trended similarly (Table 2.1). The threshold times of the benchtop RT-LAMP-

assay and microfluidic-based RT-LAMP correlated linearly ($R^2 = 0.7$). The aggregated data of all the threshold times in our chip (regardless of the target type) exhibited a weaker correlation ($R^2 = 0.4$, Fig. 2.11A) with the qRT-PCR threshold cycle. A stronger correlation was, however, obtained ($R^2 = 0.8 - 0.9$) when each pathogen was analyzed separately (Fig. 2.12).

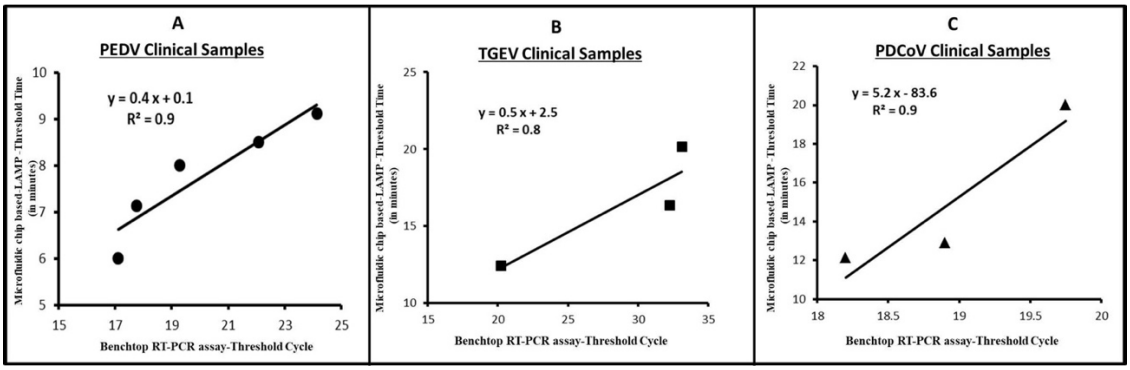

Fig. 2.12: Testing of clinical samples from diseased piglets with the microfluidic based-LAMP and benchtop RT-PCR assays. Microfluidic-based LAMP-threshold time as a function of qRT-PCR threshold cycle for PEDV (A), TGEV (B), and PDCoV (C) clinical samples.

2.4 Discussion and Conclusions

Swine enteric viruses such as PEDV, TGEV, and PDCoV are a major threat to the pig industry, causing substantial economic losses [1, 4]. For example, losses due to PEDV are estimated at $300,000 per year for a single 700 sow farrow-to-finishing herd [31]. To rapidly implement suitable control measures to contain the infection, rapid molecular testing of suspected animals is needed. Since PEDV, TGEV, and PDCoV are co-endemic and cause similar symptoms in animals, it is highly desirable to co-test for all three pathogens. Currently, diagnosis for PEDV, TGEV, and PDCoV in suspected pigs is carried out with laboratory-based RT-PCR assays. A previous report [32] described multiplexed molecular detection of swine enteric coronaviruses with RT-PCR combined with post-amplification detection with gel electrophoresis. In addition to the complex, time-consuming operation, the necessity to open amplicon-rich tubes endangers contamination of the workspace. Another report [33] described a multiplexed assay that uses TaqMan-probes for specific detection of enteric coronavirus targets with real-time qRT-PCR.

Such an assay requires an expensive thermal cycler with a multicolor reader, is limited in the level of multiplexing, and has a 10-fold lower sensitivity than the singleplex assays, presumably because probes emit less light than intercalating dyes and/or due to the competition for enzymes.

The various PCR-based assays require well-equipped facilities, possibly expensive instruments, and trained personnel that typically are not available on farms and often are located at a large distance away, which complicate testing and delay test results. To facilitate testing in resource-poor settings such as rural areas and developing countries, we have developed new benchtop singleplex RT-LAMP assays for detecting PEDV, TGEV, and PDCoV. RT-LAMP is more suitable for use in resource-poor settings than RT-PCR. Since LAMP operates at a fixed temperature, ranging from 60 °C to 65 °C, does not require precise incubation temperature, and does not require temperature cycling, it can be incubated with simple instruments such as ESEQuant TubeScanner (GmbH, Stockach, Germany), Genie II (Optigene, Horsham, UK), and a water bath or even instrumentation and electricity-free with heating provided by an exothermic chemical reaction of the type used in military rations and in ready-to-eat meals and temperature regulation provided with a phase-change material (PCM) [34, 35] LAMP's constant temperature operations also consume less power than the thermal cycling needed for PCR. LAMP products can be detected with intercalating dyes and molecular beacons like PCR products. But, since LAMP produces about an order of magnitude greater number of amplicons than PCR, LAMP products and by-products can also be detected with colorimetric dyes that are visible to the naked eye, eliminating the need for a reader. Furthermore, the fluorescence emission from LAMP can be detected with the ubiquitous smartphone [34, 35]. Finally, LAMP assays are more tolerant of contaminants than PCR assays [36], simplifying sample preparations. In summary, LAMP assays are highly sensitive, specific, robust, can be carried out over a temperature range of 60-65 °C in less than one hour, and are more suitable for use outside centralized laboratories than PCR [37, 38].

Our benchtop PEDV, TGEV, and PDCoV RT-LAMP assays perform on par with the gold standard qRT-PCR assays with shorter processing times. Like the benchtop qRT-PCR, our RT-LAMP assays are processed in closed tubes without a need to open the tube and transfer

amplification products to a lateral flow strip – a process that risks contaminating the workspace and rendering future negative tests false positives. Each of our RT-LAMP assays for PEDV and PDCoV has a limit of detection of 10 gRNA molecules per reaction (Fig. 2.7). Our RT-LAMP assay for TGEV has a limit of detection of 100 gRNA molecules per reaction (Fig. 2.7). These detection limits are appropriate for early-stage infection detection [14, 39, 40]. Our assays' threshold times correlate linearly with the log of template concentration, enabling the estimation of the number of viruses in the sample.

To confirm our assays' clinical performance for virus detection, we tested eleven clinical specimens from diseased pigs with our benchtop RT-LAMP assays. Our LAMP test results are in excellent agreement with the gold standard qRT-PCR. We believe that our assays are ready for field tests.

To enable convenient co-detection of co-endemic targets, we developed a microfluidic system comprising a 3D-printed microfluidic chip and a simple processor. The 3D-printing technology allows us rapid, low-cost prototyping. From earlier works on LAMP on chips that typically process a single target at a time [28, 41], our chip hosts four independent reaction chambers, enabling the co-testing for multiple co-endemic pathogens in a single sample at the point of need. Three of our reaction (test) chambers are customized for testing each of the pathogens PEDV, TGEV, and PDCoV by pre-storing the corresponding primer sets in the reaction chambers. The fourth reaction chamber serves as a negative control. Our chip architecture can readily accommodate a larger number of reaction chambers to enable the co-detection of a larger number of targets if needed.

The loading and drying operations in our chip are driven by capillary forces and do not require external instruments for flow control, in contrast to many other microfluidic devices that require syringe pumps and centrifugal forces [42, 43]. We rely on capillary imbibition and capillary valves to take an aliquot from the sample among the various reaction chambers and, after sample filling, to sever the connections among the reaction chambers to eliminate any crosstalk and false positives. Our chips self-seal with a temperature-actuated phase-change material (PCM). During incubation, the melted PCM prevents evaporation in the reaction chambers and amplicons from

escaping and contaminating the workspace. After amplification, the PCM solidifies, tombing the reaction mix. Given the limited scope of this study, we were not able to dry-store reagents inside our chip. In the future, we will store all reagents inside the chip in dry form for long-term (over one year) refrigeration-free shelf-life, and the sample will include only the extracted nucleic acids.

We demonstrated that our RT-LAMP chip has similar performance to our benchtop RT-LAMP assays and that we can detect any of the targeted analytes in a single process as well as comorbidities. The chip required a bit longer processing times than our benchtop RT-LAMP, which we attribute to the lower performance of our heating system compared to the benchtop equipment. We anticipate that with further improvements, our microfluidic system would enable affordable molecular testing at the point of need by minimally trained personnel, providing timely and actionable information to farmers. In conclusion, our field-deployable real-time RT-LAMP assays and microfluidic chips have the potential to facilitate rapid, inexpensive, multiplexed molecular detection and quasi-quantification of PEDV, TGEV, and PDCoV in basic veterinary laboratories and pigs' farms.

References

[1] Q. Wang, A. N. Vlasova, S. P. Kenney, and L. J. Saif, "Emerging and re-emerging coronaviruses in pigs," *Current opinion in virology,* vol. 34, pp. 39-49, 2019.

[2] V. Gerdts and A. Zakhartchouk, "Vaccines for porcine epidemic diarrhea virus and other swine coronaviruses," *Veterinary microbiology,* vol. 206, pp. 45-51, 2017.

[3] D. Brian and R. Baric, "Coronavirus genome structure and replication," *Coronavirus replication and reverse genetics,* pp. 1-30, 2005.

[4] M. Niederwerder and R. Hesse, "Swine enteric coronavirus disease: a review of 4 years with porcine epidemic diarrhoea virus and porcine deltacoronavirus in the United States and Canada," *Transboundary and emerging diseases,* vol. 65, no. 3, pp. 660-675, 2018.

[5] E. Bohl, "Enteric viral infections as related to diarrhea in swine," in *Proceedings of the 3rd international symposium on neonatal diarrhea. Veterinary Infectious Diseases Organization, Saskatoon, Saskatchewan, Canada*, 1981, pp. 1-9.

[6] E. H. Bohl, R. P. Gupta, M. F. Olquin, and L. J. Saif, "Antibody responses in serum, colostrum, and milk of swine after infection or vaccination with transmissible gastroenteritis virus," *Infection and immunity,* vol. 6, no. 3, pp. 289-301, 1972.

[7] L. Kim, K.-O. Chang, K. Sestak, A. Parwani, and L. J. Saif, "Development of a reverse transcription-nested polymerase chain reaction assay for differential diagnosis of transmissible gastroenteritis virus and porcine respiratory coronavirus from feces and nasal swabs of infected pigs," *Journal of veterinary diagnostic investigation,* vol. 12, no. 4, pp. 385-388, 2000.

[8] A. N. B. Salem, A. C. Sergei, P. B. Olga, G. A. Olga, A. Mahjoub, and B. P. Larissa, "Multiplex nested RT-PCR for the detection of porcine enteric viruses," *Journal of virological methods,* vol. 165, no. 2, pp. 283-293, 2010.

[9] T. Oka *et al.*, "Cell culture isolation and sequence analysis of genetically diverse US porcine epidemic diarrhea virus strains including a novel strain with a large deletion in the spike gene," *Veterinary microbiology,* vol. 173, no. 3-4, pp. 258-269, 2014.

[10] X. Liu *et al.*, "Determination of the infectious titer and virulence of an original US porcine epidemic diarrhea virus PC22A strain," *Veterinary research,* vol. 46, no. 1, pp. 1-6, 2015.

[11] H. Hu *et al.*, "Isolation and characterization of porcine deltacoronavirus from pigs with diarrhea in the United States," *Journal of clinical microbiology,* vol. 53, no. 5, pp. 1537-1548, 2015.

[12] D. Song *et al.*, "Molecular characterization and phylogenetic analysis of porcine epidemic diarrhea viruses associated with outbreaks of severe diarrhea in piglets in Jiangxi, China 2013," *PloS one,* vol. 10, no. 3, p. e0120310, 2015.

[13] K. Jung, T. Annamalai, Z. Lu, and L. J. Saif, "Comparative pathogenesis of US porcine epidemic diarrhea virus (PEDV) strain PC21A in conventional 9-day-old nursing piglets vs. 26-day-old weaned pigs," *Veterinary microbiology,* vol. 178, no. 1-2, pp. 31-40, 2015.

[14] C.-M. Lin *et al.*, "Experimental infection of a US spike-insertion deletion porcine epidemic diarrhea virus in conventional nursing piglets and cross-protection to the original US PEDV infection," *Veterinary research,* vol. 46, no. 1, pp. 1-13, 2015.

[15] C.-M. Lin *et al.*, "Antigenic relationships among porcine epidemic diarrhea virus and transmissible gastroenteritis virus strains," *Journal of virology,* vol. 89, no. 6, pp. 3332-3342, 2015.

[16] L. Wang, B. Byrum, and Y. Zhang, "Detection and genetic characterization of deltacoronavirus in pigs, Ohio, USA, 2014," *Emerging infectious diseases,* vol. 20, no. 7, p. 1227, 2014.

[17] P. Li and X. Ren, "Reverse transcription loop-mediated isothermal amplification for rapid detection of transmissible gastroenteritis virus," *Current microbiology,* vol. 62, no. 3, pp. 1074-1080, 2011.

[18] X. Yu *et al.*, "Development of a real-time reverse transcription loop-mediated isothermal amplification method for the rapid detection of porcine epidemic diarrhea virus," *Virology journal,* vol. 12, no. 1, pp. 1-8, 2015.

[19] F. Zhang *et al.*, "A simple and rapid identification method for newly emerged porcine Deltacoronavirus with loop-mediated isothermal amplification," *Biological research,* vol. 50, no. 1, pp. 1-7, 2017.

[20] T. N. Mai *et al.*, "Development of pooled testing system for porcine epidemic diarrhoea using real-time fluorescent reverse-transcription loop-mediated isothermal amplification assay," (in eng), *BMC Vet Res,* vol. 14, no. 1, p. 172, May 29 2018, doi: 10.1186/s12917-018-1498-9.

[21] K. Nagamine, T. Hase, and T. Notomi, "Accelerated reaction by loop-mediated isothermal amplification using loop primers," *Molecular and cellular probes,* vol. 16, no. 3, pp. 223-229, 2002.

[22] O. A. Gandelman *et al.*, "Novel bioluminescent quantitative detection of nucleic acid amplification in real-time," *PloS one,* vol. 5, no. 11, p. e14155, 2010.

[23] G. Kiddle *et al.*, "GMO detection using a bioluminescent real time reporter (BART) of loop mediated isothermal amplification (LAMP) suitable for field use," *BMC Biotechnology,* vol. 12, no. 1, p. 15, 2012/04/30 2012, doi: 10.1186/1472-6750-12-15.

[24] X. Zhang, S. B. Lowe, and J. J. Gooding, "Brief review of monitoring methods for loop-mediated isothermal amplification (LAMP)," *Biosensors and Bioelectronics,* vol. 61, pp. 491-499, 2014.

[25] Q. Yang, K. J. Domesle, F. Wang, and B. Ge, "Rapid detection of Salmonella in food and feed by coupling loop-mediated isothermal amplification with bioluminescent assay in real-time," *BMC Microbiology,* vol. 16, no. 1, p. 112, 2016/06/17 2016, doi: 10.1186/s12866-016-0730-7.

[26] J. Song *et al.*, "Smartphone-Based Mobile Detection Platform for Molecular Diagnostics and Spatiotemporal Disease Mapping," (in eng), *Anal Chem,* vol. 90, no. 7, pp. 4823-4831, Apr 3 2018, doi: 10.1021/acs.analchem.8b00283.

[27] J. Li, J. Macdonald, and F. von Stetten, "Review: a comprehensive summary of a decade development of the recombinase polymerase amplification," *Analyst,* 10.1039/C8AN01621F vol. 144, no. 1, pp. 31-67, 2019, doi: 10.1039/C8AN01621F.

[28] K. Kadimisetty *et al.*, "Fully 3D printed integrated reactor array for point-of-care molecular diagnostics," *Biosensors and Bioelectronics,* vol. 109, pp. 156-163, 2018/06/30/ 2018, doi: https://doi.org/10.1016/j.bios.2018.03.009.

[29] T. H. G. Thio *et al.*, "Theoretical development and critical analysis of burst frequency equations for passive valves on centrifugal microfluidic platforms," *Medical & Biological Engineering & Computing,* vol. 51, no. 5, pp. 525-535, 2013/05/01 2013, doi: 10.1007/s11517-012-1020-7.

[30] N. Zhang *et al.*, "Development of one-step SYBR Green real-time RT-PCR for quantifying bovine viral diarrhea virus type-1 and its comparison with conventional RT-PCR," *Virology Journal,* vol. 8, no. 1, p. 374, 2011, doi: 10.1186/1743-422x-8-374.

[31] L. Weng, A. Weersink, Z. Poljak, K. de Lange, and M. von Massow, "An economic evaluation of intervention strategies for Porcine Epidemic Diarrhea (PED)," *Preventive veterinary medicine,* vol. 134, pp. 58-68, 2016.

[32] G. Ding *et al.*, "Development of a multiplex RT-PCR for the detection of major diarrhoeal viruses in pig herds in China," *Transboundary and emerging diseases,* vol. 67, no. 2, pp. 678-685, 2020.

[33] X. Huang, J. Chen, G. Yao, Q. Guo, J. Wang, and G. Liu, "A TaqMan-probe-based multiplex real-time RT-qPCR for simultaneous detection of porcine enteric coronaviruses," *Applied Microbiology and Biotechnology,* vol. 103, no. 12, pp. 4943-4952, 2019, doi: 10.1007/s00253-019-09835-7.

[34] S. C. Liao *et al.*, "Smart cup: A minimally-instrumented, smartphone-based point-of-care molecular diagnostic device," *Sensor Actuat B-Chem,* vol. 229, pp. 232-238, Jun 28 2016, doi: 10.1016/j.snb.2016.01.073.

[35] H. H. Bau, C. Liu, M. Mauk, and J. Song, "Is instrument-free molecular detection possible?," *Expert Review of Molecular Diagnostics,* vol. 17, no. 11, pp. 949-951, 2017, doi: 10.1080/14737159.2017.1374855.

[36] Q. Yang, F. Wang, W. Prinyawiwatkul, and B. Ge, "Robustness of Salmonella loop-mediated isothermal amplification assays for food applications," *Journal of Applied Microbiology,* vol. 116, no. 1, pp. 81-88, 2014, doi: 10.1111/jam.12340.

[37] Y. Mori and T. Notomi, "Loop-mediated isothermal amplification (LAMP): a rapid, accurate, and cost-effective diagnostic method for infectious diseases," (in eng), *J Infect Chemother,* vol. 15, no. 2, pp. 62-9, Apr 2009, doi: 10.1007/s10156-009-0669-9.

[38] P. A. Kokkinos, P. G. Ziros, M. Bellou, and A. Vantarakis, "Loop-Mediated Isothermal Amplification (LAMP) for the Detection of Salmonella in Food," *Food Analytical Methods,* vol. 7, no. 2, pp. 512-526, 2014, doi: 10.1007/s12161-013-9748-8.

[39] Q. Chen *et al.*, "Pathogenicity and pathogenesis of a United States porcine deltacoronavirus cell culture isolate in 5-day-old neonatal piglets," *Virology,* vol. 482, pp. 51-59, 2015.

[40] R. Magtoto *et al.*, "Evaluation of the serologic cross-reactivity between transmissible gastroenteritis coronavirus and porcine respiratory coronavirus using commercial blocking enzyme-linked immunosorbent assay kits," *Msphere,* vol. 4, no. 2, 2019.

[41] K. Yin *et al.*, "Real-time Colorimetric Quantitative Molecular Detection of Infectious Diseases on Smartphone-based Diagnostic Platform," *Scientific Reports,* vol. 10, no. 1, p. 9009, 2020/06/02 2020, doi: 10.1038/s41598-020-65899-w.

[42] A. Perebikovsky *et al.*, "Rapid sample preparation for detection of antibiotic resistance on a microfluidic disc platform," *Lab Chip,* 10.1039/D0LC00838A 2021, doi: 10.1039/D0LC00838A.

[43] E. J. S. Brás, A. M. Fortes, T. Esteves, V. Chu, P. Fernandes, and J. P. Conde, "Microfluidic device for multiplexed detection of fungal infection biomarkers in grape cultivars," *The Analyst,* vol. 145, no. 24, pp. 7973-7984, 2020, doi: 10.1039/d0an01753a.

Chapter 3 Refrigeration-free Ready-to-use Microfluidic Chip for Single-stage NAATs

3.1 Introduction

In this chapter, we describe an inexpensive, portable, refrigeration-free, ready-to-use 3D-printed microfluidic device for real-time multiplexed molecular detection of the human immunodeficiency virus (HIV), hepatitis B virus (HBV), and hepatitis C virus (HCV). In addition, an Android-based smartphone application was developed to capture real-time images in the case of colorimetric detection, carry out time-series image analysis of fluorescent images imported from a USB camera, and interpret results.

Bloodborne viral infections are threats to global public health. Over 400 million people worldwide are infected or co-infected with the three bloodborne viruses, Hepatitis B Virus (HBV), Hepatitis C virus (HCV), and Human immunodeficiency virus (HIV) [1-5]. In the absence of early diagnosis and treatment, blood virus infections have high morbidity and mortality, cause chronic diseases, and endanger the blood supply. HBV causes liver hepatitis, cirrhosis, and hepatocellular carcinoma, infecting nearly 1.5 million people and causing an estimated 0.8 million deaths annually. Over 296 million people are living with HBV [6], of whom 90% are unaware of their infection [7]. The hepatitis virus HCV causes both acute and chronic liver diseases, including cancer [8], with roughly 1.5 million new infections and 0.3 million deaths annually. About 58 million people worldwide are currently infected with HCV [9]. HIV targets humans' immune systems, making infected people immunodeficient [10] and causing an estimated 0.7 million deaths and 1.5 million new infections annually [11]. Only 60 % of HIV patients are continuously taking antiviral drugs, and over 20% of infected individuals are unaware of their condition. Approximately 2.3 million HIV-infected people are co-infected with HCV, and 2.6 million HIV-infected individuals are co-infected with HBV [12]. There is an urgent need for co-detection of HIV, HBV, and HCV due to their common path of transmission, the impact of co-infections on therapy, and the need to inform public health officials to enable them to enact informed policies

and control measures. In view of the availability and affordability of treatments, simple, rapid, and reliable point-of-care testing is essential, especially in resource-poor conditions.

The current standard HIV, HBV, and HCV diagnoses require a molecular test such as PCR. A PCR-based molecular test requires stringent sample processing, skilled personnel, a cold chain, and expensive laboratory-based equipment [13, 14], making it unfeasible and unaffordable in resource-limited settings. Point-of-care testing that distinguishes between an active state of infection and past infection can provide a direct linkage to care, keep patients engaged, increase the number of tested patients, and provide means to monitor therapy's efficacy [15].

Isothermal enzymatic nucleic acid amplification provides opportunities for simple and sensitive molecular tests at the point of care. One such isothermal amplification method, loop-mediated isothermal amplification (LAMP), uses up to six primers to obtain target-specific amplification with strand displacement polymerase [16, 17]. LAMP has demonstrated high sensitivity compared to other isothermal methods and has been successfully applied in various tests. LAMP is an attractive alternative to the PCR test in point-of-care settings since LAMP does not require thermal cycling and has greater tolerance to contaminants than PCR [18, 19]. Combined with simple platforms such as microfluidic chips and paper-based devices, LAMP provides a promising means for point-of-care molecular tests [13, 20-24].

A simple, rapid, point-of-care diagnosis can play a key role in identifying infected individuals during a visit to a doctor's or dentist's office, enabling proper follow-up and care. To enable molecular diagnostics at the point of need such as patients' home, it is desirable to eliminate the need for cold-chain refrigeration.

Herein, we demonstrate an inexpensive, portable, refrigeration-free, and ready-to-use microfluidic device for multiplexed molecular detection of HIV, HBV, and HCV. All the components of the LAMP assay are dried on chip, enabling refrigeration-free storage under room conditions. Our device with the dry-stored reagents utilizes the same capillary circuit that we described in Chapter 2 for auto-distribution of sample solution and auto-sealing with the phase-change material. Our chip consists of four reaction chambers, one for each of the three targets (HIV, HBV, and HCV) and one for negative control. Detection can be carried out at the end of the

process colorimetrically without any instrumentation or in real-time with a fluorescent dye. Incubation and detection were carried out with our portable, low-cost, custom processor that comprises an electric resistance heater and a USB camera, which can be easily produced in resource-poor settings.

3.2 Materials and Methods

3.2.1 Materials

KCl, $MgSO_4$, $(NH_4)_2SO_4$, betaine, tween 20, polyethylene glycol (PEG) 930 for auto-sealing, PEG 3350 for coating, and hydroxynaphthol blue (HNB) were purchased from Sigma-Aldrich (St. Louis, MO, USA). Tris-HCl was purchased from Boston Bioproducts (Ashland, MA, USA). dNTPs were purchased from Denville Scientific (South Plainfield, NJ, USA). 20X EvaGreen dye was purchased from Biotium Inc. (Hayward, CA, USA). Warmstart Bst 2.0 polymerase was purchased from New England Biolab (Ipswich, MA, USA). HBV plasma sample was purchased from Seracare life science (Milford, MA, USA). HCV genotype 1 clinical research sample was purchased from Discovery life science Inc. (Huntsville, AL, USA). HIV-1 control and isopropyl alcohol (IPA) were purchased from Thermo Fisher Scientific (Waltham, MA, USA). Clear resin for 3D printing was purchased from Formlabs (Somerville, MA, USA).

3.2.2 Nucleic acid extraction

HIV (Thermo Fisher Scientific, Waltham, MA, USA), HBV (LGC Clinical Diagnostics, Milford, MA), and HCV (Discovery Life Science, Huntsville, AL, USA) plasma samples were stored at -20 ^oC prior to use. HBV dsDNA was extracted with Qiamp DNA extraction kit (Qiagen, Hilden, Germany). HIV RNA and HCV RNA were extracted with Qiamp viral RNA extraction kits (Qiagen). The concentrations of the purified nucleic acids were estimated with Qubit DNA assay kit, NA HS assay kit, and fluorimeter (molecular probe life science, Waltham, MA, USA). Copy numbers of each sample were calculated based on molecular masses (NCBI) and then mixed with molecular water to form dilution series. Our estimated viral loads favorably agreed with the

vendor's (Thermofisher, Seracare, Discovery) data after converting international units (IU) to copy numbers [25-27].

3.2.3 Chip fabrication

Our microfluidic chip was designed with SolidWorks 2020 (Dassault Systèmes, Vélizy-Villacoublay, France) and saved as an STL file. The file was processed with PreForm (Formlabs, Somerville, MA, USA) - a print preparation software that generates print supports and controls print layout and orientation. Then, devices were fabricated with Form 3 (Formlabs, Somerville, MA, USA), a low-force stereolithography (LFS) resin-based desktop 3D printer. After 3D printing, the chip was thoroughly IPA rinsed with Form Wash (Formlabs, Somerville, MA, USA) for 15 min and post-cured with Form Cure (Formlabs, Somerville, MA, USA) at 60 °C for 15 min. Next, the inner surfaces of microfluidic channels were coated with a 2% aqueous solution of PEG 3350 [23, 28].

3.2.4 Ready-to-use microfluidic chip

Our portable, 3D-printed, ready-to-use microfluidic device has a compact size (23 mm *L* x 27 mm *W* x 10 mm *H*). The chip (Fig. 3.1a) consists of four independent LAMP reactors. Each of the first three reactors pre-stores primer set specific to a designated target. The fourth reactor does not store any primers and serves as a non-primer, negative control. All other LAMP assay components were dry-stored on chip and re-activated with the sample elution buffer prior to use. Both fluorometric and colorimetric detections were used, allowing, respectively, real-time monitoring with a fluorescence camera and endpoint detection with either a smartphone or the naked eye.

Each reactor (Fig. 3.1a) has a volume of 20 µL and a slanted roof to siphon any air bubbles away from the observation window so that the air bubbles do not interfere with the signal acquisition (Fig. 3.2). On one end, all four reactors connect to a common distribution conduit that links to the inlet port of the chip. On their other ends, reactors connect to a side opening dedicated to reaction mix insertion. The two sides of the reaction chambers are interconnected to

prevent pressure differences (Fig. 3.3a). Our LAMP assay comprises two parts: A and B, each stored separately [29]. Component A is stored in the reaction chambers next to their distal ends, and component B is stored at the sample injection port. The reagents are introduced in liquid form through the designated openings and dried in-situ under ambient conditions. Detailed chip dimensions are shown in Fig. 3.1b. A 3D CAD drawing and a real photograph of the device after LAMP incubation with the left three chambers showing positive and the rightmost one displaying negative signals are shown in Fig. 3.1c - 3.1d.

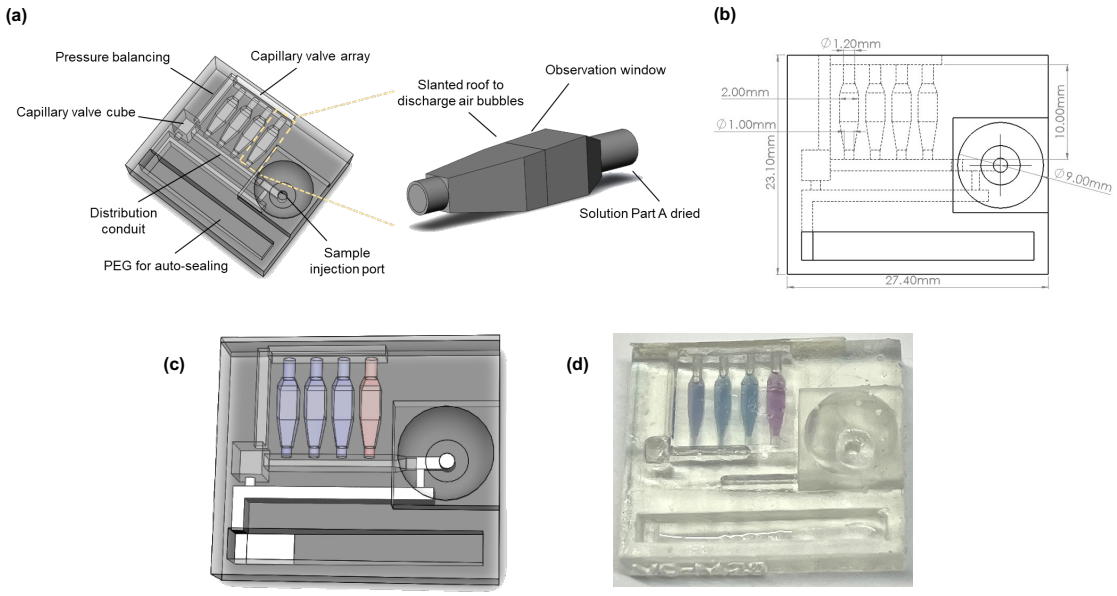

Fig. 3.1: (a) Chip architecture and the tapered geometry of each reaction chamber to accommodate bubble migration away from the imaging region. (b) Chip dimensions. (c) 3D rendering and (d) photograph of the chip after LAMP amplification with left three reaction chambers showing positive signals and the rightmost chamber as a negative control.

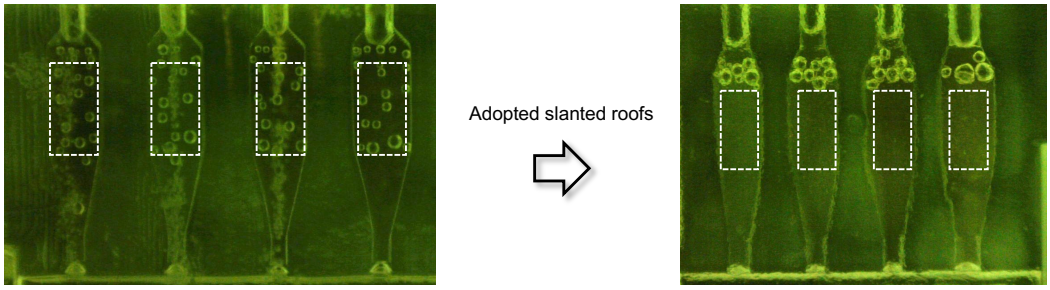

Fig. 3.2: Slanted roofs siphon air bubbles away from the observation windows with gravity. The observation windows, enclosed by the dash lines, are the regions analyzed to calculate the chamber-averaged fluorescence intensity.

The 3D-printed resin has a static water contact angle of 47 degrees (Formlabs, Somerville, MA, USA) that enables the capillary imbibition of aqueous solutions into the microfluidic chip. To control spontaneous liquid distribution driven by capillary forces, capillary valves were integrated onto the chip. The capillary valve array prevents the reactors from overflowing during auto-distribution and locks liquids within each reactor when the liquid in the distribution conduit is drained with an absorption pad. The capillary valve cube (Fig. 3.1a) comprises two capillary valves on two sides and prevents aqueous solutions from flowing into the PEG channel and vice versa. To stop undesired fluid flow during chip preparation, all air vents are blocked to build up downstream pressure inside the chip that counteracts the capillary action.

PEG 930 has a static contact angle smaller than 90 degrees with the 3D printing material, which allows the capillary imbibition of the molten PEG 930 into the microfluidic chip to perform sealing. With a melting temperature of around 37 °C, PEG 930 remains solid at room temperature. The chip is auto-sealed after its temperature exceeds the PEG's melting temperature before the LAMP amplification starts.

3.2.5 Chip preparation

Since each reactor is dedicated to a designated target or negative control, it requires specialized LAMP mixes with primer sets specific to the designated targets. The LAMP reaction mix was stored in two parts. Both parts were applied to the chip in liquid form, and the solvent was allowed

to evaporate. Part A in liquid form (10 μL) comprises target-specific primers (10.4 μM), Bst polymerase (0.64 U), dNTPs (2.8 mM of each), $MgSO_4$ (16 mM), and $(NH_4)_2SO_4$ (20 mM). Part B in liquid form (60 μL) comprises Tris-HCl (40 mM), KCl (20 mM), betaine (1.6 M), HNB (240 μM), EvaGreen (5.0 μM). Part A is specific to each reaction chamber and defines the chamber's designation. In contrast, component B is common to all reaction chambers. Thus, component B is dry stored at the sample injection port and, after hydration, shared by the entire reactor array.

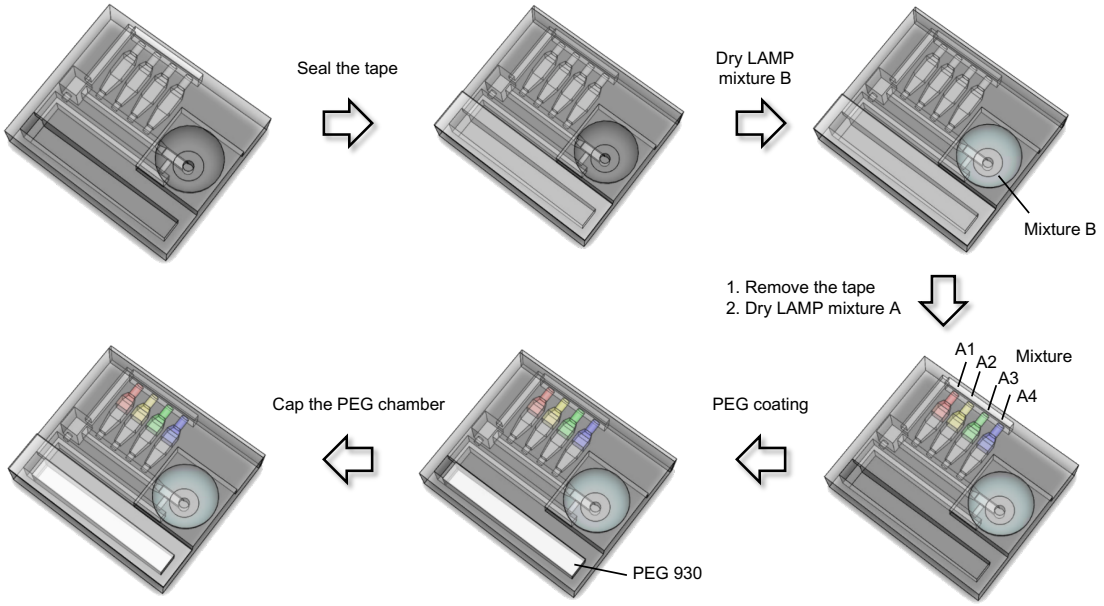

Fig. 3.3: Schematic illustration of the chip preparation process.

After chip fabrication, the PEG chamber and the side opening were sealed with PCR tapes. LAMP mixture part B was then loaded into the reservoir and air-dried at 60 °C for 2 hr. After component B formed a powder, we removed all the PCR tapes, inserted LAMP mixtures A with specific primer sets into the corresponding reaction chambers via the side opening, and air-dried the chip at room temperature for 4 hr. Next, the chip was placed on a cooled surface. Then, molten PEG was poured into the PEG chambers and solidified immediately. Last, PCR tapes were used to seal all openings leaving the sample injection port as the only port of the chip. The chip preparation process is depicted in Fig. 3.3.

3.2.6 Device operation

For each test, the extracted nucleic acids were eluted in nuclease-free water to a total volume of 120 µL and then inserted into the chip through its inlet port. The loading process can be done either with a pipette or a dropper. Next, the PCR tape on top of the PEG chamber was peeled off to trigger capillary action for the auto-distribution of the sample. The chip utilizes capillary circuits for the uniform distribution of the sample among the reaction chambers. As the sample solution enters each reactor, it hydrates and reconstitutes the LAMP reaction mix. After the four LAMP reactors had been fully filled, we placed an absorption pad at the inlet port, draining liquid from the distribution conduit while the liquids in the reaction chambers were retained in place with the capillary valves located at the distal ends of the reaction chambers.

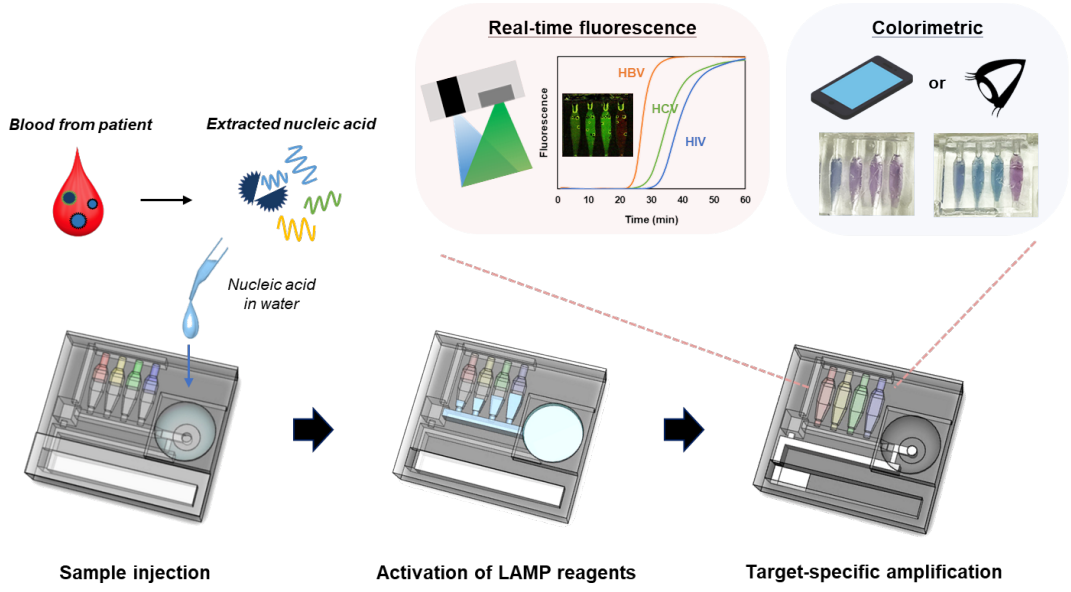

Fig. 3.4: Workflow of the ready-to-use chip for real-time amplification and detection. Nuclease-free water laden with target nucleic acids hydrates and reconstitutes the LAMP reaction mix, enabling LAMP amplification at the proper incubation temperature with both real-time and endpoint detection.

Next, the chip was incubated with our custom processor that comprises a microcontroller Raspberry Pi 4 Model B (Raspberry Pi Foundation, Cambridge, UK), a flexible thin-film heater Thermofoil HK6911 (Minco, Minneapolis, MN, US), a thermocouple TT-K-30-SLE (Omega Engineering, Norwalk, CT, US), and a portable fluorescence camera Dino-Light AM4113TGFBW (AnMo Electronics, Taiwan, China). The system was programmed to first hold the microfluidic chip at 50 °C for 5 min for auto-sealing and then at 63 °C for 1 hr for LAMP amplification.

3.2.7 Real-time fluorescence detection

Our processor provides a dark chamber during LAMP amplification that blocks all ambient light. The fluorescence camera mounted over the chip was programmed to take one fluorescence image every 1 min. The camera has built-in blue LEDs that excite the EvaGreen dye. In the presence of dsDNA amplicons, the dye emits green fluorescence that can be detected through a 510 nm emission filter with the CCD camera. When LAMP amplification takes place, the emission intensity of the fluorescent dye increases with time. Reactors that light up with fluorescence indicate the presence of their designated targets.

The fluorescence images were saved as JPG files and then analyzed with MATLAB R2021b (MathWorks, Natick, MA, US). The MATLAB program used the RGB values in the first image as the baseline and subtracted these values from all subsequent images to create a new set of image files. Next, the program automatically detected the locations of LAMP reactors. Alternatively, the user can specify manually the regions within the reactors to be analyzed for emission intensity. After reactor identification, the program calculates the average G (green) value of the pixels within each reactor region for each image, normalizes these values with the maximum G value observed among all four reactors throughout the entire incubation time, and plots the normalized G values as functions of time (Fig. 3.11).

3.2.8 Colorimetric detection

HNB is a colorimetric indicator that monitors the presence of Mg^{2+} ions under alkaline conditions [30]. Since the LAMP amplification produces byproducts such as pyrophosphate ion that reacts with Mg^{2+} ions, the Mg^{2+} ion concentration decreases during the LAMP reaction, resulting in the color change of HNB from violet to blue [31]. Reactors that change color indicate the presence of their designated targets. A cellphone (iPhone 12 Pro, Apple, Cupertino, CA, US) was used to capture a photo of the microfluidic chip after 60-min LAMP amplification. The photo was then analyzed with MATLAB R2021b (MathWorks, Natick, MA, US). Similar to the fluorescence image analysis mentioned above, the locations of each reactor in the photo were identified first with auto-detection or by manual selection. Then, the MATLAB program extracted R (red) and B (blue) values from each imaging region, calculated the average B to R ratio for each reactor, normalized these ratios with the value of the negative control, and plotted the ratio as bar charts (Fig. 3.8).

3.2.9 Smartphone application for image analysis

An Android-based smartphone application was developed with the platform MIT App Inventor [32]. Four screens (Fig. 3.5) were created and dedicated, respectively, to program selection (screen 1), camera settings (screen 2), region of interest identification (screen 3), and real-time monitor and result interpretation (screen 4). Once the application is opened, the user is directed to the home screen (screen 1) to select one from the three programs, i) real-time monitoring, ii) colorimetric detection, and iii) fluorometric detection.

If the first program, real-time monitoring, is selected, the user is then transferred to screen 2 (Fig. 3.5) to make any adjustment to the default camera settings, including camera index (which specific camera to use – smartphones usually have multiple built-in cameras), flash mode, focus mode, exposure compensation, etc. Once the camera settings are finalized, the application transfers to screen 3 (Fig. 3.5), asking the user to confirm the reactor number and the regions of interest for chamber-averaged intensity analysis. Next, the application switches to the last screen (Fig. 3.5) and prompt the user to confirm the incubation time and the image acquisition frequency. The default settings are 60 min of incubation and a photo capture frequency of one per minute.

During incubation, the application acquires a photo at the specified frequency, displays the photo on screen 4, calculates chamber-averaged signal intensities, and updates the real-time amplification curve on screen 4. At the end of the incubation time, the application displays the diagnostic results, pointing out which target pathogens are present.

If the second program, colorimetric detection, is selected, the user will go through a similar process, confirming the camera settings (screen 2) and the regions of interest (screen 3). On the final screen (screen 4), the application will take an endpoint photo of the chip, plot each reactor's chamber-averaged B to R ratio in a bar chart, and display the detection results.

If the third program, fluorometric detection, is selected, the program skips the camera settings (screen 2) and goes through the same process for observation window confirmation (screen 3). On the final screen (screen 4), the application is given access to the fluorescence images uploaded to the smartphone. It then performs time-series image analysis, plots amplification curves on screen 4, and displays the diagnostic results. All the tests of the application were done with an Android smartphone (Mate 20 Pro, Huawei, Shenzhen, China). More details of the application are provided in Supplementary Information.

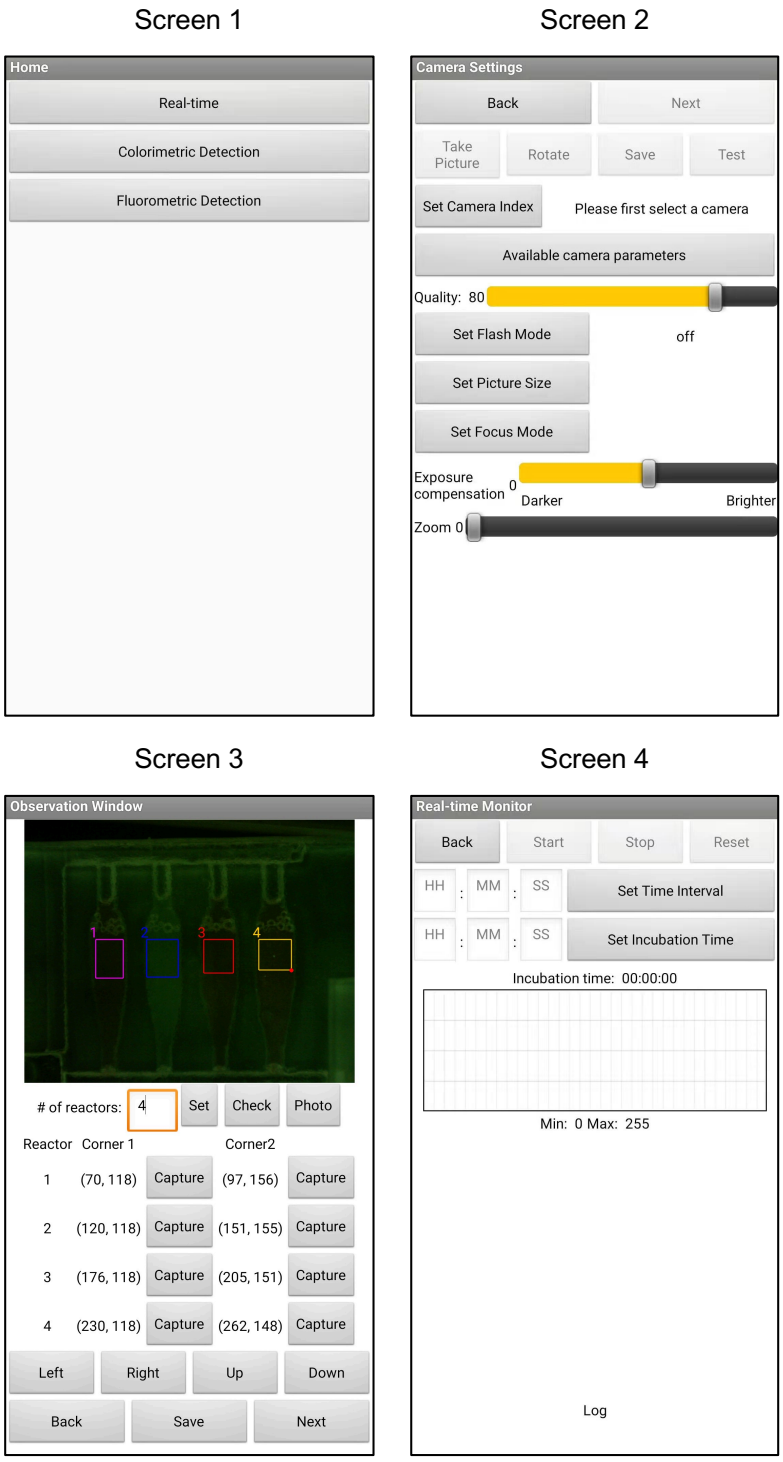

Fig. 3.5: User interface (UI) of the Android-based smartphone application developed with the MIT App Inventor platform. Screen 1 is the home screen for program selection that appears when the application is opened; Screen 2 allows camera setting adjustments; Screen 3 enables the user to

confirm regions of interest; Screen 4 provides real-time monitoring, result display, and data interpretation.

3.2.10 Estimation of potential cross-talk: primer migration

A 3D model with geometries complementary to our microfluidic chip was designed with SolidWorks 2020 (Dassault Systèmes, Vélizy-Villacoublay, France) and saved as a STEP file. The file was then imported into COMSOL Multiphysics (COMSOL, Stockholm, Sweden), providing the geometry for the computational domain (Fig. 3.6). The simulation is based on a time-dependent diffusive transport module with no-flux boundary conditions everywhere. The diffusion coefficient for the primers was estimated based on the primer with the shortest length (17 nt, Table 3.1) as 1.5×10^{-10} m^2/s [33]. The reaction mix part A is assumed rehydrated when all four reaction chambers are fully filled with the sample elution buffer and reconstituted in a 0.1-mm thick layer coating the half of the LAMP reactors' surface close to the side opening. Without loss of generality, we report on the diffusion of primers from the second reactor from the left (Fig. 3.6). The primer concentration is normalized with its initial concentration. That is, the initial primer concentration in the coated region is 1 and 0 elsewhere.

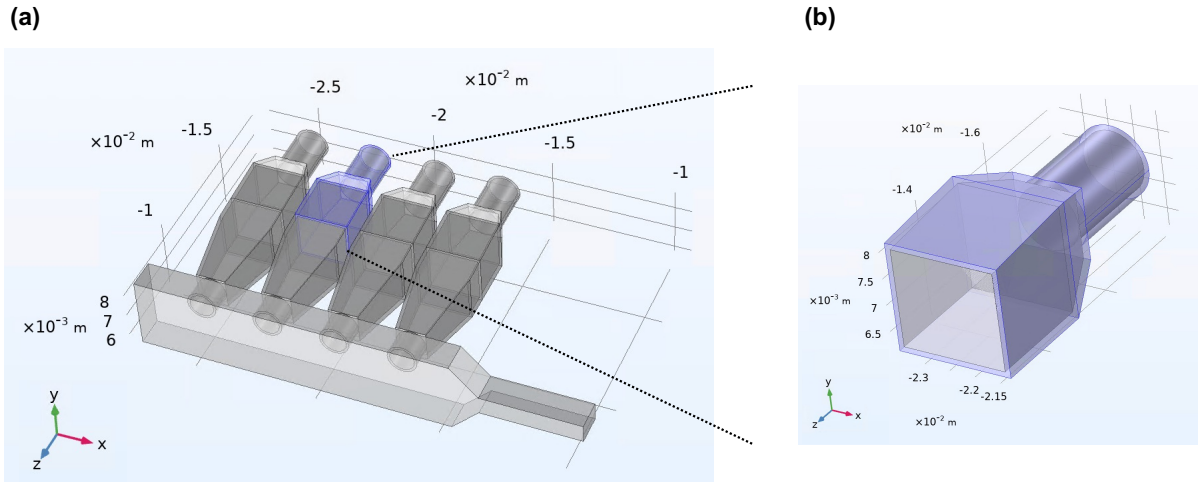

Fig. 3.6: Geometry of the microfluidic chip with four LAMP reaction chambers and the common distribution for COMSOL simulation. The region highlighted is the 0.1-mm thick layer surrounding

the half of the second LAMP chamber close to the side channel (representing reconstituted part A of the reaction mix), where the normalized initial primer concertation was set to 1. The other domains have a normalized initial primer concentration of 0.

3.3 Results

3.3.1 Simulation results

During the auto-distribution of the sample (~2 min), the various LAMP reactors are interconnected via the distribution conduit. The COMSOL simulation was carried out to examine potential primer migration among the LAMP reactors (cross-talk). As expected, our simulations indicate that an insignificant quantity (< 0.01 %) of primers migrated out of their original reactor (Fig. 3.7a). The primer concentration at the inlet of the adjacent reaction chamber (Fig. 3.7b) is negligible (less than 0.01 % of the nominal primer concentration needed for LAMP amplification) within the 3-min time interval when the passage among reactors is available for diffusion. The simulations suggest that the cross-talk and false positives resulting from primers' migrations (Fig. 3.7a - 3.7b) are unlikely. The results of our numerical simulations were validated with a mesh-size convergence (Fig. 3.7a) and a mass conservation (Fig. 3.7c) study. Our simulation is conservative, assuming that i) the dried LAMP mixture A re-suspends immediately once all reaction chambers are filled with the hydration solution, ii) the hydration solution remains quiescent and only diffusion contributes to the migration, and iii) all six LAMP primers have the same diffusion coefficient of 1.5×10^{-10} m^2/s obtained based on the shortest primer (Table 3.1). In practice, i) dried assay resuspension requires time, up to minutes; ii) during the loading of the hydration solution, there is advection in the direction from the common distribution conduit to reaction chambers' distal ends that would counteract diffusion; and iii) longer primers (Table 3.1) have even smaller diffusion coefficients, which further lessen the possibility of cross-talk.

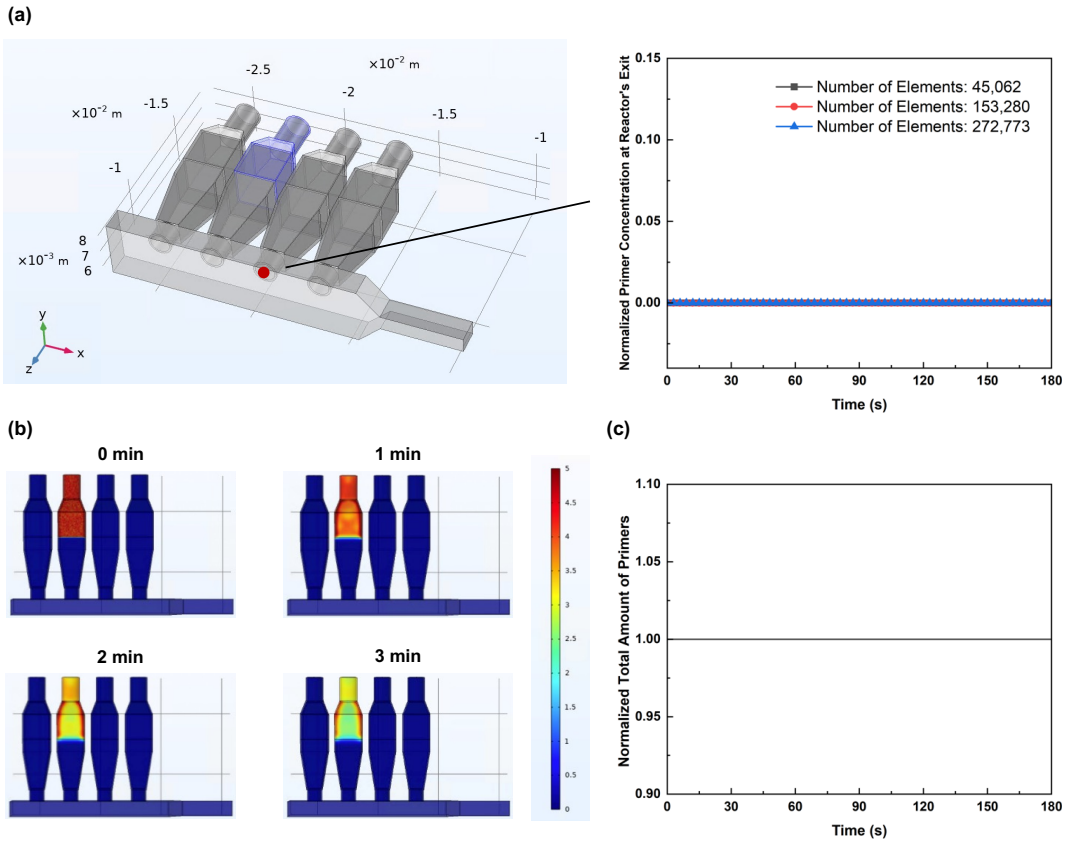

Fig. 3.7: Simulations to estimate the primer migration from the second (from the left) reaction chamber to the other reaction chambers. (a) Normalized primer concentration calculated with three different mesh sizes at the inlet of the third (from the left) reaction chamber as a function of time. (b) Representative images of primer concentration distributions within the reaction chambers during the first few minutes after hydration prior to the draining of the distribution conduit. (c) Total primer mass as a function of time.

Table 3.1: Primer sequences of HIV, HBV, and HCV.

Target	Primer	Sequence
HBV	F3	TTGGGACTCTCTCGTCCCCTTCTCCGTCTG
	B3	CCCAGTCTTTAAACAAACAGTCTTTGAAGTATGCC
	FIP	GAAGCGAAGTGCACACGGTCCGCGCACCTCTCTTTACGC
	BIP	CACCGTGAACGCCCACCAAAGGTCGGTCGTTGACATTGC
	LF	GCAGATGAGAAGGCACAGAC
	LB	TGCCCAAGGTCTTACATAAGAGGAC

Target	Primer	Sequence
HCV	F3	AGTGTCGTGCAGCCTCC
	B3	GCACTCGCAAGCACCCTAT
	FIP	CGGTCGTCCTGGCAATTCCGTTTTCCGGGAGAGCCATAGTGG
	BIP	TTGGATCAACCCGCTCAATGCCTTTTCCTTTCGCGACCCAACAC
	LF	CTCACCGGTTCCGCAGA
	LB	TGCCCCCGCAAGACTGCTA

Target	Primer	Sequence
HIV	F3	ATTATCAGAAGGAGCCACC
	B3	CATCCTATTTGTTCCTGAAGG
	FIP	CAGCTTCCTCATTGATGGTTTCTTTTTAACACCATGCTAAACACAGT
	BIP	TGTTGCACCAGGCCAGATAATTTTGTACTGGTAGTTCCTGCTATG
	LF	TTTAACATTTGCATGGCTGCTTGAT
	LB	GAGATCCAAGGGGAAGTGA

*HBV primer sequences were adapted from [34], HCV from [35], and HIV from [36].

3.3.2 Detection of HIV, HBV, and HCV

We prepared microfluidic chips for the multiplexed detection of HIV, HBV, and HCV in the left three reactors, leaving the rightmost one primer-free as a negative control. Fig. 3.8 shows the multiplexed LAMP results for six cases when 1) HBV only is present in the sample, 2) HCV only is present in the sample, 3) HIV only is present in the sample, 4) HBV and HCV are present in the sample, 5) all three targets are present in the sample, and 6) there are no targets present (no template control).

The chips were incubated at 63 °C for 60 min in our custom processor with real-time fluorometric (EvaGreen dye) and colorimetric (HNB dye) monitoring. We did not observe any cross-talk, contamination, false positives, or false negatives.

Fig. 3.8a displays fluorescence images taken at the end of each incubation. In each test, only the reactors corresponding to the targets present in the sample lighted up, and the other reactors remained dark. The normalized fluorescence emission intensities in each reaction chamber are shown in the bar chart in Fig. 3.8a. Green fluorescence from dsDNA intercalating dye increases as the number of LAMP amplicons increases. All the experiments single-plex – (1), (2), (3), multiplex – (4), (5), and no-target control (6) show target-specific results. The assay specificity was tested with samples laden with other pathogens such as HPV-16, HPV-18, and ZIKV available in our lab. None produced any false positive (Fig. 3.9).

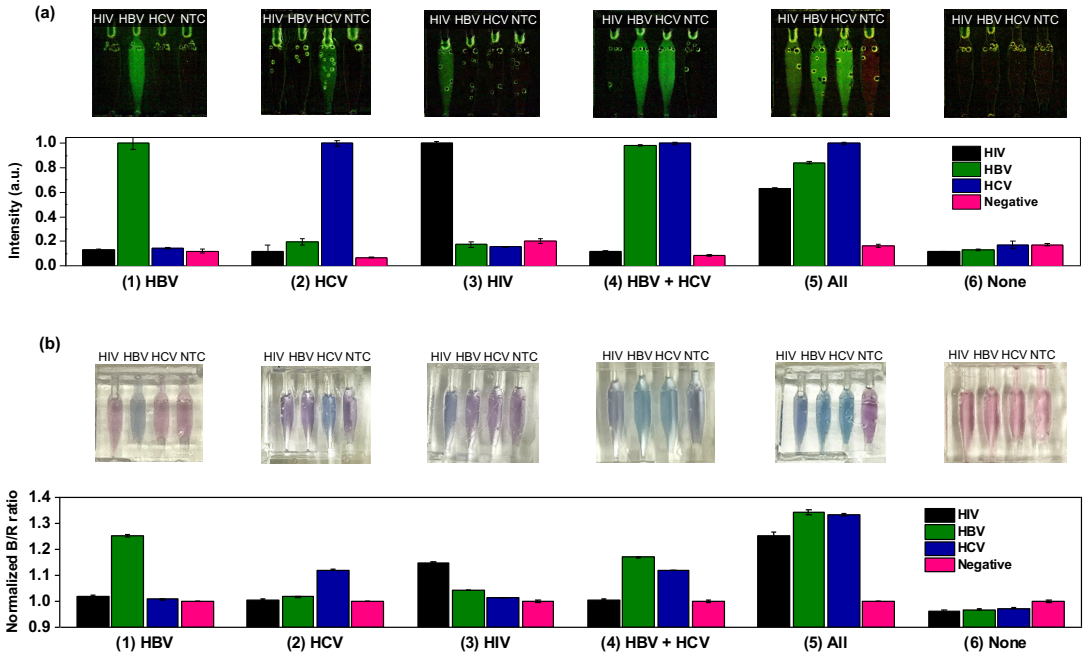

Fig. 3.8: Results of multiplexed LAMP amplification under various sample conditions with concurrent use of a fluorescent intercalating dye (EvaGreen) and a colorimetric dye (HNB). (a) Fluorescence images at the end of the 60-min incubation (top row), and the fluorescence intensity of each reaction chamber (bottom row) normalized with the maximum fluorescence intensity observed from all four chambers on the same chip. (b) Photographs of the colorimetric dye (top row) and color quantification (bottom row). The sample contains (1) only HBV; (2) only HCV; (3) only HIV; (4) both HBV and HCV; (5) HBV, HCV, and HIV; (6) non-template control.

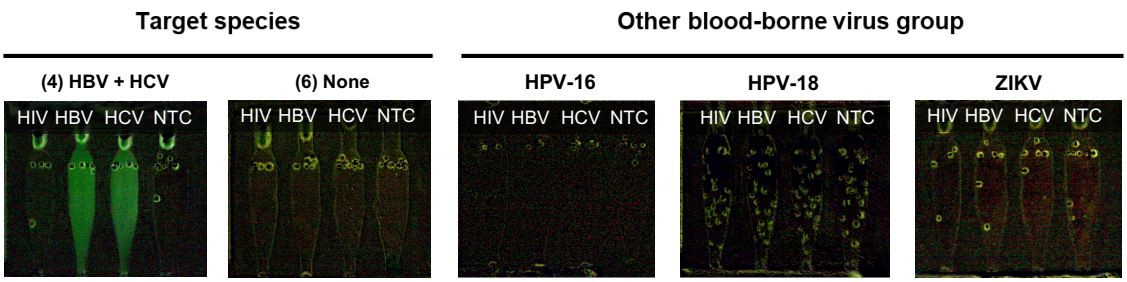

Fig. 3.9: Specificity test of our microfluidic chip with samples containing HBV, HCV, Human papillomavirus (HPV-16 and HPV-18), and zika virus (ZIKV).

The test results can be captured both in real-time (Fig. 3.8a) and at the end of the incubation (Fig. 3.8b). Real-time measurement is carried out with a fluorescent dye whose emission intensity is proportional to the number of amplicons. Fluorescence emission can also be detected at the endpoint in the visible spectrum. It is also possible to detect that LAMP amplification took place with a colorimetric dye such as HNB. The color of HNB dye changes from violet to blue with successful LAMP amplification [31]. Here, we use both fluorescent intercalating dye EvaGreen and colorimetric dye HNB. Both EvaGreen and HNB dye are pre-stored on chip in the dry form together with the LAMP reagents. The detection results are read with the naked eye and the smartphone application. To quantify the color signature, we extracted the R (red) and B (blue) values from the pixels in the imaging region in each reactor, calculated the B/R ratio, normalized this ratio with the corresponding value of the negative (non-template) control (Fig. 3.8b and Fig. 3.10c - 3.10d). We automated this whole with the custom-written smartphone application, which can be used at the POCT without a need for any specialized instrumentation (Fig. 3.10). The colorimetric results after 60-min amplification are displayed in Fig. 3.8b and are consistent with the fluorometric detection (Fig. 3.8a).

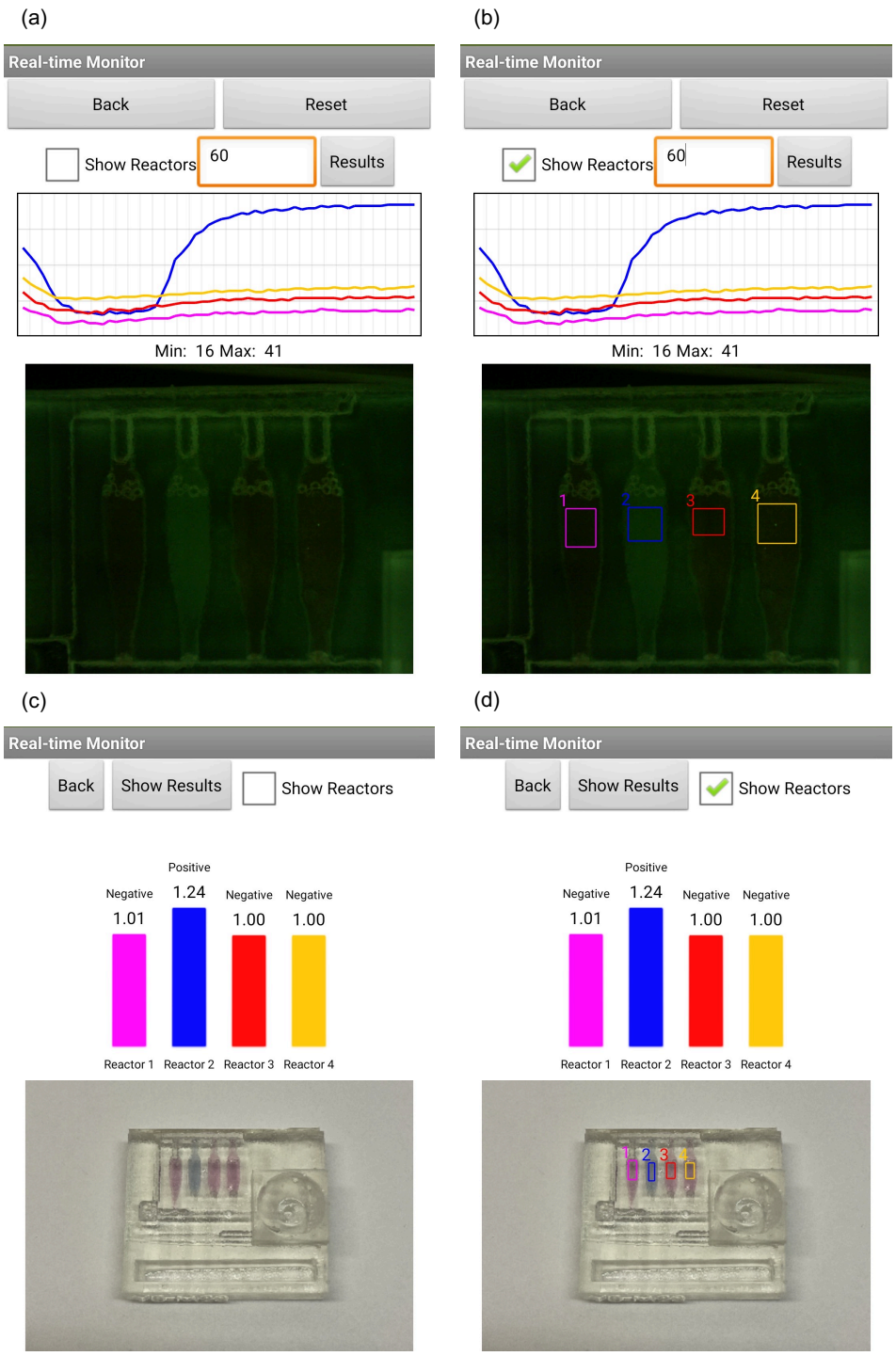

Fig. 3.10: Screenshots of the Android-based application for image analysis and result interpretation. (a) The application performed time-series image analysis and plotted amplification curves for each reactor. The plot is consistent with the result obtained with MATLAB. (b) The same result as (a) with the region of interest of each reactor being specified. (c) The application

performed image analysis, plotted each reactor's chamber-averaged B to R ratio, and displayed that the result for the second (from the left) reactor was positive. (d) The same result as (c) with the region of interest of each reactor being specified.

3.3.3 Real-time analysis for HIV, HBV, HCV specific amplification

The amplification process was also monitored in real-time during incubation. Fig. 3.11a and Fig. 3.11b depict, respectively, two representative cases when only a single target (HBV) is present and when all three targets (HIV, HBV, and HCV) are present. The figure also reports fluorescence images at 0 min, 20 min, and 60 min of the LAMP amplification. Only reactors specific to the present target(s) lighted up during incubation time.

Real-time curves enable us to estimate the target concentration in the sample based on the time needed for the amplification curve to exceed threshold intensity. The threshold time was defined as the time when the fluorescence emission reaches its half peak intensity. To demonstrate the capability of quasi-quantitative analysis of our microfluidic chip, we performed real-time LAMP with samples containing various concentrations of HBV and HCV. Samples were serial diluted in nuclease-free water and transported to a ready-to-use chip for LAMP amplification. Fig. 3.11c and Fig. 3.11d depict results with various concentrations of HBV DNA and HCV RNA samples, respectively. The real-time curves in Fig. 3.11c and Fig. 3.11d are sigmoid-shaped and shift to the right as the target concentration decreases. Similar to the threshold cycle analysis of quantitative PCR, the threshold time of LAMP increases linearly as a function of the logarithm of the target concentration in the sample (Fig. 3.11e - 3.11f). To establish limits of detection, we need to carry out a much greater number of experiments than we have done here. Our results indicate that we can detect down to 24 copies of HBV DNA and 76 copies of HCV RNA on chip. This detection sensitivity is comparable to that of the benchtop laboratory equipment [4, 15, 37].

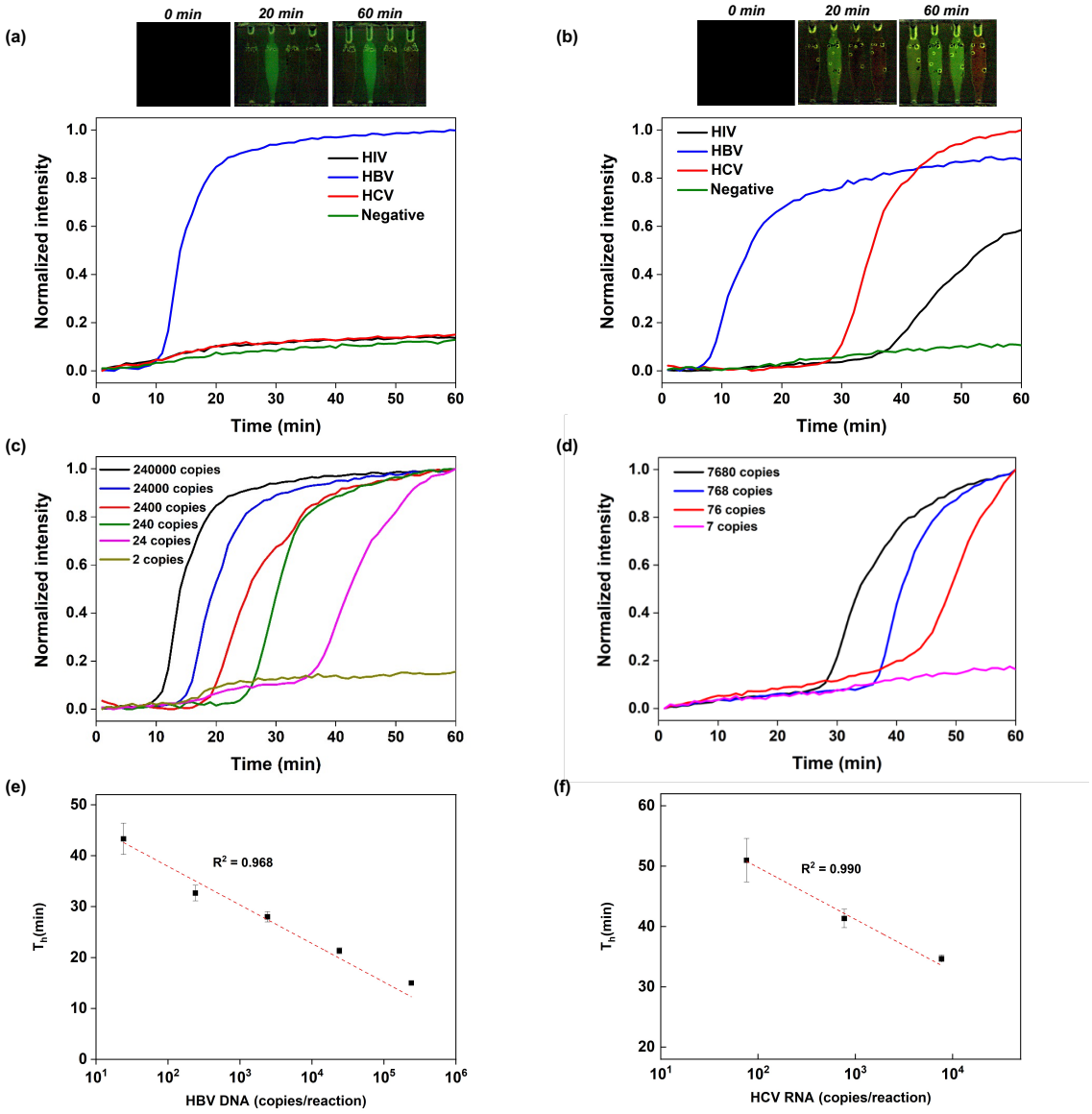

Fig. 3.11: Real-time amplification curves for multiplexed detection of targets on chip. (a) Fluorescent intensity emitted by an intercalating dye during the incubation of a sample containing only HBV (2.4×10^5 copies), (b) Fluorescent intensity emitted by an intercalating dye during the incubation of a sample containing HBV (2.4×10^5 copies), HIV (6.5×10^4 copies), and HCV (7680 copies). (c) Amplification curves for a dilution series of HBV DNA. (d) Amplification curves for a dilution series of HCV RNA. (e) LAMP threshold times as functions of the number of HBV DNA templates in the reaction volume. (f) LAMP threshold times as functions of the number of HCV RNA templates in the reaction volume.

3.3.4 Refrigeration-free storage of the microfluidic chip

To test the stability of our on-chip dried LAMP reagents, we prepared a few ready-to-use chips for HBV detection, stored them in a dark environment at room temperature and humidity, and tested the chips as a function of storage duration using the threshold time as the figure of merit. The reagents were dried in ambient conditions without any stabilizers. The performance of our dried reagents gradually decreased with storage time (Fig. 3.12), as reflected by the increase in the threshold time of the LAMP tests. Our dry storage, refrigeration-free method enables us to store chips for about 10 weeks in refrigeration-free conditions. This is likely insufficient for a commercial product but good enough for laboratory testing of chip efficacy.

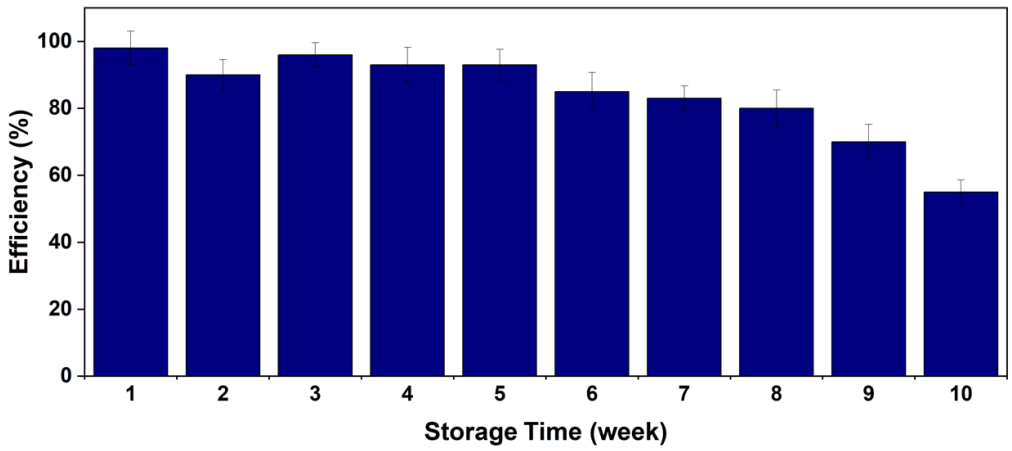

Fig. 3.12: Stability test of our on-chip dried LAMP reagents as a function of storage duration under ambient conditions. Efficiency (y-axis) is defined as $(Tt-Tt_0)/Tt_0$, where Tt and Tt_0 are, respectively, the measured threshold time and the threshold time measured with freshly dried reagents.

3.4 Discussion and Conclusions

We demonstrated a ready-to-use microfluidic device for multiplexed molecular detection of the bloodborne pathogens: HIV, HBV, and HCV extracted from human plasma. Co-detection of these pathogens is of significance since the routes of transmission of these three pathogens are similar,

and many HIV-infected patients are also infected with HCV and HBV. Furthermore, in the case of HCV, the standard of care mandates an antibody test followed up with a molecular test. A procedure results in many patients being lost to care for the lack of follow-up. A rapid molecular test at the point of need would facilitate the test and treat strategy.

Our device has several novel features and advantages. First, the flow control is based on capillary circuits that enable spontaneous chip filling driven by capillary forces and eliminates the need for more expensive moving members. Second, our thermally activated sealing with a phase-change material performs auto-sealing, which further simplifies the operational complexity and increases user-friendliness. Third, both the chip and the custom processor are portable for POCT. Fourth, fluorometric and colorimetric detections are carried out concurrently. The fluorometric detection enables real-time monitoring of the LAMP amplification reaction and quasi-quantification of the target concentration. Colorimetric detection enables readout with the naked eye, eliminating the need for instrumentation. Fifth, we developed an Android-based smartphone application that can process fluorescence images and endpoint photos to automate image analysis and result interpretation, replacing the previously used laptop computer running MATLAB. Sixth, all LAMP reagents were dry-stored on chip, making our chip ready-to-use and refrigeration-free. With our current storage method, the dried LAMP reagents on chip last for at least 10 weeks stored in a dark environment at room temperature and humidity. Seventh, the four-channel design enables multiplexed molecular detection of HIV, HBV, and HCV, together with a negative control. And we have shown that our chip has detection sensitivity comparable to the state-of-art.

A low-cost, user-friendly, and refrigeration-free ready-to-use microfluidic device is the key to molecular point-of-care testing for untrained individuals and resource-limited settings. Our microfluidic device has demonstrated its feasibility to eliminate the needs of centralized laboratory facilities and professional operators while maintaining a high detection sensitivity and specificity.

In future work, 1) the chip will be integrated with a superhydrophobic plasma separator [38] to provide sample-to-answer capability; 2) the smartphone application will be augmented to

provide thermal control for the incubation process in addition to the image acquisition and data analysis.

References

[1] UNAIDS. "AIDS statistics - 2021 fact sheet.".

[2] C. Beyrer and A. Pozniak, "HIV drug resistance—an emerging threat to epidemic control," *New England Journal of Medicine,* vol. 377, no. 17, pp. 1605-1607, 2017.

[3] H. W. Chen, T. Belinskaya, Z. Zhang, and W. M. Ching, "Simple Detection of Hepatitis B Virus in Using Loop-Mediated Isothermal Amplification Method," *Mil Med,* vol. 184, no. 7-8, pp. e275-e280, Jul 1 2019, doi: 10.1093/milmed/usy421.

[4] D. J. Shin, A. Y. Trick, Y. H. Hsieh, D. L. Thomas, and T. H. Wang, "Sample-to-Answer Droplet Magnetofluidic Platform for Point-of-Care Hepatitis C Viral Load Quantitation," *Sci Rep,* vol. 8, no. 1, p. 9793, Jun 28 2018, doi: 10.1038/s41598-018-28124-3.

[5] M. J. Alter, "Epidemiology of viral hepatitis and HIV co-infection," *Journal of Hepatology,* vol. 44, pp. S6-S9, 2006/01/01/ 2006, doi: https://doi.org/10.1016/j.jhep.2005.11.004.

[6] WHO. "Hepatitis B." https://www.who.int/news-room/fact-sheets/detail/hepatitis-b.

[7] D. Razavi-Shearer *et al.*, "Global prevalence, treatment, and prevention of hepatitis B virus infection in 2016: a modelling study," *The lancet Gastroenterology & hepatology,* vol. 3, no. 6, pp. 383-403, 2018.

[8] B. Maasoumy and H. Wedemeyer, "Natural history of acute and chronic hepatitis C," *Best practice & research Clinical gastroenterology,* vol. 26, no. 4, pp. 401-412, 2012.

[9] WHO. "Hepatitis C." https://www.who.int/news-room/fact-sheets/detail/hepatitis-c (accessed.

[10] P. Piot, M. Bartos, P. D. Ghys, N. Walker, and B. Schwartländer, "The global impact of HIV/AIDS," *Nature,* vol. 410, no. 6831, pp. 968-973, 2001, doi: 10.1038/35073639.

[11] WHO. "HIV/AIDS." https://www.who.int/news-room/fact-sheets/detail/hiv-aids (accessed.

[12] L. R. Saud *et al.*, "Hepatocellular carcinoma in patients coinfected with hepatitis B or C and HIV: more aggressive tumor behavior?," *European Journal of Gastroenterology & Hepatology,* vol. 33, no. 4, pp. 583-588, 2021.

[13] B. S. Batule, Y. Seok, and M. G. Kim, "Paper-based nucleic acid testing system for simple and early diagnosis of mosquito-borne RNA viruses from human serum," *Biosens Bioelectron,* vol. 151, p. 111998, Mar 1 2020, doi: 10.1016/j.bios.2019.111998.

[14] M. Kubista *et al.*, "The real-time polymerase chain reaction," *Molecular Aspects of Medicine,* vol. 27, no. 2, pp. 95-125, 2006/04/01/ 2006, doi: https://doi.org/10.1016/j.mam.2005.12.007.

[15] Y. Seok, Q. Yin, H. Bai, and H. H. Bau, "Sensitive, Single-Pot, Two-Stage Assay for Hepatitis Viruses," *Analytical Chemistry,* 2022.

[16] N. Tomita, Y. Mori, H. Kanda, and T. Notomi, "Loop-mediated isothermal amplification (LAMP) of gene sequences and simple visual detection of products," *Nat Protoc,* vol. 3, no. 5, pp. 877-82, 2008, doi: 10.1038/nprot.2008.57.

[17] T. Notomi *et al.*, "Loop-mediated isothermal amplification of DNA," *Nucleic acids research,* vol. 28, no. 12, pp. e63-e63, 2000.

[18] L. Becherer, N. Borst, M. Bakheit, S. Frischmann, R. Zengerle, and F. von Stetten, "Loop-mediated isothermal amplification (LAMP) – review and classification of methods for sequence-specific detection," *Analytical Methods,* vol. 12, no. 6, pp. 717-746, 2020, doi: 10.1039/c9ay02246e.

[19] N. A. Tanner, Y. Zhang, and T. C. Evans, Jr., "Visual detection of isothermal nucleic acid amplification using pH-sensitive dyes," *Biotechniques,* vol. 58, no. 2, pp. 59-68, Feb 2015, doi: 10.2144/000114253.

[20] R. R. G. Soares *et al.*, "Sub-attomole detection of HIV-1 using padlock probes and rolling circle amplification combined with microfluidic affinity chromatography," *Biosens Bioelectron,* vol. 166, p. 112442, Oct 15 2020, doi: 10.1016/j.bios.2020.112442.

[21] S. Hongjaisee *et al.*, "Rapid visual detection of hepatitis C virus using a reverse transcription loop-mediated isothermal amplification assay," *Int J Infect Dis,* vol. 102, pp. 440-445, Jan 2021, doi: 10.1016/j.ijid.2020.10.082.

[22] H. Kong *et al.*, "A RT-LAMP based hydrogen ion selective electrode sensing for effective detection HIV-1 RNA with high-sensitivity," *Sensors and Actuators B: Chemical,* vol. 329, 2021, doi: 10.1016/j.snb.2020.129118.

[23] M. El-Tholoth, H. Bai, M. G. Mauk, L. J. Saif, and H. H. Bau, "A Portable, 3-D Printed, Microfluidic Device for Multiplexed, Real Time, Molecular Detection of Porcine Epidemic Diarrhea Virus, Transmissible Gastroenteritis Virus, and Porcine Deltacoronavirus at the Point of Need," *Lab Chip,* 10.1039/D0LC01229G 2021, doi: 10.1039/D0LC01229G.

[24] S. C. Liao *et al.*, "Smart cup: A minimally-instrumented, smartphone-based point-of-care molecular diagnostic device," *Sensor Actuat B-Chem,* vol. 229, pp. 232-238, Jun 28 2016, doi: 10.1016/j.snb.2016.01.073.

[25] J. Saldanha *et al.*, "An international collaborative study to establish a World Health Organization international standard for hepatitis B virus DNA nucleic acid amplification techniques," *Vox Sanguinis,* vol. 80, no. 1, pp. 63-71, 2001, doi: https://doi.org/10.1046/j.1423-0410.2001.00003.x.

[26] J. Saldanha *et al.*, "World Health Organization collaborative study to establish a replacement WHO international standard for hepatitis C virus RNA nucleic acid amplification technology assays," *Vox Sanguinis,* vol. 88, no. 3, pp. 202-204, 2005, doi: https://doi.org/10.1111/j.1423-0410.2005.00606.x.

[27] J. Song, C. Liu, M. G. Mauk, J. Peng, T. Schoenfeld, and H. H. Bau, "A Multifunctional Reactor with Dry-Stored Reagents for Enzymatic Amplification of Nucleic Acids," *Anal Chem,* vol. 90, no. 2, pp. 1209-1216, Jan 16 2018, doi: 10.1021/acs.analchem.7b03834.

[28] K. Kadimisetty *et al.*, "Fully 3D printed integrated reactor array for point-of-care molecular diagnostics," *Biosensors and Bioelectronics,* vol. 109, pp. 156-163, 2018/06/30/ 2018, doi: https://doi.org/10.1016/j.bios.2018.03.009.

[29] Y. Seok, B. S. Batule, and M.-G. Kim, "Lab-on-paper for all-in-one molecular diagnostics (LAMDA) of zika, dengue, and chikungunya virus from human serum," *Biosensors and Bioelectronics,* vol. 165, p. 112400, 2020.

[30] A. Ito and K. Ueno, "Successive chelatometric titration of calcium and magnesium using Hydroxy Naphthol Blue (HNB) indicator," *Bunseki kagaku,* vol. 19, no. 3, pp. 393-397, 1970, doi: 10.2116/bunsekikagaku.19.393.

[31] M. Goto, E. Honda, A. Ogura, A. Nomoto, and K. Hanaki, "Colorimetric detection of loop-mediated isothermal amplification reaction by using hydroxy naphthol blue," *Biotechniques,* vol. 46, no. 3, pp. 167-72, Mar 2009, doi: 10.2144/000113072.

[32] Shaileen and Jos\'e, "MIT App Inventor: Enabling Personal Mobile Computing," *arXiv pre-print server,* 2013-10-24 2013, doi: None arxiv:1310.2830.

[33] I.-C. Yeh and G. Hummer, "Diffusion and Electrophoretic Mobility of Single-Stranded RNA from Molecular Dynamics Simulations," *Biophysical Journal,* vol. 86, no. 2, pp. 681-689, 2004, doi: 10.1016/s0006-3495(04)74147-8.

[34] Y. Seok, Q. Yin, H. Bai, and H. H. Bau, "Sensitive, Single-Pot, Two-Stage Assay for Hepatitis Viruses," *Analytical Chemistry,* vol. 94, no. 3, pp. 1778-1786, 2022, doi: 10.1021/acs.analchem.1c04480.

[35] L. V, "Application of Real Time Loop Mediated Isothermal Amplification Assay on Dried Blood Spots in the Detection of HCV RNA among High Risk Patients," *Journal of Emerging Diseases and Virology,* vol. 2, no. 1, 2016, doi: 10.16966/2473-1846.111.

[36] J. Song *et al.*, "Smartphone-Based Mobile Detection Platform for Molecular Diagnostics and Spatiotemporal Disease Mapping," (in eng), *Anal Chem,* vol. 90, no. 7, pp. 4823-4831, Apr 3 2018, doi: 10.1021/acs.analchem.8b00283.

[37] N. B. Quoc, N. D. N. Phuong, and N. N. B. Chau, "Closed tube loop-mediated isothermal amplification assay for rapid detection of hepatitis B virus in human blood," *Heliyon,* vol. 4, no. 3, p. e00561, 2018.

[38] C. Liu *et al.*, "A high-efficiency superhydrophobic plasma separator," *Lab Chip,* vol. 16, no. 3, pp. 553-560, 2016, doi: 10.1039/c5lc01235j.

Chapter 4 Microfluidic Device with Capillary Circuits for Multiplexed, Two-stage NAATs

4.1 Introduction

The microfluidic devices previously discussed in chapters 2 and 3 were developed for multiplexed, single-stage NAATs. We have demonstrated with the LAMP assay that our devices can be successfully used for the co-detection of three co-endemic pig viruses (PEDV, TGEV, and TGEV) and three human bloodborne viruses (HIV, HBV, and HCV) that co-infect a significant number of individuals worldwide. In earlier work, our group has developed a two-stage isothermal enzymatic amplification that combines RPA and LAMP, dubbed Penn RAMP, to achieve a high level of multiplexing. In some cases, Penn RAMP has also achieved higher sensitivity and better tolerance to inhibitors than the standalone LAMP [1-4].

In benchtop settings (Fig. 4.1a), the first stage of Penn-RAMP is multiplexed RPA at 37 °C for 10-20 min in a single tube with RPA primer sets for all targets of interest; Next, the RPA products are aliquoted into multiple LAMP tubes, each with a unique LAMP primer set dedicated to a single target. The multiple LAMP reactors are then incubated with a thermal cycler at 63 °C for 1 hr. The Penn RAMP in its benchtop format requires the user to open the amplicon-rich RPA tube to aliquot the RPA products into various LAMP tubes [1], which risks contamination of the workspace with amplicons and false-positive results in future tests.

To address this issue, our group developed a single-tube Penn RAMP, wherein the RPA solution is loaded to the tube's lid while the LAMP solution is loaded into the tube's body (Fig. 4.1b). The thermal cycler's block and lid temperatures are first set to the RPA incubation temperature of 38-42 °C for 10-20 min. Next, the RPA solution in the lid is either spined down into the tube with a centrifuge or mixed with the tube's contents by turning the closed tube upside down a few times. The tube is then incubated for 20-40 min with the block and lid temperatures set to the LAMP incubation temperature of about 63 °C. During this entire process, the Penn RAMP tube remains closed, eliminating the risk of contamination [3].

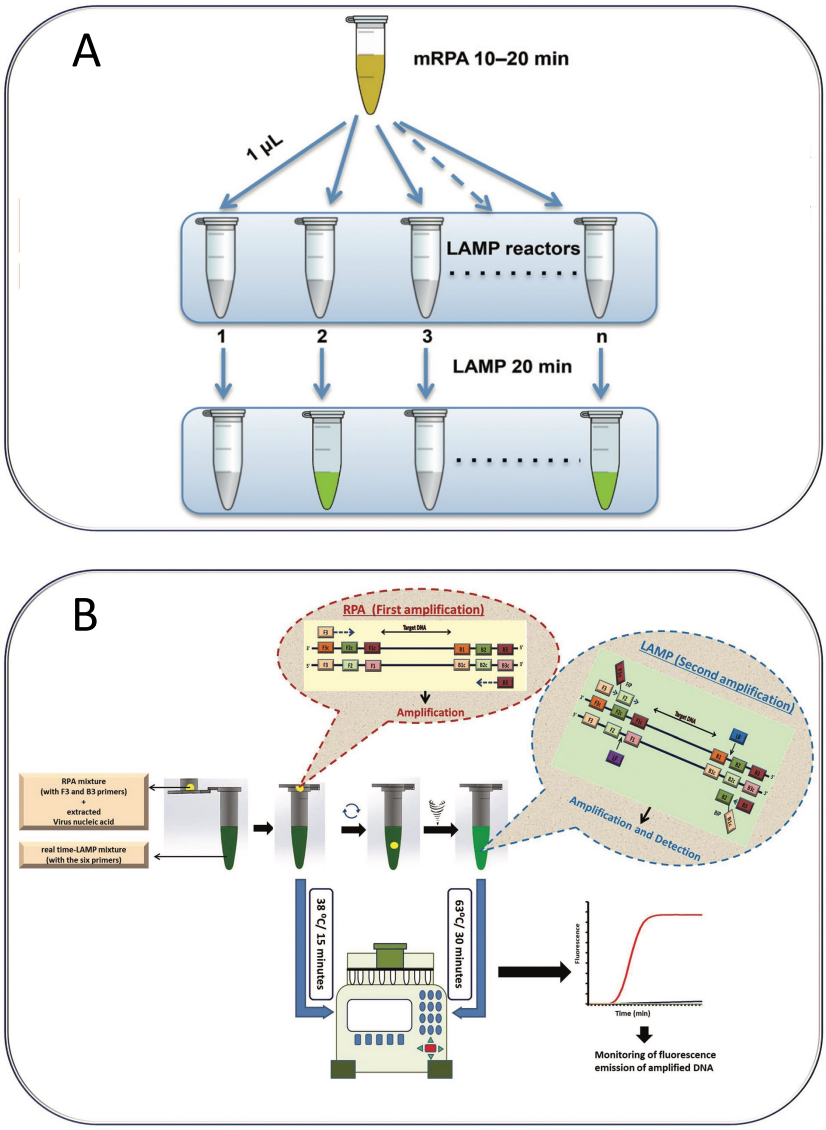

Fig. 4.1: A schematic illustration of Penn RAMP in benchtop settings: (A) Penn RAMP comprises a single tube for multiplexed RPA and multiple LAMP tubes, each dedicated to a single target [1]; (B) Penn RAMP in a single-tube format. The RPA is performed in the tube's lid while the LAMP is carried out in the tube's body. The tube remains sealed at all times [3].

However, the Penn RAMP in a single-tube format has certain limitations: 1) Unless probes with distinct emission spectra are used, the process is limited to detecting a single target; 2) The RPA and LAMP buffers are incompatible. The optimal RPA:LAMP volume ratio is around 1/15 [3]. When carried out in a single tube, typically, the RPA volume in the lid is 5 µL, which

requires about 70-µL LAMP solution in the tube while a standalone LAMP can be carried out with a volume of 10-20 µL. That is, the single-tube Penn RAMP consumes more reagents and is, therefore, less cost-effective than standalone LAMP. In this chapter, we introduce a portable, low-cost, rapid, 3D-printed microfluidic device with capillary circuits for real-time molecular detection of infectious laryngotracheitis virus (ILTV) in chickens with Penn RAMP.

ILTV is a DNA virus that belongs to the Gallid alphaherpesvirus 1 (GaHV-1) species of the *Alphaherpesvirinae* subfamily within the *Herpesviridae* family [5-7] and causes a common respiratory disease in chickens. The disease causes respiratory distress and leads to significant production losses due to diminished egg production, poor feed conversion rates, high mortality rates, and increased susceptibility to other respiratory tract pathogens [6, 8]. The rapid, specific, simple molecular detection of ILTV at the point of need is crucial to enable chicken farms to take timely action and contain the spread of infection.

Traditional diagnosis of the disease depends on clinical signs and necropsy findings. Confirmative laboratory diagnosis of ILT is performed by virus isolation, immunofluorescence techniques, neutralization assay, enzyme-linked immunosorbent assay (ELISA), as well as conventional PCR and quantitative real-time PCR (qPCR) [6, 9-18]. However, the above-mentioned diagnostic methods are unsuitable for simple, specific, and rapid ILTV detection outside centralized laboratories, such as at rudimentary veterinary stations and particularly in developing countries where expensive equipment and skilled staff are in short supply. The need to send samples to centralized laboratories and await results may delay the implementation of control measures with significant adverse consequences.

Loop-mediated isothermal amplification (LAMP) of nucleic acids is a simpler alternative to PCR with a comparable sensitivity [19-23]. Penn RAMP is a two-stage isothermal molecular detection that uses recombinase polymerase amplification (RPA) as the first-stage amplification, followed by LAMP, the second stage [1, 3, 4]. Both LAMP and Penn RAMP use a strand-displacing polymerase, obviating the need for a high-temperature ‘melting’ step and the temperature cycling used in PCR. In contrast to PCR that uses a pair of primers, LAMP employs four primers, in addition to two loop primers, which anneal to different regions of the nucleic acid

template. The additional primers may improve specificity [24]. Moreover, compared to the standalone LAMP assay, the two-stage nested Penn RAMP is more sensitive and tolerant to inhibitors [1-4].

A molecular diagnostics test (NAAT, nucleic acid amplification test) comprises two major components: (A) Enzymatic amplification and (B) Detection of the amplification product, either during amplification (real-time) or post-amplification (end-point detection). Multiple methods have been reported for amplicon detection in LAMP assays, including gel electrophoresis [25], fluorescence [25], naked eye (turbidity or color change) [25], and bioluminescence [26-28]. In bioluminescence and fluorescence-based detection, LAMP amplicons are monitored in a real-time manner, enabling quantification [29-31].

NAATs can be implemented in microfluidic formats, such as palm-sized plastic cartridges with microscale fluid circuits for sample processing and analysis [32, 33]. Such microfluidic chips offer lower cost, automated and streamlined operation, portability, sample containment, and ease of use, facilitating operation by laypeople. Multiple unit operations (e.g., lysis, nucleic extraction) can be integrated into single-use (disposable) chips for nucleic acid amplification tests [34, 35].

This chapter describes a LAMP assay and a Penn RAMP assay for ILTV detection and the implementation of these assays in a microfluidic chip suitable for field molecular detection and quasi-quantification of ILTV infection. Our microfluidic chip had four reaction chambers, one of which acts as a negative control. The other three chambers can be used either to test three different samples for the same pathogen or a single sample split across the three chambers to detect co-morbidity with different pathogens.

4.2 Materials and Methods

4.2.1 Chemicals and materials

The clear resin FLGPCL04 for 3D printing was supplied from Formlabs™ (Somerville, MA, USA). Polyethylene glycol (PEG) 3350 for chip surfaces' coating was obtained from Sigma Aldrich, Inc. (St. Louis, MO, USA). AM1836 5× MagMax 96 Viral Extraction kit was adopted from Life Technologies™ (Ambion®, Austin, TX, USA). RPA and LAMP primers were ordered from

Integrated DNA Technologies, Inc. (Coralville, IA, USA). Loop amp DNA amplification Kit was supplied from Eiken Chemicals Co. (Tokyo, Japan). Bst 2.0 WarmStartTM DNA polymerase was purchased from New England Biolabs (Ipswich, MA, USA). EvaGreen® dye was supplied from Biotium Inc. (Hayward, CA, USA). Nuclease-free water was acquired from Invitrogen (Carlsbad, CA, USA). OptiGene ISO-001 isothermal mastermix was purchased from Pro-Lab Diagnostics, Inc. (Round Rock, TX, USA). TwistAmp® Basic kit was purchased from TwistDx^{TM} (Cambridge, UK).

4.2.2. Virus and clinical samples

Previously isolated ILTV and 11 clinical samples from diseased chickens with respiratory distress were supplied by the Department of Molecular Biology, School of Veterinary Medicine, University of Pennsylvania (Philadelphia, PA, USA). The ILTV was propagated on chorioallantoic membranes (CAM) of embryonated chicken eggs (ECEs), followed by identification using histopathology for the intranuclear inclusions detection and the virus detected molecularly by conventional PCR [14]. The number of genomic DNA copies of ILTV was quantified as previously reported [36]. The genomic concentration is 5×10^5 copies per µL.

4.2.3 DNA extraction

DNA/RNA extraction was carried out with AM1836 5× MagMax 96 Viral Extraction kit (Ambion®, Austin, TX, USA) following the instructions from the manufacturer.

4.2.4 RPA and LAMP primers

Genomic sequences of various ILTV strains from the GeneBank were analyzed after alignment to identify conserved sequences. A 296-nt sequence in the polymerase gene of ILTV was used as a target due to its high similarity among the analyzed strains. The RPA and LAMP primers (Fig. 4.2) were designed with the PrimerExplorer V5 software (Eiken Chemical Co. Ltd.). The designed primers were screened using NCBI database BLAST (http://www.ncbi.nlm.nih.gov, accessed on 2

February 2020) for cross-reaction with other chicken respiratory tract viruses, including Mareks disease virus (MDV), Newcastle disease virus, and avian influenza viruses (H5N1, H9N2, and H5N8). No cross-reaction was detected. The RPA and LAMP primers were diluted to a 100 µM concentration using nuclease-free water.

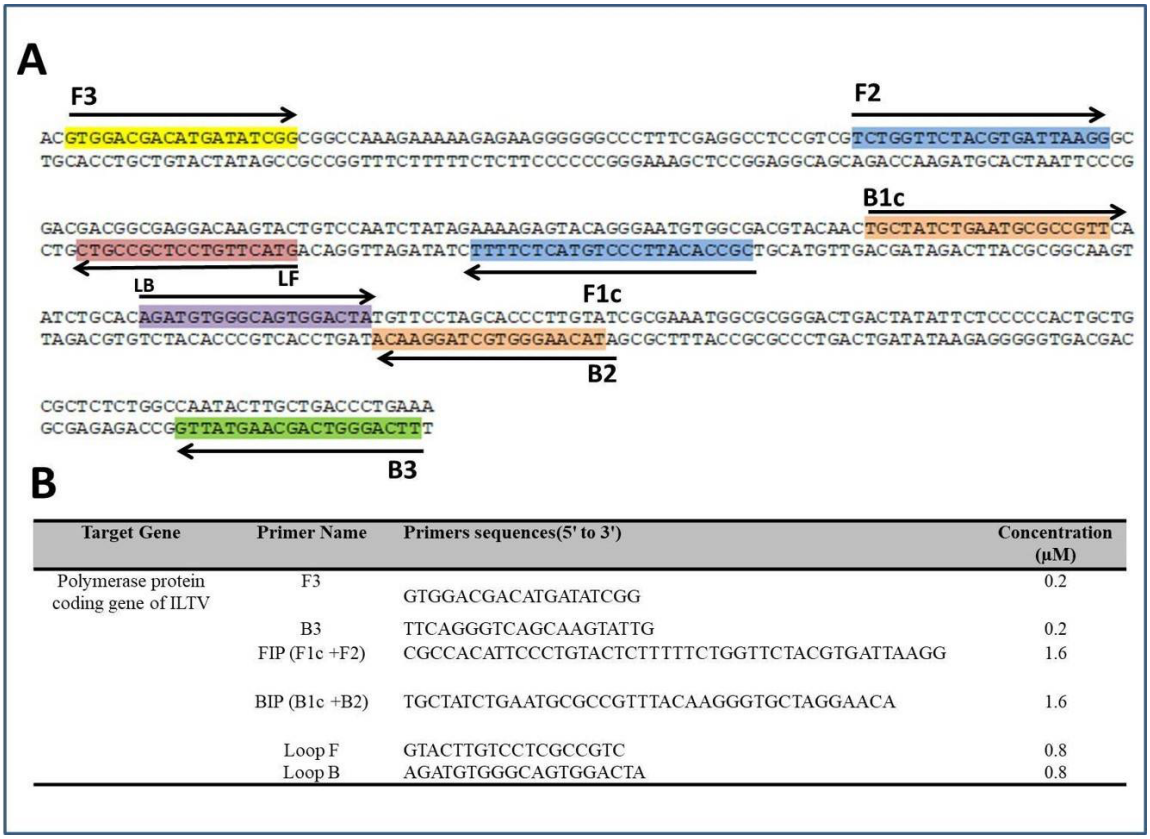

Target Gene	Primer Name	Primers sequences(5' to 3')	Concentration (µM)
Polymerase protein coding gene of ILTV	F3	GTGGACGACATGATATCGG	0.2
	B3	TTCAGGGTCAGCAAGTATTG	0.2
	FIP (F1c +F2)	CGCCACATTCCCTGTACTCTTTTTCTGGTTCTACGTGATTAAGG	1.6
	BIP (B1c +B2)	TGCTATCTGAATGCGCCGTTTACAAGGGTGCTAGGAACA	1.6
	Loop F	GTACTTGTCCTCGCCGTC	0.8
	Loop B	AGATGTGGGCAGTGGACTA	0.8

Fig. 4.2: RPA and LAMP primers aligned along the ILTV amplicon. (A) ILTV amplified sequence with the primers sites: F3, B3, BIP, FIP, LF, and LB. Arrows show the direction of extension. (B) Primers sequence for ILTV RPA and LAMP assays. F3 and B3 primers were used for RPA, while all six primers were used for LAMP.

4.2.5 Benchtop LAMP amplification

The LAMP assay was performed to detect the polymerase gene of ILTV using the loop amp DNA amplification Kit. The 10-µL reaction mixture consisted of LAMP primers (Fig. 4.2B), 5 µL of 2× Reaction Mix, 0.4 µL of Bst 2.0 WarmStart DNA polymerase, 0.5 µL of 1× EvaGreen® dye

(Biotium Inc., Hayward, CA, USA), 0.6 µL of viral DNA template, and nuclease-free water to the total volume of 10 µL. Fluorescence signals from DNA amplificons were observed with the 7500 Fast Real-Time PCR system (Applied Biosystems, Carlsbad, CA, USA) for 30 min at 63 °C. Template-free controls were included in each run to guarantee the absence of contamination. Nucleic acid extracts of Escherichia Coli isolate, Newcastle disease virus (NDV), and infectious bronchitis virus (IBV) were used as negative controls.

4.2.6 Microfluidic chip for Penn RAMP and LAMP

Our 3D-printed microfluidic chip (31 mm × 25 mm × 3 mm, Fig. 4.3a) consists of one RPA chamber with a volume of 45 µL and four 20-µL LAMP reaction chambers. The chip was designed with SolidWorks 2020 (DS SolidWorks™, Waltham, MA, USA) and fabricated with a low-force Stereolithography (LFS) 3D printer Form 3 (Formlabs™, Somerville, MA, USA) using the clear resin FLGPCL04 (Formlabs™, Somerville, MA, USA). Fig. 4.3b - 4.3e depicts the chip processing steps: The 3D-printed chips were post-processed with Form Wash (Formlabs™, Somerville, MA, USA) and Form Cure (Formlabs™, Somerville, MA, USA) following the manufacturer's instructions; The inner surface of the LAMP and RPA reaction chambers were then coated with polyethylene glycol (PEG) 3350 aqueous solution (2%) for 30 min to reduce the absorbance of polymerase by the 3D-printed materials [37, 38]; Next, solutions with different LAMP primers were loaded into the various LAMP reactors via the uncapped distribution channel, and the chip was air-dried at room temperature for 2 hr; Last, the open distribution channel was capped with a PCR tape.

4.2.7 Penn RAMP and LAMP amplification on chip

Since LAMP primers (Fig. 4.2B) were pre-stored in individual LAMP reactors during chip preparation (Fig. 4.3c - 4.3d), the generic LAMP mixture (OptiGene ISO-001 isothermal mastermix) sans primers could be loaded into the chip. The 20-µL generic LAMP mix comprised 12 µL of ISO-001 mastermix (OptiGene, Horsham, UK), 1 µL of EvaGreen® dye (Biotium Inc., Hayward, CA, USA), and nuclease-free water to the total volume of 20 µL. The 45-µL RPA

reaction mix consisted of 1× rehydrated TwistAmp® Basic reaction mix (TwistDx™, Cambridge, UK), F3 and B3 primers (480 nM, Fig. 4.2B), 14 mM of MgAc, 2.7 µL of DNA template with various concentrations, and nuclease-free water to 45 µL. When performing LAMP-only tests, the pseudo-RPA reaction mix that does not include TwistAmp® Basic reaction mix was used. When performing limit of detection tests with standalone LAMP, 1.2 µL of viral DNA template was added to the 20-µL LAMP mixture, and the RPA chamber was left empty at all times.

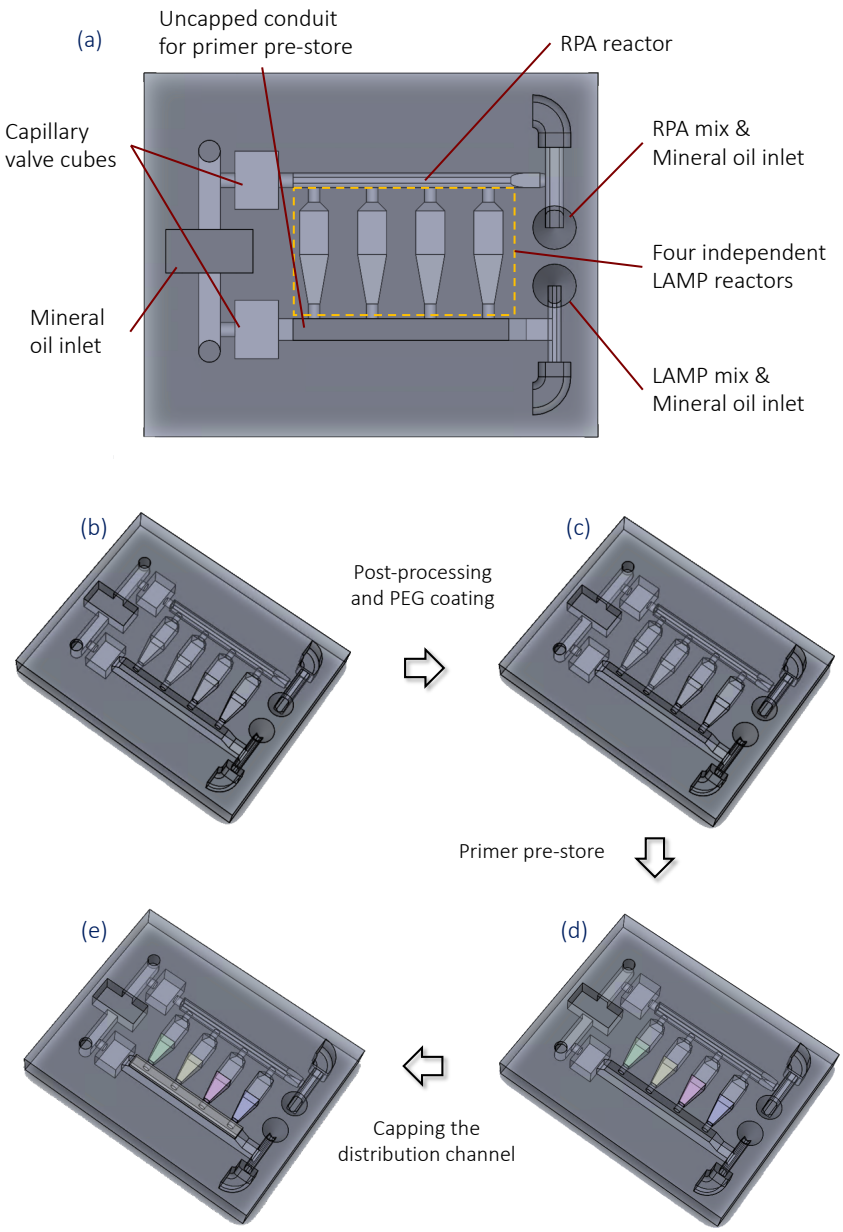

Fig. 4.3: Schematic illustration of microfluidic chip design and chip preparation process.

Fig. 4.4 depicts the chip preparation: First, the generic LAMP mixture was loaded via the LAMP inlet, followed by a draining step to remove the liquid from the common distribution channel (Fig. 4.4A). In this process, the capillary valves retain the reaction mix in the LAMP reaction chambers. Second, the RPA mixture was loaded via the RPA inlet followed by a draining process to clear the head of the T-junction, taking advantage of a capillary vale to keep the RPA solution

in place (Fig. 4.4B); Last, mineral oil was inserted to provide oil seal by isolating the reaction solutions from the ambient (Fig. 4.4C). The chip was then ready for incubation. Next, the chip was incubated with our custom processor (Fig. 2.1) that comprises an electric resistant heater Thermofoil HK6911 (Minneapolis, MN, USA), a Type-K thermocouple Omega Engineering TT-K30-SLE (Norwalk, CT, USA), a Raspberry Pi 4 Model B (Cambridge, UK), and a portable USB camera DinoLite AM4113TGFBW (Taiwan, China). The Raspberry Pi works as a central controller, reading the temperatures measured by the thermocouple, calculating the appropriate power to be supplied to the heater based on a proportional-integral-derivative (PID) algorithm, and adjusting the heater power with pulse-width modulation (PWM). The USB camera includes seven built-in blue light-emitting diodes (LEDs) for excitation, an emission filter with a 510-nm wavelength cut-off, a CCD camera detection, and a USB connection. This microscope is appropriate for EvaGreen® dyes and can monitor all reactors simultaneously without the need for scanning. The USB camera was mounted on the top of the custom processor and programmed to take a fluorescence image every minute. During incubation, the chip was first heated up to 37 °C for 10 min, followed by 63 °C for 30 min (Fig. 4.4D).

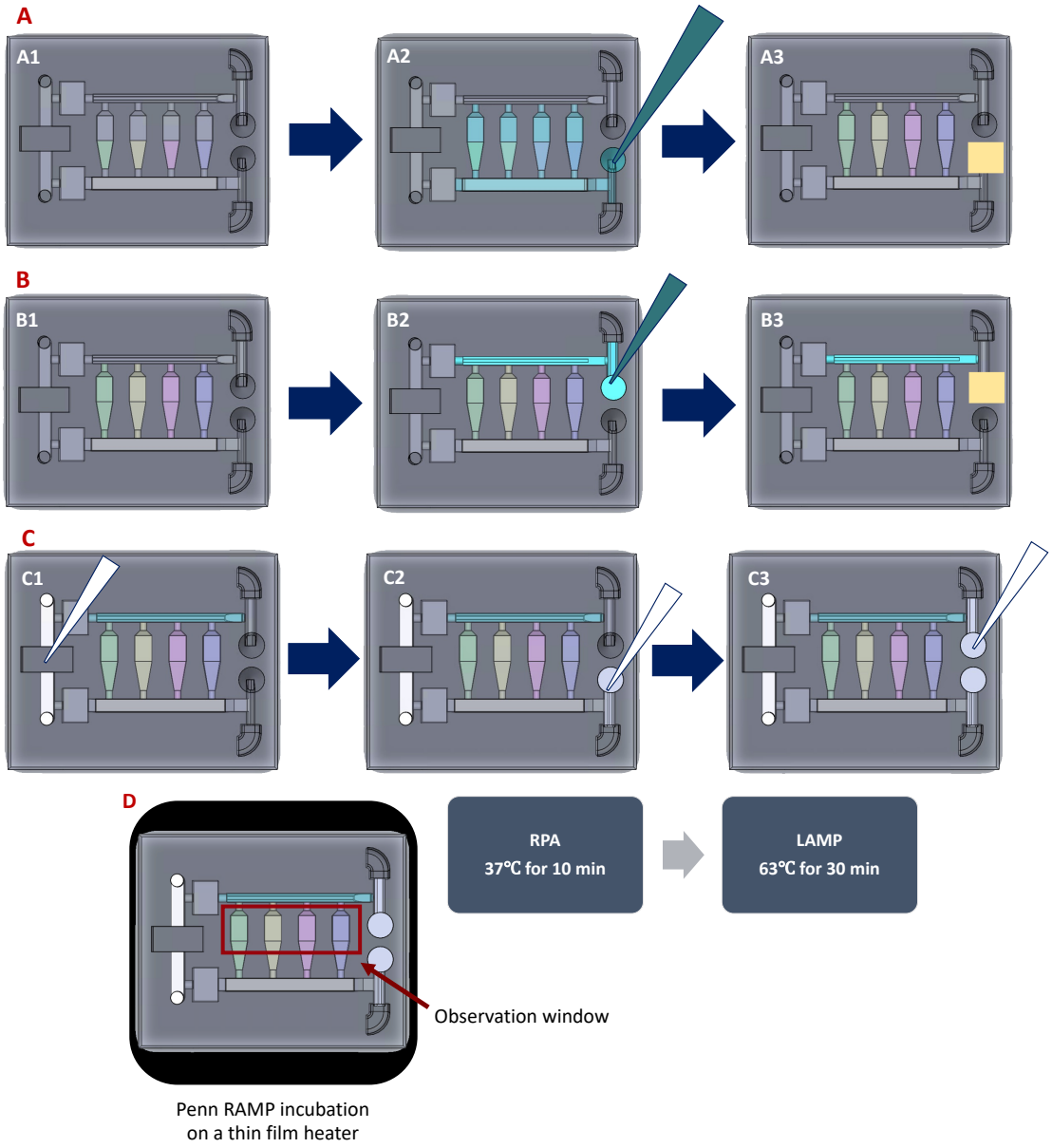

Fig. 4.4: A schematic depiction of device operation: (A) Loading the LAMP reaction mix for the second-stage amplification (A2) followed by draining the common conduit that connects the various LAMP chambers (A3). (B) Loading the RPA reaction mix for the first-stage amplification (B2) followed by a draining excess RPA solution to make room for the sealing mineral oil (B3). (C) Insertion of mineral oil for sealing. (D) Two-stage incubation with our custom processor.

The fluorescence images in JPG format were then analyzed with MATLAB R2021b (MathWorks, Natick, MA, US) and our Android-based smartphone application previously reported in Chapter 3. Normalized fluorescence intensities of each LAMP reaction chamber were plotted versus time. We defined the threshold time as the time when the fluorescence emission reaches its half peak intensity.

The specificity of our microfluidic chip was assessed by testing various pathogens available in our laboratory such as IBV (8×10^5 gRNA copies per µL), NDV (10^3 gRNA copies per µL), E. coli (10^{10} PFU per µL), transmissible gastroenteritis virus (TGEV, 10^3 gRNA copies per µL), porcine epidemic diarrhea virus (PEDV, 10^3 gRNA copies per µL), and porcine deltacoronavirus (PDCoV, 10^3 gRNA copies per µL). Each microorganism was tested three times and presented a negative result, while controls tested with appropriate primers and, otherwise, identical conditions were positive.

4.2.8 Penn RAMP simulation

The Penn RAMP on-chip implementation was examined with a COMSOL simulation to better understand the migration of primers, reaction buffers, and nucleic acid amplicons among the various reaction chambers. A 3D model of our microfluidic chip (Fig. 4.3a) was constructed with SolidWorks 2020 (DS SolidWorks™, Waltham, MA, USA) and imported into the COMSOL Multiphysics (COMSOL, Stockholm, Sweden) software, providing the geometry for the numerical simulations (Fig. 4.5). COMSOL's *Chemistry*, *Transport of Diluted Species*, and *Laminar Flow* modules were selected to simulate, respectively, on-chip RPA amplification, on-chip LAMP amplification, and evaporation-induced fluid flow. The *Transport of Diluted Species* module was also used to study the convective and diffusive transport of all species of interest.

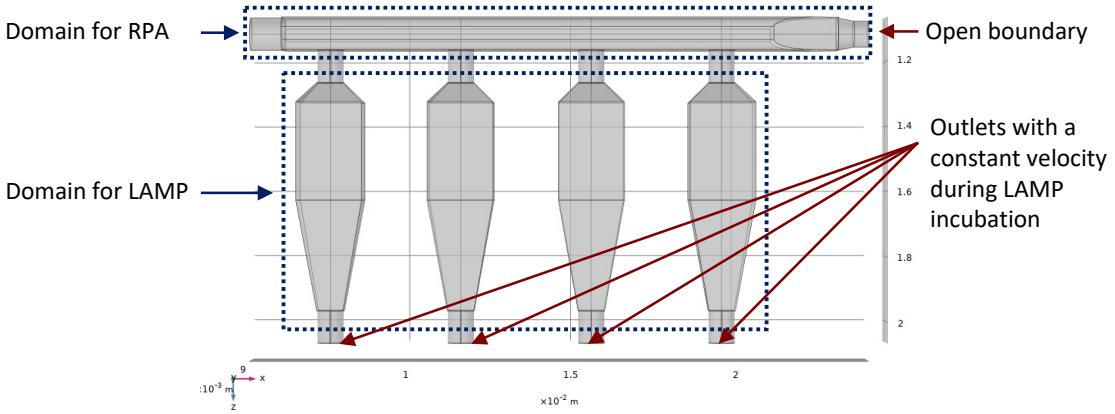

Fig. 4.5: Geometry complementary to the microfluidic chip with one RPA and four LAMP reaction chambers for COMSOL simulation.

The simulation of the RPA amplification involves 15 species (Table 4.1) and 12 chemical reactions as reported in Moody [39] with a few modifications/corrections (Table 4.2). The simulation of LAMP was implemented with an empirical mathematical model previously reported in Liu [40]. The empirical LAMP model is a logistic equation that requires the minimum and maximum concentrations of the target nucleic acids and a single reaction rate constant (obtained from Liu's paper [40]) as inputs. To examine the interference between RPA and LAMP buffers, we use $C_{\text{LAMP buffer}}$ and $C_{\text{RPA buffer}}$ to denote, respectively, the dimensionless LAMP buffer and the RPA buffer concentrations normalized with their initial values. That is, the initial $C_{\text{LAMP buffer}}$ is 1 in the LAMP reaction chambers and 0 in the RPA chamber, while the initial $C_{\text{RPA buffer}}$ is 0 in the LAMP reaction chambers and 1 in the RPA chamber. Due to the evaporation during the LAMP amplification and the resulting advection, the $C_{\text{LAMP buffer}}$ in the LAMP chambers gets concentrated. We hypothesize that the LAMP reaction would only occur where the local $C_{\text{LAMP buffer}}$ is smaller than 1.2. Since the LAMP amplification works reasonably well when blended with the RPA buffer in the ratio of 1:9 [3], we assume that the LAMP reaction takes place only when the local $C_{\text{LAMP buffer}}$ is larger than 0.9 and the local $C_{\text{RPA buffer}}$ is smaller than 0.1. Next, according to our heating settings, we limited the RPA reaction to the first 10 min and the LAMP amplification between 15 and 60 min. We assumed that the heating and the RPA reaction start immediately

after filling. The time window between 10 and 15 min is for temperature ramp-up from the RPA to the LAMP working temperature.

Table 4.1: Species of interest involved in simulating the RPA amplification as reported in Moody [39].

Species	Description
D	DNA template
F	Primers
G	Single-stranded DNA binding protein
P	Polymerase
R	Recombinase complex
dNTP	Deoxyribonucleotide triphosphate
PPi	Inorganic pyrophosphate
FD	The complex formed between *F* and *D*
FG	The complex formed between *F* and *G*
FGR'	The unstable complex formed among *F*, *G*, and *R*
FGR	The stable complex formed among *F*, *G*, and *R*
FGnR'	The complex formed among *F*, *G*, and *R*
FnR	The complex formed between *F* and *R*
FnRD	The complex formed among *F*, *R*, and *D*
PFD	The complex formed among *P*, *F*, and *D*

Table 4.2: Chemical reactions involved in the RPA amplification as reported in Moody [39] with few corrections. m and n are, respectively, the number of binding sites for G and R on a primer.

Chemical Equations	
$\boldsymbol{m \times G + F \rightleftharpoons FG}$	
$\boldsymbol{R + FG \rightleftharpoons FGR'}$	
$\boldsymbol{FGR' \longrightarrow FGR}$	
$\boldsymbol{FGR + (n-1) \times R \rightleftharpoons FGnR'}$	Corrected
$\boldsymbol{FGnR' \longrightarrow FnR + (m-1) \times G}$	Corrected
$\boldsymbol{FnR + D \rightleftharpoons FnRD}$	Corrected
$\boldsymbol{FnRD + n \times ATP \longrightarrow FD + n \times R + n \times AMP + n \times PPi}$	
$\boldsymbol{FnRD + n \times ATP \longrightarrow FD + n \times R + n \times ADP + H_3PO_4}$	Corrected
$\boldsymbol{FD + P \rightleftharpoons PFD}$	
$\boldsymbol{PFD + 2 \times B \times dNTP \longrightarrow P + 2 \times B \times PPi + 2 \times D}$	
$\boldsymbol{FD + np \times PPi \longrightarrow D + np \times dNTP}$	
$\boldsymbol{D + B \times PPi \longrightarrow B \times dNTP + FD}$	

The *Laminar Flow* module comprised an open boundary at the inlet of the RPA chamber, four outlets with the same velocity of 5 x 10^{-7} m/s at the inlets of LAMP reactors, and a no-flux boundary condition for all other surfaces (Fig. 4.5). In reality, the inlet of the RPA chamber is

sealed with mineral oil. When evaporation takes place at the water-air interface between the LAMP reaction chambers and the common distribution conduit, the mineral oil penetrates the RPA chamber. By measuring the distance that the water-oil interface has advanced during incubation and assuming a constant evaporation speed, the constant velocity at the four outlets was determined experimentally.

The *Transport of Diluted Species* module was coupled with the *Laminar Flow* module and used the flow field calculated by the *Laminar Flow* module to simulate advective and diffusive species transport. The *Transport of Diluted Species* module had zero-flux boundary conditions everywhere. The diffusion coefficients of all species of interest except the DNA amplicons and primers were set to 10^{-9} m^2/s. The DNA template's and primer oligos' diffusion coefficients were set to 10^{-10} m^2/s [40].

The mesh was set to *Free Tetrahedral*, followed by a *Corner Refinement* and a *Boundary Layers* mesh with default settings. The default, time-dependent segregated solver was selected.

To validate the simulation results, we performed (i) a mass conservation study where C_{LAMP} was integrated over the entire domain, normalized with its initial value, and plotted versus time, and (ii) a mesh convergence study.

4.2.9 Analytical sensitivity

To determine the minimum number of ILTV nucleic acids that our LAMP assay could detect with our microfluidic device, we carried out ten-fold serial dilutions of ILTV (2.5×10^4 genome copies per reaction) suspended in nuclease-free water. Each dilution was tested three times.

4.2.10 Detection of nucleic acids from clinical samples

Extraction of the nucleic acids from 11 nasal swabs collected from diseased chickens was carried out with AM1836 5× MagMax 96 Viral Extraction kit. The extracted nucleic acids were tested for ILTV by PCR as previously described [14]. The extracted nucleic acids were analyzed for ILTV with our microfluidic chip. Positive and negative controls were included in all tests.

4.3 Results

4.3.1 ILTV LAMP performs on par with qPCR

We carried out amplification of a dilution series of ILTV with LAMP. As the genome concentration decreases, qPCR's threshold cycle (Ct) increases nearly linearly as a function of the logarithm of the template's concentration [41]. Like the PCR threshold cycle, the LAMP threshold time (Tt) is a linear function of the log of template concentration (Fig. 4.6). The smallest detectable ILTV genome copies are 250 copies per reaction volume for both the qPCR [41] and the LAMP assays (Fig. 4.6).

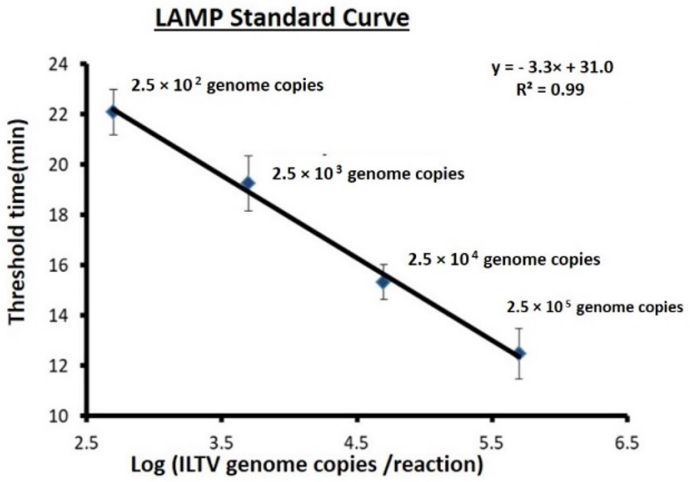

Fig. 4.6: Quantitative detection of ILTV with real-time LAMP: The LAMP threshold time (minutes) as a function of the log of ILTV concentration (genomic DNA copies per reaction). N = 3.

4.3.2 Auto-distribution driven by capillary forces

The auto-distribution of the reaction mix driven by capillary forces was imaged with yellow and blue food coloring (McCormick). Water with yellow food dye was used to represent the LAMP solution, while water with blue food dye was used to mimic the RPA reaction mix. The on-chip capillary circuits successfully i) aliquoted the LAMP solution into the four LAMP reaction chambers (Fig. 4.7a - 4.7c), ii) allowed an absorption pad to drain liquid from the distribution

channel while maintaining the solution in the LAMP reaction chambers intact (Fig. 4.7d - 4.7f), iii) filled RPA chamber (Fig. 4.7g - 4.7i), and iv) enabled the removal of excess RPA solution without draining the RPA reaction mix (Fig. 4.7j - 4.7l). Our chip with capillary circuits accommodates the loading of two different solutions into adjacent chambers while maintaining a clear interface between the two miscible solutions (Fig. 4.7l).

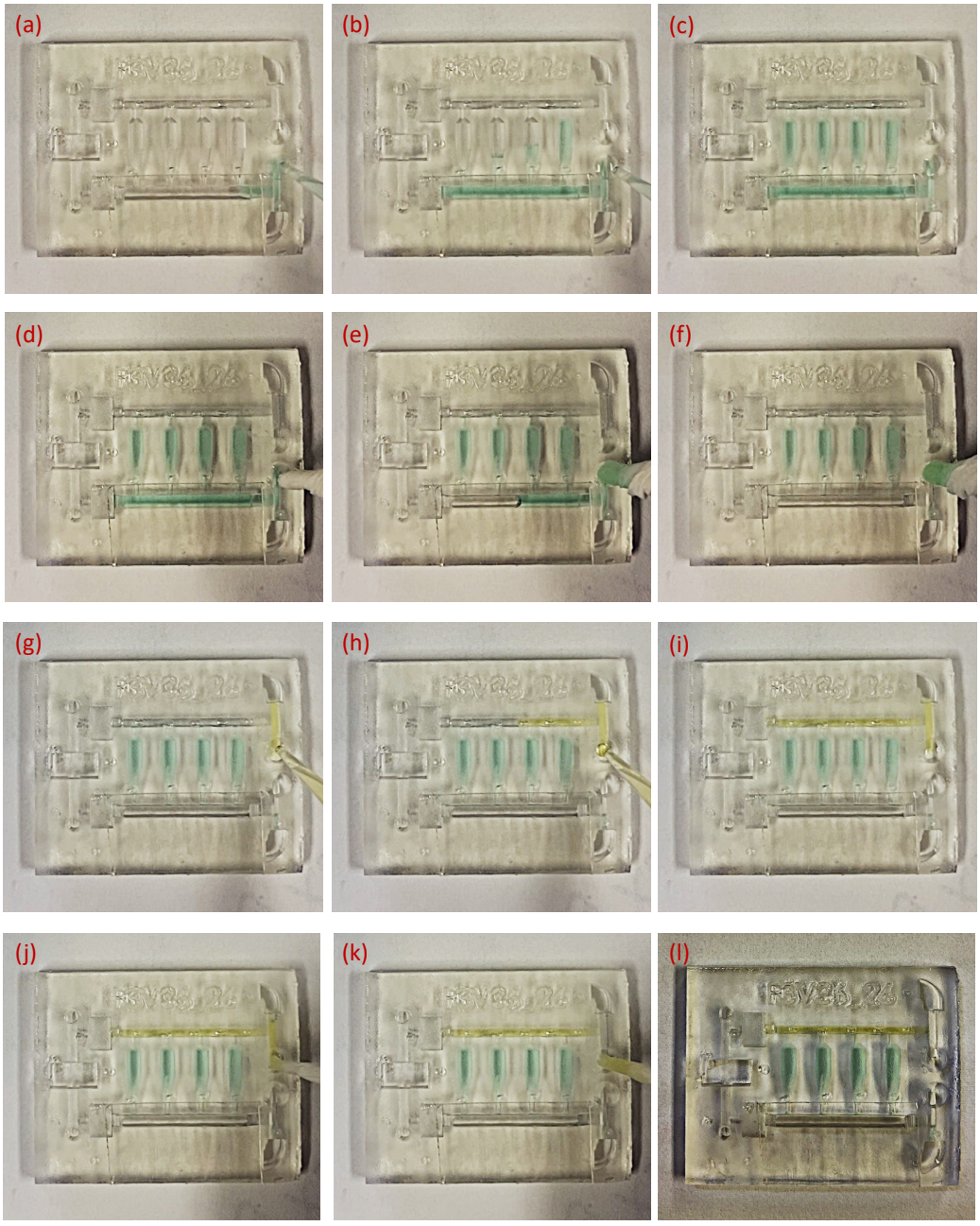

Fig. 4.7: Demonstration of the operation of the capillary circuit for auto-liquid distribution. Water dyed with blue and yellow food coloring is used, respectively, as a surrogate for the LAMP and RPA reaction buffers.

4.3.3 COMSOL simulation results

In contrast with the Penn RAMP's benchtop settings, wherein RPA and LAMP solutions are separate during the first-stage incubation and have an RPA:LAMP volume ratio of 1/15 in the second stage, the RPA and LAMP reaction chambers on chip stay interconnected at all times. We performed a COMSOL simulation to assess potential interference between RPA and LAMP buffers and evaluate the potential risk of cross-contamination caused by the migration of LAMP primers and LAMP amplicons from one LAMP reaction chamber to another LAMP reaction chamber.

The interference between RPA and LAMP was simulated by assigning a representative concentration to each buffer. $C_{\text{LAMP buffer}}$ and $C_{\text{RPA buffer}}$ represent, respectively, the LAMP buffer concentration and the RPA buffer concentration normalized with their initial concentrations. The presence of LAMP buffer in the RPA chamber $C_{\text{LAMP buffer}}$ was computed at the end of the RPA reaction (time = 600 s) along the central line of the RPA chamber (Fig. 4.8a) and across the entire domain. At the end of the RPA reaction, the central line of the RPA chamber has $C_{\text{LAMP buffer}}$ smaller than 0.1 (Fig. 4.8b), which is deemed small enough not to affect the RPA reaction significantly.

$C_{\text{RPA buffer}}$ was computed at the end of the LAMP reaction (time = 3600 s), along the central line of the first (from left) LAMP chamber (Fig. 4.8a) and across the entire domain. The simulation results (Fig. 4.8c) show that by the end of the LAMP reaction, the entire region of interest within the LAMP chamber has $C_{\text{RPA buffer}}$ smaller than 0.2, and in the majority of the reaction chamber, $C_{\text{RPA buffer}}$ is smaller than 0.1. Based on prior reports [3], LAMP performs reasonably well when blended with RPA buffer in the ratio of 1:9. Thus, it is hypothesized that the current chip design does not significantly decrease the efficiency of the LAMP reaction.

The DNA amplicon concentrations at three selected locations in the RPA chamber (Fig. 4.8d) were computed during the RPA reaction between 0 s and 600 s. Since the diffusion was enabled for all the species involved in the RPA reaction (Table 4.1), the RPA reaction is under suboptimal conditions. The closer to the LAMP reaction chambers, the lower the RPA amplification efficiency (Fig. 4.8d). The initial amount of the DNA template in the RPA chamber is

3.3×10^{-15} mol (initial concentration: 1×10^{-7} mol/m^3). At the time (t = 900 s) when the LAMP amplification starts, a total of 7.2×10^{-14} mol RPA amplicons have migrated into the four LAMP chambers, 1.8×10^{-14} mol each, which is 5 times the initial amount of DNA template added into the RPA chamber. For the primer-free, negative control where the LAMP amplification is disabled, at the end of the LAMP incubation (t = 3600 s), there are in total 2.2×10^{-13} mol RPA amplicons that have been transported to the LAMP reactors, 5.5×10^{-14} mol each LAMP chamber which is 16 times the initial amount of DNA template added into the RPA chamber. The RPA amplicon distributions were shown in Fig. 4.8e. The simulation results proved our microfluidic chip design is effective in aliquoting the first-stage amplicons into second-stage reaction chambers and consistent with the observation that the two-stage amplification is about 10-fold more sensitive than the standalone LAMP.

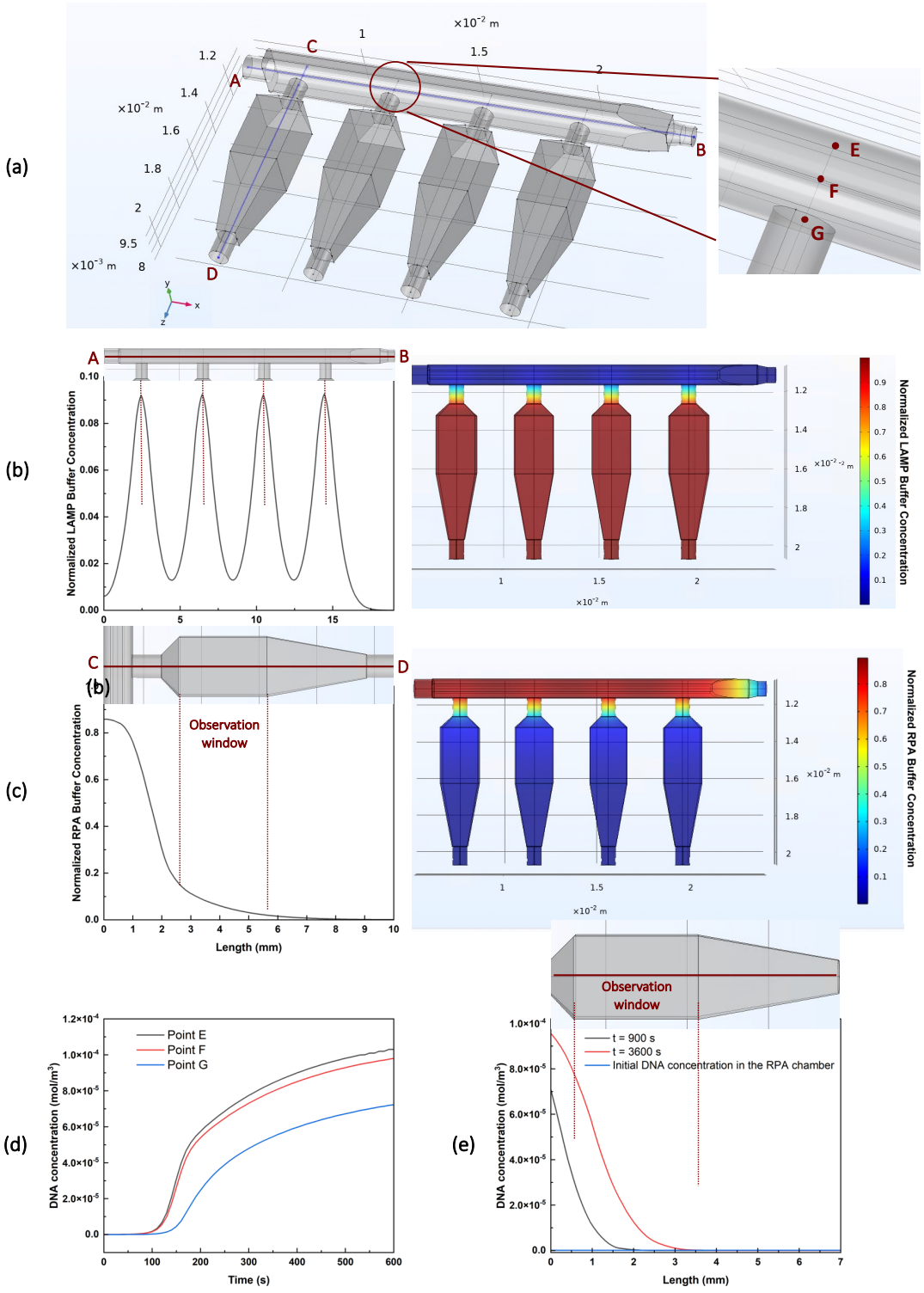

Fig. 4.8: Simulation results of RPA-LAMP interference at the end of the RPA and the LAMP reactions. (A) The computational domain and the locations of the RPA chamber's central line $\overline{AB}$,

the central line $\overline{CD}$ of the first (from the left) LAMP chamber, and the locations of points E, F, and G in the RPA chamber. (b) The normalized LAMP buffer concentration at the end of the RPA reaction (time = 600 s) as a function of position along the RPA chamber's central line $\overline{AB}$ and across the entire domain (color-coded). (c) The concentration of the normalized RPA buffer concentration at the end of the LAMP reaction (time = 3600 s) as a function of position along the LAMP chamber's central line $\overline{CD}$ and across the entire domain (color-coded). (d) RPA amplicon concentrations at three selected locations during RPA reaction as functions of time during the RPA reaction. The initial DNA template concentration in the RPA chamber is 1×10^{-7} mol/m^3. (e) RPA amplicon concentrations at the beginning (t = 900 s) and the end (t = 3600 s) of the LAMP reaction as a function along the central line of the primer-free LAMP reaction chamber (negative control).

The risk of cross-contamination was estimated based on primer migration and LAMP amplicon migration among reaction chambers. $C_{\text{LAMP primer}}$ denotes the LAMP primer concentration normalized with its initial value. Since typically primers are provided in large excess, we do not account for primer depletion during the LAMP amplification. We examined the case when the leftmost LAMP reaction chamber is the primer-free, negative control and the other reactors are positive controls. That is, the initial $C_{\text{LAMP primer}}$ is 0 in the leftmost LAMP chamber and 1 in the other LAMP chambers. This is the worst-case scenario because there is a net flow from right to left in the RPA chamber and there are net flows from the RPA chamber into the LAMP reactors due to the evaporation at the air-liquid interface between the liquid-free distribution channel and the LAMP reactors. As mentioned in the methods section, this evaporation rate was measured experimentally and specified in the numerical model as flow boundary conditions facilitating advection. At the end of the Penn RAMP process (time = 3600 s), a negligible number of primers (less than 0.01 % of the nominal primer concentration needed to support LAMP amplification) has migrated out from their home chambers to the primer-free control chamber (Fig. 4.9a), suggesting that false positives due to primer migration are unlikely. At the end of the

Penn RAMP process (time = 3600 s), the observation window of the primer-free control has local DNA amplicon concentrations smaller than 4% of the value in the test LAMP reaction chamber (Fig. 4.9b), indicating that the template migration is unlikely to produce any signal (false positive). Since the worst-case scenario was simulated, our estimates of primer and amplicon migration among reaction chambers are conservative.

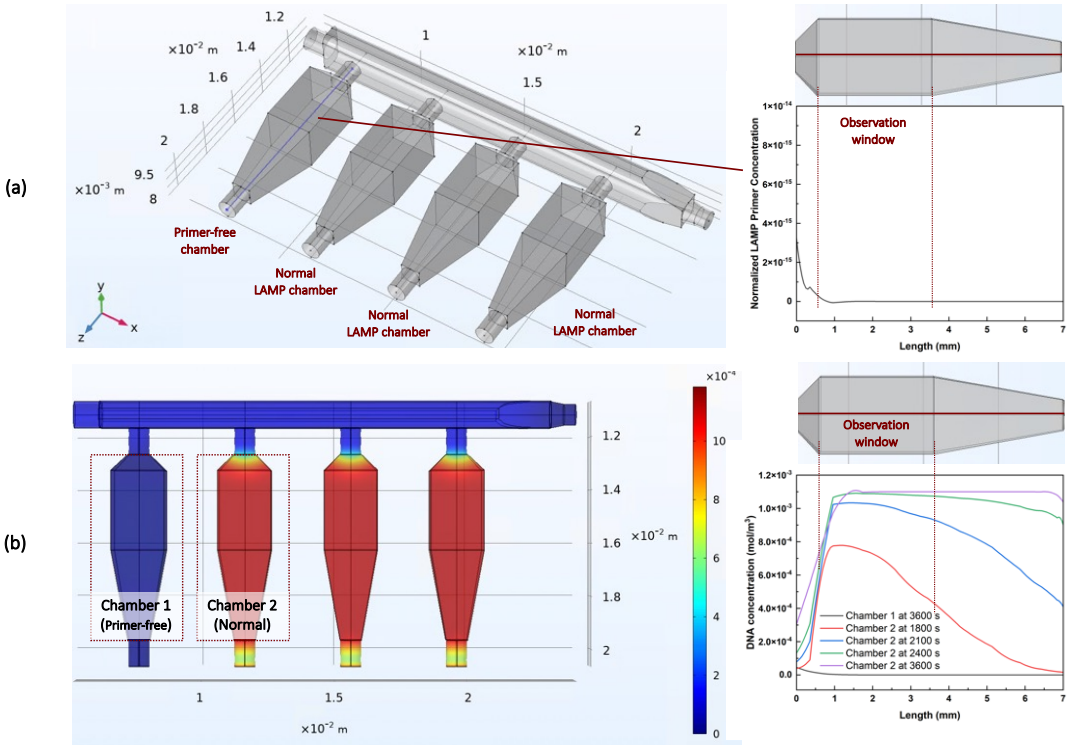

Fig. 4.9: Simulation results of primer migration among reaction chambers in Penn RAMP. The leftmost LAMP chamber is primer-free control. (a) Computed normalized LAMP primer's concentration along the central line of the primer-free LAMP chamber at the endpoint of Penn RAMP (time = 3600 s). (b) Computed distribution of DNA amplicons across the entire domain at the endpoint of Penn RAMP (time = 3600 s) and the concentration of DNA amplicons along the central lines of the primer-free chamber and a positive LAMP chamber at various times (time = 1800 s, 2100 s, 2400 s, 3600 s).

Furthermore, to verify our simulation setup, we monitored the mass conservation during the entire simulation (Fig. 4.10a) and performed a mesh convergence study (Fig. 4.10b). The mass conservation study was carried out by integrating the LAMP buffer concentration $C_{\text{LAMP Buffer}}$ over the entire domain and normalizing it with its initial value. During the simulation, the LAMP buffer mass increased by 0.9 % (Fig. 4.10a), which we consider reasonable. To verify that the numerical simulation converges, we examined the effect of mesh refinement on the RPA amplicon distribution at the end of the RPA reaction (time = 600 s). The DNA amplicon concentrations were computed along the central line of the leftmost LAMP reactor. The results (Fig. 4.10b) suggest that our results are reasonably mesh-size independent.

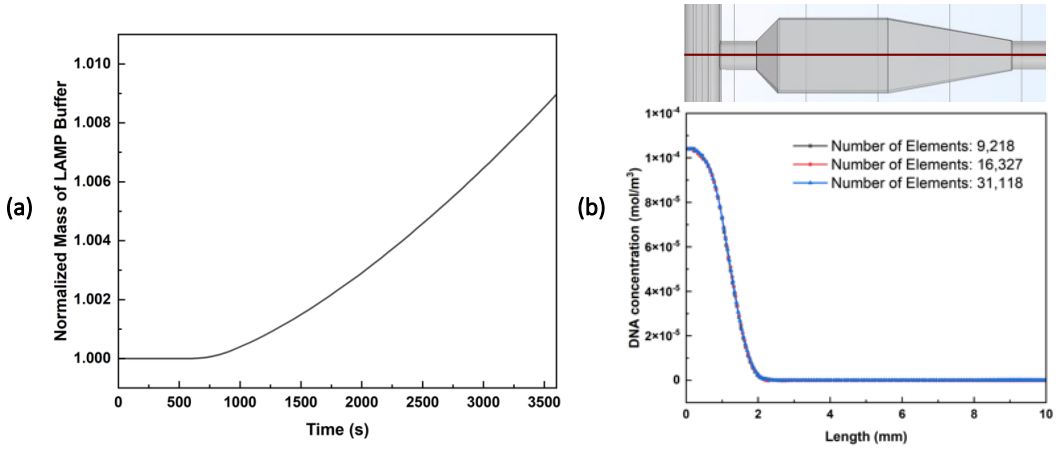

Fig. 4.10: Examination of the viability of the numerical simulations. (a) Mass conservation during the simulation – $C_{\text{LAMP Buffer}}$ was integrated over the entire domain and normalized with its initial value. (b) Mesh convergence result – The DNA amplicon concentrations along the central line of the leftmost LAMP reaction chamber at the endpoint of the RPA reaction (time = 600 s) were computed with different mesh sizes.

4.3.4 ILTV detection on chip with real-time LAMP

The microfluidic chip used in our study has four independent LAMP reactors (Fig. 4.3a). Nucleic acid amplification was monitored in real-time by observing the fluorescence emission of the

EvaGreen® dye included in the LAMP reaction mix. When a template was present in the sample, the corresponding LAMP chamber emitted fluorescence, while the chambers specialized for the absent templates and the negative control chamber remained dark during the entire incubation. In our experiments, three reaction chambers (1, 2, and 3) store primers for ILTV, while the fourth chamber is a no primer control (Fig. 4.11). We carried out serial dilution LAMP on chip with the number of templates ranging from 25 to 25,000 copies per reactor. Fluorescence emission was detected in real-time with our homemade processor. Our microfluidic chip successfully detected 250 copies of ILTV (Fig. 4.11A), providing comparable sensitivity to the benchtop settings (Fig. 4.6). The threshold time correlated linearly with the log of the template concentration (Fig. 4.11B). Fig. 4.11C is the fluorescence image of the chip after LAMP amplification, wherein only the reaction chambers (1, 2, and 3) that contained primer sets for ILTV emitted fluorescence while the non-primer control remained dark, consistent with our numerical simulations' predictions (Fig. 4.9b). To examine specificity, we tested other samples available in our laboratory: IBV, NDV, E. coli, TGEV, PEDV, and PDCoV (Fig. 4.12). None caused any fluorescent emission. That is, there were no false positives.

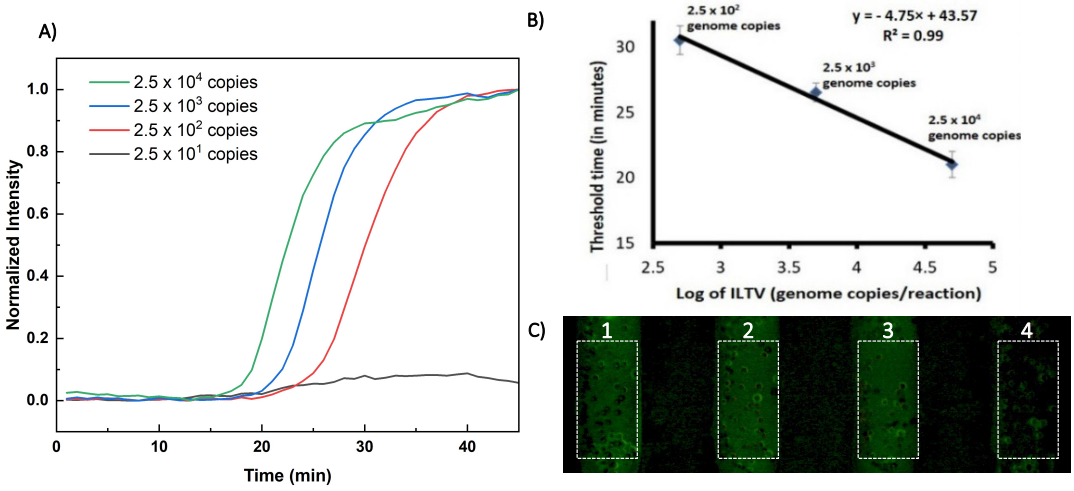

Fig. 4.11: (A) Real-time amplification curves of microfluidic chip-based ILTV LAMP assays with 25000, 2500, 250, and 25 genome copies per reaction. (B) Fluorescence image of LAMP reactors

(1, 2, 3: reaction chambers pre-stored with ILTV primers; 4: primer-free control). (C) The microfluidic chip-based LAMP threshold time Tt (minutes) as a function of the log of ILTV concentration.

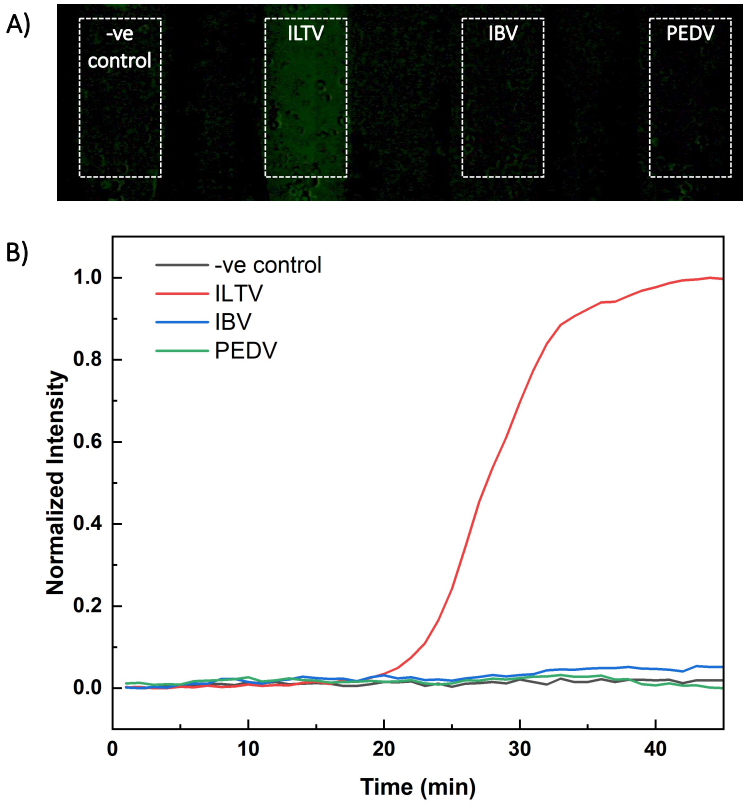

Fig. 4.12: (A) End-point fluorescence image of the LAMP assay specificity test on chip with 1) negative control, 2) ILTV positive sample, 3) IBV positive sample, and 4) PEDV positive sample. (B) Reactor-averaged fluorescence intensities as functions of time, showing successful amplification of the ILTV sample only.

4.3.5. LAMP assay performance with clinical samples

Eleven field samples collected from diseased chicken flocks were used to screen for ILTV with our benchtop real-time LMAP and our microfluidic device. Both our benchtop and on-chip ILTV LAMP detection had 100% sensitivity and 100% selectivity in comparison with the gold-standard

qPCR (Table 4.3, [41]). The on-chip (Fig. 4.13A) and benchtop (Fig. 4.13B) LAMP threshold times correlated linearly with the qPCR threshold cycle and were shorter than the PCR processing time. The threshold times of benchtop and microfluidic-based LAMP assays correlated linearly (Fig. 4.13C). The benchtop LAMP threshold times were shorter than the microfluidic LAMP due to the higher temperature ramping rate of the former.

Table 4.3: Results of clinical performance of our developed assays for ILTV detection. The qPCR incubation time equals $t_I + t_c \times C_t$, where t_I is the initial incubation time of 2 min at 95 °C and t_c is the cycle time of 35 s (95 °C for 30 s and 60 °C for 5 s). The PCR assay performance was published in Mohamed [41].

Sample No.	ILTV Detection Threshold Time		
	qPCR (Ct)	LAMP (Min)	LAMP on chip (Min)
1	21	14	18
2	-	-	-
3	26	17	21
4	22	15	19
5	-	-	-
6	25	16	20
7	22	15	21
8	21	14	18
9	28	19	22
10	-	-	-
11	25	16	21
Negative control	-	-	-

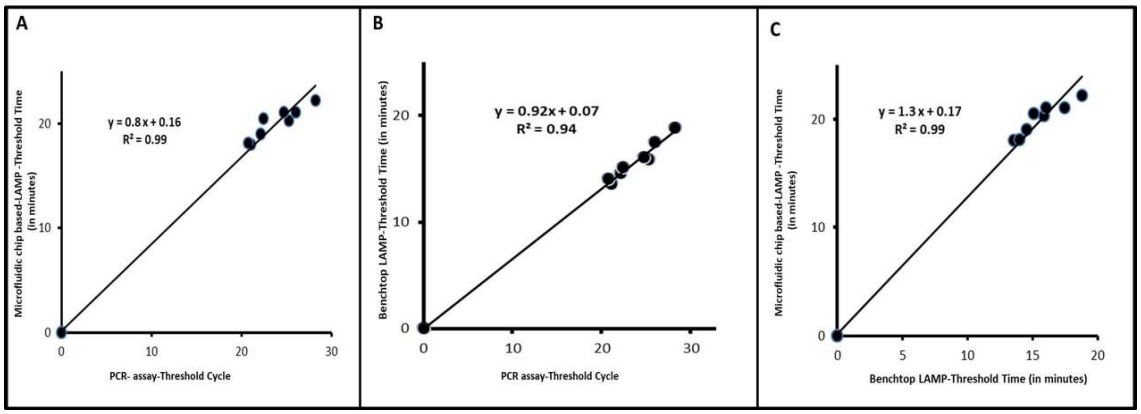

Fig. 4.13: Clinical performance of our benchtop LAMP, benchtop PCR, and on-chip LAMP when testing samples from diseased chickens. (A) Microfluidic chip-threshold time as a function of PCR threshold cycle. (B) Benchtop LAMP threshold time as a function of PCR threshold cycle. (C) Microfluidic device threshold time as a function of benchtop LAMP threshold time. The PCR assay data was published in Mohamed [41].

4.3.6 On-chip Penn RAMP

We carried out a control experiment to verify that 1) both stages of amplification are functioning on chip and 2) the sensitivity of Penn RAMP outperforms standalone LAMP. 102 copies of ILTV were added to the RPA reaction mix and shared by all four LAMP reaction chambers, resulting in an effective sample concentration of 25 copies per LAMP reaction. We used pseudo-RPA solution without TwistAmp® Basic reaction mix as the control, while our experimental group used standard RPA solutions. As before, ILTV primer sets were pre-stored in three out of four reaction chambers, leaving the last one a primer-free negative control. In the absence of RPA enzymes, the LAMP chambers did not emit any fluorescence, while in the presence of RPA enzymes, fluorescence emission was detected, enabling the construction of amplification curves (Fig. 4.14), suggesting that both RPA and LAMP functioned on chip. All the three reactors in our test group detected 25 copies of ILTV, indicating that the sensitivity of our Penn RAMP is about 10-fold better than the sensitivity of our standalone LAMP (Fig. 4.11). The Android-based smartphone application that was introduced in chapter 3 was also used to carry out the image analysis of our Penn-RAMP chip. Instead of analyzing the fluorescence images with the MATLAB software on a

laptop computer, the images were imported into the smartphone and processed with the Android-based application discussed in Chapter 3.2.9. The smartphone's results (Fig. 4.14c) are consistent with the results generated with the laptop computer (Fig. 4.14a).

The multiplexing capability of Penn RAMP was demonstrated with on-chip Penn RAMP detection of contrived samples comprising chicken virus ILTV and E. coli. In each test, only the chambers with primers specific to the targets present in the sample lighted up, and the other reactors remained dark (Fig. 4.15). No false positives were observed.

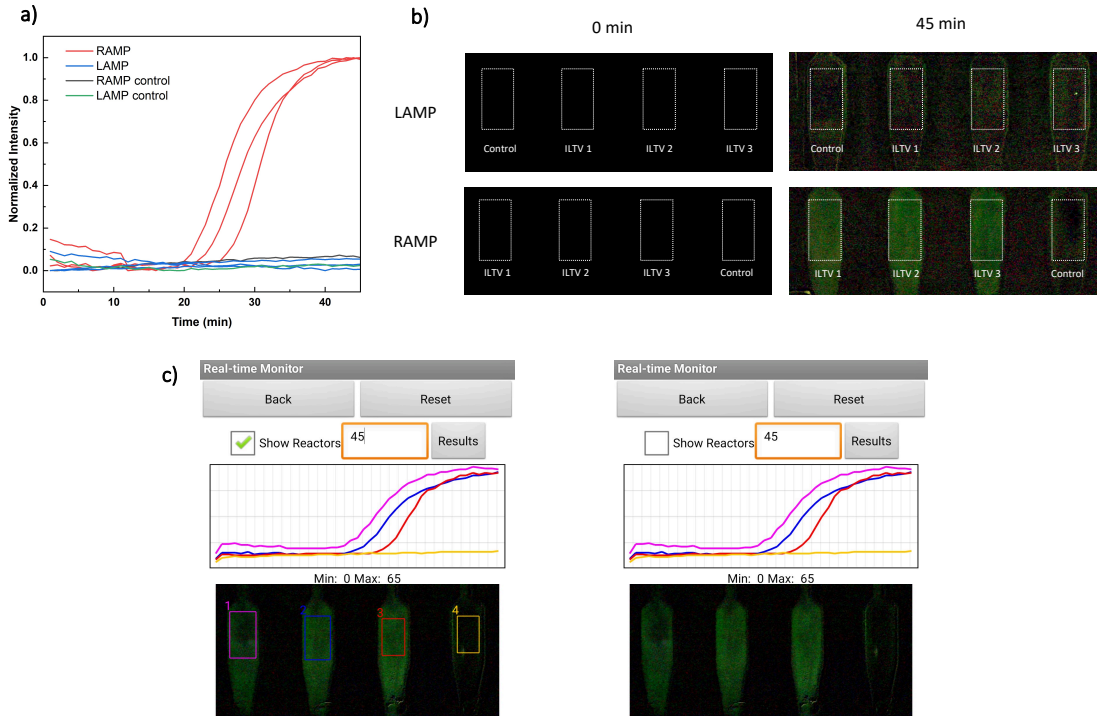

Fig. 4.14: Comparison of Penn RAMP chip and standalone LAMP chip. Penn RAMP successfully detected 25 copies of ILTV in all three reaction chambers while the standalone LAMP failed to detect 25 copies per reaction volume: (a) Real-time chamber-averaged fluorescence intensities as functions of time, (b) Initial and end-point images of LAMP reaction chambers, and (c) Screenshots of the Android-based smartphone application used for analyzing the time-series images of Penn RAMP with and without the regions of interest specified.

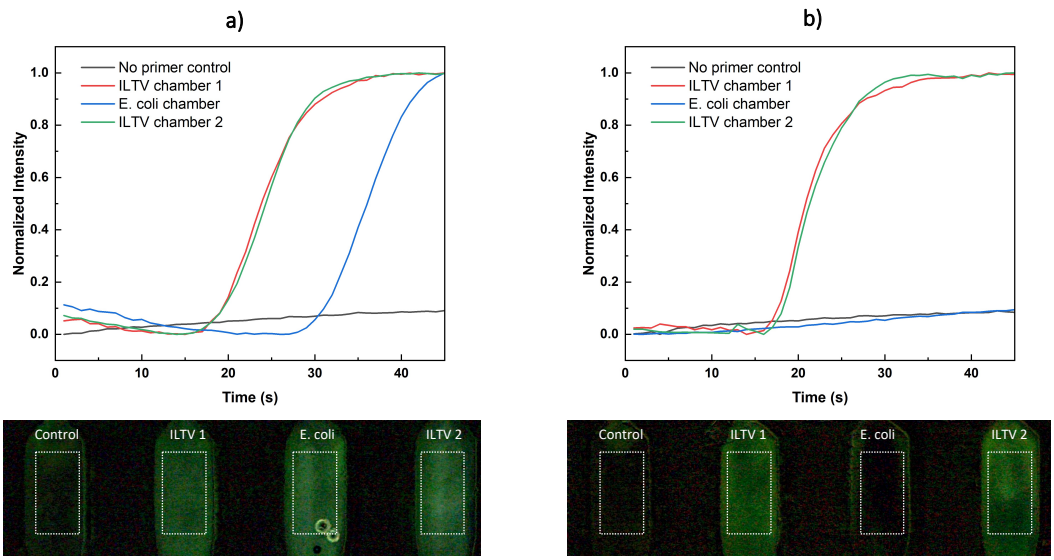

Fig. 4.15: Chamber-averaged fluorescence intensities as functions of time and end-point fluorescence images of Penn RAMP and standalone LAMP microfluidic chips customized to detect both ILTV and E. Coli. Sample (a) contains both ILTV (1020 copies per RPA reaction volume) and E. coli (1000 copies per RPA reaction volume), and sample (b) contains only ILTV (1020 copies per RPA reaction volume). In each case, the leftmost reaction chamber is primer-free, serving as a negative control, and the other three chambers pre-store, respectively, ILTV, E. coli, and ILTV primer sets.

4.4 Discussion and Conclusions

ILT presents a major risk to the chicken industry [8]. Rapid, point-of-need molecular detection methods are critical to promptly instigate control measures to contain the spread of the disease in the flock. This requires samples from suspected animals to be tested either in or in proximity to poultry farms. Simple molecular tests that can be carried out by minimally trained personnel and without sophisticated equipment would enable poultry farms operators to guard their farms against devastating diseases.

To address this need, we have developed a new LAMP and Penn RAMP assay for ILTV nucleic acids. LAMP and Penn RAMP assays have proven to be sensitive, specific, and robust [1,

3, 32, 42] and share a few important advantages over the PCR used in centralized laboratories. LAMP and Penn RAMP operate at fixed temperatures and do not require temperature cycling, which significantly diminishes equipment complexity, power consumption, and total setup cost. Furthermore, the isothermal incubation for LAMP and Penn RAMP can be carried out even electricity-free with a heat-generating, exothermic reaction and a phase-change material to regulate the temperature [43]. Moreover, LAMP and Penn RAMP assays tolerate inhibitors effects better than PCR [1, 44], allowing less stringent sample preparations. Finally, LAMP and Penn RAMP produce more amplicons than PCR, facilitating instrument-free detection with a variety of colorimetric dyes.

Our ILTV LAMP and Penn RAMP assay can be carried out in benchtop settings in a tube with standard laboratory equipment or in a microfluidic device. Here, we describe a 3D-printed microfluidic chip with one RPA chamber and four LAMP reaction chambers for Penn RAMP or LAMP-only assays on chip. The chip utilizes capillary circuits, encoding the desired liquid distribution within the geometry design. The aliquoting of RPA amplicons relies on convection-diffusion effects, facilitating uniform distribution of first-stage amplicons into multiple second-stage reactors without the need for actuators. The chips described herein comprise 4 LAMP reaction chambers. The concept can be expanded, however, to include much greater number of LAMP reaction chambers to facilitate high-level multiplexing. Our microfluidic chip mates with an inexpensive, portable processor that provides temperature control and fluorescence detection.

Our ILTV LAMP assay, either on the benchtop or in microfluidic format, performs on par with the gold-standard qPCR assay, and the sensitivity of our Penn RAMP assay outperforms our LAMP-only assay by about 10-fold. Both our assays combine amplification and detection in a closed system without the need to transfer amplicons to a lateral flow strip or electrophoresis gel, avoiding exposing amplicon-rich solutions to the ambient and risking possible contamination of the workplace, which may render false positives in subsequent tests. The threshold times of both our benchtop and chip-based LAMP correlate linearly with the logarithm of initial ILTV DNA concentration. Thus, we can use the threshold time to estimate the viral/pathogen load. The somewhat longer threshold times in our microfluidic-based LAMP compared to benchtop assays

result from the one-sided heating of our chip. In the benchtop instrument, the reaction chamber (tube) is inserted into a heated metal block. In contrast, our microfluidic chip is heated only at its bottom and is exposed to the ambient at its top. The heating efficiency can be, however, improved with two-sided heating with a slight increase in complexity and cost, which were deemed non-essential.

Both our benchtop and microfluidic ILTV LAMP assays achieved the sensitivity of 250 genomic copies per reaction, while the ILTV Penn RAMP demonstrated a higher sensitivity of 25 genomic copies per LAMP reaction chamber. During the early stage of infection, a chicken typically has ILTV in respiratory tissues and secretions exceeding 10^3 genome copies/μL [16, 17]. Therefore, our assays' detection limits are more than sufficient for virus detection during the seroconversion window.

To evaluate the clinical utility of our ILTV LAMP assay and its implementation in the microfluidic format, we tested 11 clinical samples from diseased chickens, demonstrating concordance with the gold-standard PCR and no interference from the inhibitors in clinical veterinary samples.

In future work, it may be desirable to differentiate vaccines from pathogen strains. This would require the design of more specific primers to inform appropriate control measures. Additionally, integrating a simple and rapid technique for pathogen nucleic acids extraction and concentration from crude samples with the chip would enable higher sensitivity [43].

References

[1] J. Song *et al.*, "Two-Stage Isothermal Enzymatic Amplification for Concurrent Multiplex Molecular Detection," *Clinical Chemistry,* Article vol. 63, p. 714, 2017.

[2] H. H. Bau, M. G. Mauk, S. Jinzhao, and C. Liu, "Multiple stage isothermal enzymatic amplification," ed: Google Patents, 2019.

[3] M. El-Tholoth, E. Anis, and H. H. Bau, "Two stage, nested isothermal amplification in a single tube," *The Analyst,* vol. 146, no. 4, pp. 1311-1319, 2021, doi: 10.1039/d0an01835j.

[4] Y. Seok, Q. Yin, H. Bai, and H. H. Bau, "Sensitive, Single-Pot, Two-Stage Assay for Hepatitis Viruses," *Analytical Chemistry,* vol. 94, no. 3, pp. 1778-1786, 2022, doi: 10.1021/acs.analchem.1c04480.

[5] A. J. Davison *et al.*, "The order Herpesvirales," *Archives of Virology,* vol. 154, no. 1, pp. 171-177, 2009, doi: 10.1007/s00705-008-0278-4.

[6] V. Gowthaman *et al.*, "Infectious laryngotracheitis: Etiology, epidemiology, pathobiology, and advances in diagnosis and control – a comprehensive review," *Veterinary Quarterly,* vol. 40, no. 1, pp. 140-161, 2020, doi: 10.1080/01652176.2020.1759845.

[7] K. R. Menendez, M. García, S. Spatz, and N. L. Tablante, "Molecular epidemiology of infectious laryngotracheitis: a review," *Avian Pathology,* vol. 43, no. 2, pp. 108-117, 2014, doi: 10.1080/03079457.2014.886004.

[8] M. García, J. Volkening, S. Riblet, and S. Spatz, "Genomic sequence analysis of the United States infectious laryngotracheitis vaccine strains chicken embryo origin (CEO) and tissue culture origin (TCO)," (in eng), *Virology,* vol. 440, no. 1, pp. 64-74, May 25 2013, doi: 10.1016/j.virol.2013.02.007.

[9] P. R. Ide, "Sensitivity and specificity of the fluorescent antibody technique for detection of infectious laryngotracheitis virus," (in eng), *Can J Comp Med,* vol. 42, no. 1, pp. 54-62, Jan 1978.

[10] M. Kotiw, C. R. Wilks, and J. T. May, "Differentiation of infectious laryngotracheitis virus strains using restriction endonucleases," (in eng), *Avian Dis,* vol. 26, no. 4, pp. 718-31, Oct-Dec 1982.

[11] R. G. Russell and A. J. Turner, "Characterization of infectious laryngotracheitis viruses, antigenic comparison by kinetics of neutralization and immunization studies," (in eng), *Can J Comp Med,* vol. 47, no. 2, pp. 163-71, Apr 1983.

[12] J. J. York, J. G. Young, and K. J. Fahey, "The appearance of viral antigen and antibody in the trachea of naive and vaccinated chickens infected with infectious laryngotracheitis virus," *Avian Pathology,* vol. 18, no. 4, pp. 643-658, 1989, doi: 10.1080/03079458908418639.

[13] M. W. Shirley, D. J. Kemp, M. Sheppard, and K. J. Fahey, "Detection of DNA from infectious laryngotracheitis virus by colourimetric analyses of polymerase chain reactions," (in eng), *J Virol Methods,* vol. 30, no. 3, pp. 251-9, Dec 1990, doi: 10.1016/0166-0934(90)90067-p.

[14] A. Vögtlin, L. Bruckner, and H. P. Ottiger, "Use of polymerase chain reaction (PCR) for the detection of vaccine contamination by infectious laryngotracheitis virus," (in eng), *Vaccine,* vol. 17, no. 20-21, pp. 2501-6, Jun 4 1999, doi: 10.1016/s0264-410x(99)00068-7.

[15] J. Humberd, M. García, S. M. Riblet, R. S. Resurreccion, and T. P. Brown, "Detection of infectious laryngotracheitis virus in formalin-fixed, paraffin-embedded tissues by nested polymerase chain reaction," (in eng), *Avian Dis,* vol. 46, no. 1, pp. 64-74, Jan-Mar 2002, doi: 10.1637/0005-2086(2002)046[0064:Doilvi]2.0.Co;2.

[16] A. Mahmoudian *et al.*, "Development of a SYBR Green quantitative polymerase chain reaction assay for rapid detection and quantification of infectious laryngotracheitis virus," *Avian Pathology,* vol. 40, no. 3, pp. 237-242, 2011, doi: 10.1080/03079457.2011.553582.

[17] Y. Zhao *et al.*, "Detection of Infectious Laryngotracheitis Virus by Real-Time PCR in Naturally and Experimentally Infected Chickens," *PLoS ONE,* vol. 8, no. 6, p. e67598, 2013, doi: 10.1371/journal.pone.0067598.

[18] N. Laamiri, R. Aouini, B. Marnissi, A. Ghram, and I. Hmila, "A multiplex real-time RT-PCR for simultaneous detection of four most common avian respiratory viruses," (in eng), *Virology,* vol. 515, pp. 29-37, Feb 2018, doi: 10.1016/j.virol.2017.11.021.

[19] H. M. Pham, C. Nakajima, K. Ohashi, and M. Onuma, "Loop-Mediated Isothermal Amplification for Rapid Detection of Newcastle Disease Virus," *Journal of Clinical Microbiology,* vol. 43, no. 4, pp. 1646-1650, 2005, doi: doi:10.1128/JCM.43.4.1646-1650.2005.

[20] H. T. Chen *et al.*, "Development of reverse transcription loop-mediated isothermal amplification for rapid detection of H9 avian influenza virus," (in eng), *J Virol Methods,* vol. 151, no. 2, pp. 200-203, Aug 2008, doi: 10.1016/j.jviromet.2008.05.009.

[21] Q. Li *et al.*, "An improved reverse transcription loop-mediated isothermal amplification assay for sensitive and specific detection of Newcastle disease virus," *Archives of Virology,* vol. 154, no. 9, pp. 1433-1440, 2009, doi: 10.1007/s00705-009-0464-z.

[22] H. T. Chen *et al.*, "Reverse transcription loop-mediated isothermal amplification for the rapid detection of infectious bronchitis virus in infected chicken tissues," (in eng), *Mol Cell Probes,* vol. 24, no. 2, pp. 104-6, Apr 2010, doi: 10.1016/j.mcp.2009.10.001.

[23] S.-C. Ou, J. J. Giambrone, and K. S. Macklin, "Comparison of a TaqMan real-time polymerase chain reaction assay with a loop-mediated isothermal amplification assay for detection of Gallid herpesvirus 1," *Journal of Veterinary Diagnostic Investigation,* vol. 24, no. 1, pp. 138-141, 2012, doi: 10.1177/1040638711427578.

[24] K. Nagamine, T. Hase, and T. Notomi, "Accelerated reaction by loop-mediated isothermal amplification using loop primers," (in eng), *Mol Cell Probes,* vol. 16, no. 3, pp. 223-9, Jun 2002, doi: 10.1006/mcpr.2002.0415.

[25] X. Zhang, S. B. Lowe, and J. J. Gooding, "Brief review of monitoring methods for loop-mediated isothermal amplification (LAMP)," *Biosensors and Bioelectronics,* vol. 61, pp. 491-499, 2014.

[26] O. A. Gandelman *et al.*, "Novel Bioluminescent Quantitative Detection of Nucleic Acid Amplification in Real-Time," *PLoS ONE,* vol. 5, no. 11, p. e14155, 2010, doi: 10.1371/journal.pone.0014155.

[27] G. Kiddle *et al.*, "GMO detection using a bioluminescent real time reporter (BART) of loop mediated isothermal amplification (LAMP) suitable for field use," *BMC Biotechnology,* vol. 12, no. 1, p. 15, 2012/04/30 2012, doi: 10.1186/1472-6750-12-15.

[28] Q. Yang, K. J. Domesle, F. Wang, and B. Ge, "Rapid detection of Salmonella in food and feed by coupling loop-mediated isothermal amplification with bioluminescent assay in real-time," *BMC Microbiology,* vol. 16, no. 1, p. 112, 2016/06/17 2016, doi: 10.1186/s12866-016-0730-7.

[29] J. Song, C. Liu, M. G. Mauk, J. Peng, T. Schoenfeld, and H. H. Bau, "A Multifunctional Reactor with Dry-Stored Reagents for Enzymatic Amplification of Nucleic Acids," *Analytical Chemistry,* vol. 90, no. 2, pp. 1209-1216, 2018/01/16 2018, doi: 10.1021/acs.analchem.7b03834.

[30] J. Song *et al.*, "Smartphone-Based Mobile Detection Platform for Molecular Diagnostics and Spatiotemporal Disease Mapping," (in eng), *Anal Chem,* vol. 90, no. 7, pp. 4823-4831, Apr 3 2018, doi: 10.1021/acs.analchem.8b00283.

[31] Y. Li *et al.*, "A real-time loop-mediated isothermal amplification method for rapid detection of Lawsonia intracellularis in porcine fecal samples," (in eng), *J Microbiol Methods,* vol. 151, pp. 62-65, Aug 2018, doi: 10.1016/j.mimet.2018.06.002.

[32] M. Dou, D. C. Dominguez, X. Li, J. Sanchez, and G. Scott, "A Versatile PDMS/Paper Hybrid Microfluidic Platform for Sensitive Infectious Disease Diagnosis," *Analytical Chemistry,* vol. 86, no. 15, pp. 7978-7986, 2014, doi: 10.1021/ac5021694.

[33] M. Dou *et al.*, "A low-cost microfluidic platform for rapid and instrument-free detection of whooping cough," (in eng), *Anal Chim Acta,* vol. 1065, pp. 71-78, Aug 13 2019, doi: 10.1016/j.aca.2019.03.001.

[34] S. Sharma, J. Zapatero-Rodríguez, P. Estrela, and R. O'Kennedy, "Point-of-Care Diagnostics in Low Resource Settings: Present Status and Future Role of Microfluidics," *Biosensors,* vol. 5, no. 3, pp. 577-601, 2015, doi: 10.3390/bios5030577.

[35] C. M. Pandey *et al.*, "Microfluidics Based Point-of-Care Diagnostics," *Biotechnology Journal,* vol. 13, no. 1, p. 1700047, 2018, doi: 10.1002/biot.201700047.

[36] N. Zhang *et al.*, "Development of one-step SYBR Green real-time RT-PCR for quantifying bovine viral diarrhea virus type-1 and its comparison with conventional RT-PCR," *Virology Journal,* vol. 8, no. 1, p. 374, 2011, doi: 10.1186/1743-422x-8-374.

[37] K. Kadimisetty *et al.*, "Fully 3D printed integrated reactor array for point-of-care molecular diagnostics," *Biosensors and Bioelectronics,* vol. 109, pp. 156-163, 2018/06/30/ 2018, doi: https://doi.org/10.1016/j.bios.2018.03.009.

[38] M. El-Tholoth, H. Bai, M. G. Mauk, L. J. Saif, and H. H. Bau, "A Portable, 3-D Printed, Microfluidic Device for Multiplexed, Real Time, Molecular Detection of Porcine Epidemic Diarrhea Virus, Transmissible Gastroenteritis Virus, and Porcine Deltacoronavirus at the Point of Need," *Lab Chip,* 10.1039/D0LC01229G 2021, doi: 10.1039/D0LC01229G.

[39] C. Moody, H. Newell, and H. Viljoen, "A mathematical model of recombinase polymerase amplification under continuously stirred conditions," *Biochemical Engineering Journal,* vol. 112, pp. 193-201, 2016/08/15/ 2016, doi: https://doi.org/10.1016/j.bej.2016.04.017.

[40] C. Liu *et al.*, "Nuclemeter: A reaction-diffusion based method for quantifying nucleic acids undergoing enzymatic amplification," *Scientific reports,* vol. 4, no. 1, pp. 1-7, 2014.

[41] M. El-Tholoth, H. Bai, M. G. Mauk, E. Anis, and H. H. Bau, "Molecular Detection of Infectious Laryngotracheitis Virus in Chickens with a Microfluidic Chip," *Animals,* vol. 11, no. 11, p. 3203, 2021. [Online]. Available: https://www.mdpi.com/2076-2615/11/11/3203.

[42] Q. Yang, F. Wang, W. Prinyawiwatkul, and B. Ge, "Robustness of Salmonella loop-mediated isothermal amplification assays for food applications," *Journal of Applied Microbiology,* vol. 116, no. 1, pp. 81-88, 2014, doi: 10.1111/jam.12340.

[43] R. J. Li, M. G. Mauk, Y. Seok, and H. H. Bau, "Electricity-free chemical heater for isothermal nucleic acid amplification with applications in COVID-19 home testing," *Analyst,* 10.1039/D1AN00309G vol. 146, no. 13, pp. 4212-4218, 2021, doi: 10.1039/D1AN00309G.

[44] M. Dou, S. T. Sanjay, D. C. Dominguez, P. Liu, F. Xu, and X. Li, "Multiplexed instrument-free meningitis diagnosis on a polymer/paper hybrid microfluidic biochip," *Biosensors and Bioelectronics,* vol. 87, pp. 865-873, 2017, doi: 10.1016/j.bios.2016.09.033.

Chapter 5 Conclusions and Outlook

5.1 Conclusions

In this thesis, three portable, low-cost, 3D-printed, microfluidic devices with capillary circuits were developed for rapid, simple, sensitive, specific, multiplexed point-of-need molecular detection of human, animal, and plant pathogens. These devices utilize capillary-driven flow to aliquot samples to multiple reaction chambers, capillary valves for flow control, and phase-change materials for device sealing. To examine the efficacy of our technology, we developed and tested assays for a few specific conditions. We developed a chip with multiple loop-mediated isothermal amplification (LAMP) reaction chambers operating with liquid reagents to co-detect three co-endemic pig viruses: PEDV, TGEV, and PDCoV (Chapter 2); a chip with multiple LAMP reactors and dry-stored reagents to co-detect the three human bloodborne viruses: HIV, HBV, and HCV (Chapter 3), and a chip that accommodates our custom-designed two-stage amplification dubbed RAMP to detect chicken respiratory viruses such as ILTV (Chapter 4). Although these various pathogens were used to assist chip development, their rapid detection is critical in many circumstances. PEDV, TGEV, and PDCoV are re-emerging coronaviruses (CoVs) that cause significant economic loss to pig farms and pork processors. HIV, HBV, and HCV have infected and co-infected more than 400 million people worldwide and are causing millions of deaths and new infections annually. ILTV presents a major risk to the chicken industry, causing a viral disease in chickens' respiratory systems and imposing considerable economic burdens on the chicken industry.

Capillary circuits are the infrastructure that enables automated flow distribution and control in all the microfluidic devices discussed in this thesis. I developed a capillary valve-controlled draining process, allowing precise removal of liquids from one of the interconnecting conduits and, more importantly, restoring function to capillary valves. In contrast to conventional capillary valves that are single-use, the capability of re-activating previously used capillary valves enables my capillary circuits to achieve more sophisticated control functions. For example, the capillary circuit in Chapter 4 demonstrates its capability of loading two miscible aqueous solutions

into adjacent microfluidic chambers while maintaining a sharp interface between the two solutions and allowing the auto-distribution of two reaction mixes for on-chip Penn RAMP. Besides aqueous solutions, the capillary circuits introduced in Chapters 2 and 3 also proved compatible with a phase-change material (PEG 930) for capillary-induced automatic sealing.

Isothermal nucleic acid amplification tests (LAMP and Penn RAMP) were adopted in all three microfluidic devices and performed on par with the gold standard PCR assays in benchtop settings that require thermal cycling. The selection of isothermal molecular detection reduced the design complexity of our microfluidic devices and heating/incubation system. Our assays are also compatible with colorimetric dyes such as HNB dye that changes color from violet to blue when successful amplification takes place, enabling instrument-free operation and result reading. To avoid the need for a cold chain, a fully dried LAMP assay was implemented in Chapter 3, demonstrating the capability of reaction mix storage at room temperature and humidity, obviating the need for storage at -20 °C. The dried LAMP reaction mix can last for at least 10 weeks of on-chip storage and perhaps much longer with further optimization.

A COMSOL-based numerical simulation was developed to model RPA and LAMP amplification, fluid flow, and the migration of species of interest on chip, ultimately guiding the microfluidic chip design. The simulations in Chapter 3 verified that the temporary liquid connection among LAMP reaction chambers does not result in a significant amount of target-specific primers migrating out of their designated chamber and into adjacent chambers. The simulation in Chapter 4 modeled the on-chip Penn-RAMP reaction, evaporation-induced fluid flow, and convective-diffusive species transport, estimating the potential risk of cross-talk and potential interference between RPA and LAMP. Our numerical simulations verified that the migration of primers and amplicons is unlikely to cause cross-contamination and the compositions of RPA and LAMP reaction mixes are not significantly changed by the end of on-chip RPA and LAMP amplification.

An Android-based smartphone application was developed to replace computers to perform image analysis. In Chapter 3, the smartphone was used to take an endpoint chip photo and interpret colorimetric detection results. In Chapters 3 and 4, the Android application was,

respectively, used to analyze time-series fluorescence images for quasi-quantification of HIV, HBV, and HCV viral loads and ILTV viral load.

5.2 Outlook

On-chip detection is rapid, sensitive, and specific, enabling the prompt implementation of appropriate control measures to contain the spread of infections. Multiplexed detection is needed to detect co-endemic pathogens that induce similar symptoms but require diverse infection management strategies and to identify co-morbidities that may alter the course of a disease and challenge standard drug therapies. Detection at the point of need is desired to provide health care providers with critical information to enable personalized medicine and public health officials with critical information to make rational policy decisions.

Our work in this thesis focused on the development and testing of the back end of the diagnostic system. We addressed the aliquoting of purified nucleic acids into specific reaction chambers, refrigeration-free reagent storage, reaction incubation, and amplicon detection. The front-end sample-specific processing, such as serum separation from whole blood and nucleic acid extraction and purification, is left to future work. It is desirable to integrate all unit operations on a single substrate to provide sample-to-answer capability. To achieve this, our devices can be combined with standalone portable devices for sample processing, such as Penn's superhydrophobic plasma separator [1]. It would, however, be more desirable to integrate all the necessary unit operations into a seamless workflow, enabling automated processing with minimal user intervention.

The capillary circuits developed herein eliminate the reliance on external control instruments such as syringe pumps and pipettes. The draining and the pumping modules form the two basic modules for my capillary circuits. More complex fluid distribution could be potentially achieved by making more extensive use of these two simple operations.

The thermal control used in my devices requires electrical power either from the grid or from a battery, a central controller to form a closed feedback loop and adjust power output based on real-time measurements, a thermocouple, and an electric resistance heater, to maintain the

desired incubation temperature. The need for such an incubator may increase the cost of our device. In the future, incubation could be performed, electricity-free, with heat from an exothermic reaction such as the one used in meals ready to eat and with phase-change material for temperature control [2, 3].

There is a large parameter space for drying conditions and on-chip storage conditions that has not been systematically explored. For example, one could optimize the temperature, humidity, pressure, and time that are used to dry the reaction mix and the use of preservatives. A better understanding of the on-chip reaction mix drying and storage will further increase the shelf time of the microfluidic chip - something that would be essential in a commercial product.

3D printing was used to fabricate all the devices discussed in this thesis. I used a commercially available 3D printer that was designed for home use. Using a professional 3D printer with higher printing resolution will allow fabricating microfluidic channels with smaller dimensions and therefore stronger capillary valves to provide more reliable flow control and achieve more sophisticated capillary circuits. Also, 3D printers with co-print capability will enable microfluidic chip fabrication with different materials to minimize self-fluorescence and enhance biocompatibility and heat conductivity. If this technology were to be commercialized, the 3D printing technology likely would need to be replaced with high throughput manufacturing such as injection molding or embossing.

My numerical simulations provided insights to chip operation. I implemented a model to simulate the RPA reaction in the presence of advection and diffusion. Similar models for LAMP do not yet exist. The availability of LAMP simulators would enable a more complete analysis of chip performance.

In the future, the smartphone can be integrated with appropriate optical filters to replace the external fluorescence camera and reduce equipment costs. The Android application has great potential for further development to guide the uninitiated user in performing the test, detect and analyze signals from all reaction chambers concurrently, interpret test results for the patient, with the patient’s permission report the results to the patient’s physician and public health officials, and provide counseling.

References

[1] C. Liu *et al.*, "A high-efficiency superhydrophobic plasma separator," *Lab Chip,* vol. 16, no. 3, pp. 553-560, 2016, doi: 10.1039/c5lc01235j.

[2] R. J. Li, M. G. Mauk, Y. Seok, and H. H. Bau, "Electricity-free chemical heater for isothermal nucleic acid amplification with applications in COVID-19 home testing," *Analyst,* 10.1039/D1AN00309G vol. 146, no. 13, pp. 4212-4218, 2021, doi: 10.1039/D1AN00309G.

[3] S. C. Liao *et al.*, "Smart cup: A minimally-instrumented, smartphone-based point-of-care molecular diagnostic device," *Sensor Actuat B-Chem,* vol. 229, pp. 232-238, Jun 28 2016, doi: 10.1016/j.snb.2016.01.073.